

REPORT DOCUMENTATION PAGE

Form Approved
OMB No. 0704-0188

Public reporting burden for this collection of information is estimated to average 1 hour per response, including the time for reviewing instructions, searching existing data sources, gathering and maintaining the data needed, and completing and reviewing this collection of information. Send comments regarding this burden estimate or any other aspect of this collection of information, including suggestions for reducing this burden to Department of Defense, Washington Headquarters Services, Directorate for Information Operations and Reports (0704-0188), 1215 Jefferson Davis Highway, Suite 1204, Arlington, VA 22202-4302. Respondents should be aware that notwithstanding any other provision of law, no person shall be subject to any penalty for failing to comply with a collection of information if it does not display a currently valid OMB control number. **PLEASE DO NOT RETURN YOUR FORM TO THE ABOVE ADDRESS.**

1. REPORT DATE (DD-MM-YYYY) 28-09-2006		2. REPORT TYPE Final		3. DATES COVERED (From - To) March 2003 - February 2005	
4. TITLE AND SUBTITLE Deployment and Intelligent Nanosatellite Operations Colorado Final Technical Report				5a. CONTRACT NUMBER	
				5b. GRANT NUMBER F49620-03-1-0150	
				5c. PROGRAM ELEMENT NUMBER	
6. AUTHOR(S) Elaine Hansen, Dave Beckwith, Chris Koehler, Steve Levin-Stankevich, Jennifer Michels, Steve Wichman				5d. PROJECT NUMBER 1536704 & 1536709	
				5e. TASK NUMBER	
				5f. WORK UNIT NUMBER	
7. PERFORMING ORGANIZATION NAME(S) AND ADDRESS(ES) Colorado Space Grant Consortium 520 UCB University of Colorado Boulder, CO 80309				8. PERFORMING ORGANIZATION REPORT NUMBER	
9. SPONSORING / MONITORING AGENCY NAME(S) AND ADDRESS(ES) Dr. Gerald Witt AFOSR/NE gerald.witt@afosr.af.mil 703-696-8571				10. SPONSOR/MONITOR'S ACRONYM(S) AFRL/VSSV	
				11. SPONSOR/MONITOR'S REPORT NUMBER(S)	

12. DISTRIBUTION / AVAILABILITY STATEMENT

Distribution Statement A: unlimited

AFRL-SR-AR-TR-06-0431

13. SUPPLEMENTARY NOTES

20061102532

14. ABSTRACT

The main purpose of the DINO satellite was to generate topographic maps of the tops of clouds through stereoscopic imaging based on photographs from the on-board digital cameras, with most processing done on the satellite itself. The attitude determination and control system was designed to be responsible for maintaining the spacecraft's orientation in order to achieve mission objectives. The system consisted of a magnetometer and three single axis rate gyroscopes. The C&DH system was responsible for storing and running all of the spacecraft's software and controlling all of the other systems - tested using two different computers: the Arcom Viper and the Arcom Mercury. The communications system was designed for establishing a two way communications link between the spacecraft and a ground station (full-duplex), using separate radios and frequencies for ground-to-satellite and satellite-to-ground links. The mechanisms system's primary objective was to safely secure all deployable systems during launch, release the deployable system when commanded during the mission, and to deploy the systems on command. DINO had four deployable systems: the antenna release, the Boom release and slow down, the FITS release, and the CTD hinge experiment release and deployment. The mission operations system was responsible for controlling and monitoring the satellite with a minimum of human intervention. The electrical power system was responsible for collecting, managing, and distributing power for the entire spacecraft - a direct energy transfer system with a secondary lithium-polymer battery for the main satellite, a primary 28V battery for the deployable devices, a main solar array, the Foldable Integrated Thin-film Stiffened (FITS), and body-mount solar arrays.

15. SUBJECT TERMS

16. SECURITY CLASSIFICATION OF:			17. LIMITATION OF ABSTRACT 100-200 words	18. NUMBER OF PAGES 190	19a. NAME OF RESPONSIBLE PERSON
a. REPORT	b. ABSTRACT	c. THIS PAGE			19b. TELEPHONE NUMBER (include area code)



Atmospheric Torque Calculation Report

DINO-ADCS-RPT-ATMTOR, Rev. A

Written by:
Stephen Stankevich

Prepared for:
Nanosat III

Table of Contents

1	Scope.....	4
1.1	Identification.....	4
1.2	Document Maintenance.....	4
1.3	Systems Overview.....	4
1.4	Document Overview.....	4
1.5	Referenced Documents.....	4
2	Atmospheric Torque Calculations.....	4

1 Scope

1.1 Identification

This document applies to the DINO project, a project undertaken by the Colorado Space Grant Consortium at the University of Colorado at Boulder. This project is part of the Nanosatellite III Program sponsored by the Air Force Office of Scientific Research (AFOSR), Air Force Research Laboratory (AFRL), Association of Aeronautics and Astronautics (AIAA), and Goddard Space Flight Center (GSFC).

1.2 Document Maintenance

This document falls under the DINO document control requirements as specified under the DINO Configuration Management plan. All changes and updates must be made in accordance with the DINO CM plan.

1.3 Systems Overview

The purpose of the student-led Deployment and Intelligent Nanosatellite Operations (DINO) mission is to determine cloud heights from space, evaluate the performance of intelligent operations, and assess deployment technologies for nanosatellites including a gravity-gradient boom, memory composite hinges, and thin-film solar arrays.

1.4 Document Overview

The atmospheric torques which will be imposed upon DINO in orbit are critical to the design of the ADC system. The torques applied to DINO will affect the attitude of the spacecraft, which the ADC system will need to maintain.

1.5 Referenced Documents

List any reference documents here.

2 Atmospheric Torque Calculations

According to the MSIS90 density plots, at 300 km we expect to see atmospheric density values of approximately $10^{-13.3}$ g/cm³ (5.012×10^{-11} kg/m³) at solar maximum and 10^{-14} g/cm³ at solar minimum. The torque applied to the DINO spacecraft will be dominated by atmospheric drag torques. Hence, DINO's gravity gradient torques should be capable of compensating for this external torque.

The relationship between atmospheric drag and atmospheric density is approximated by the following equation:

$$a_{Drag} = -\frac{1}{2} C_D \frac{A}{m} \rho v^2,$$

Eq. 2-1

where C_D is the coefficient of atmospheric drag, A is the cross-sectional area of the spacecraft, m is the mass of the spacecraft, ρ is the atmospheric density, and v is the velocity of the spacecraft with respect to the atmosphere. To determine the torque on DINO, we have approximated DINO as two masses separated by a rigid, massless rod with the following parameters:

Table 2-1

Parameter	Main Satellite	Tip-Mass
C_D	2	2
A	0.125 m ²	0.026 m ²
m	25 kg	5 kg
ρ	5.0119 x 10 ⁻¹¹ kg/m ³	5.0119 x 10 ⁻¹¹ kg/m ³
v	7,726 m/s	7,726 m/s

Using the values shown in the table above, we can determine an approximate value for the atmospheric drag that each half of DINO experiences. We find the following values:

Table 2-2

	Main Satellite	Tip-Mass
a_{Drag}	-1.496 x 10 ⁻⁵ m/s ²	-1.556 x 10 ⁻⁵ m/s ²

Now we can determine the net torque on the DINO system using the following relationship:

$$\vec{\tau}_{Drag} = \vec{r}_{Main} \times \vec{F}_{Main} + \vec{r}_{Tip} \times \vec{F}_{Tip}$$

Eq. 2-2

where r_{Main} is the vector from DINO's center of mass to the main satellite, F_{Main} is the force of drag on the main satellite, r_{Tip} is the vector from the center of mass to the tip-mass, and F_{Tip} is the force of drag on the tip-mass. In this case, assuming a circular orbit and a nadir-pointing spacecraft, the vectors are perpendicular and we can directly multiply the magnitudes of each vector. The values are given in the following table:

Table 2-3

Parameter	Main Satellite	Tip-Mass
$ r $	$L/6$	$5*L/6$
$ F $	3.7395×10^{-4} N	7.7783×10^{-5} N

L is equal to the length of the tether, equal to $r_{Main} + r_{Tip}$. The two forces produce opposing torques. If we assume a length L equal to 20 meters, we expect to see a net atmospheric torque equal to approximately 4.99×10^{-5} Nm. The figure below shows the relationship of atmospheric torque as a function of tether length for DINO.

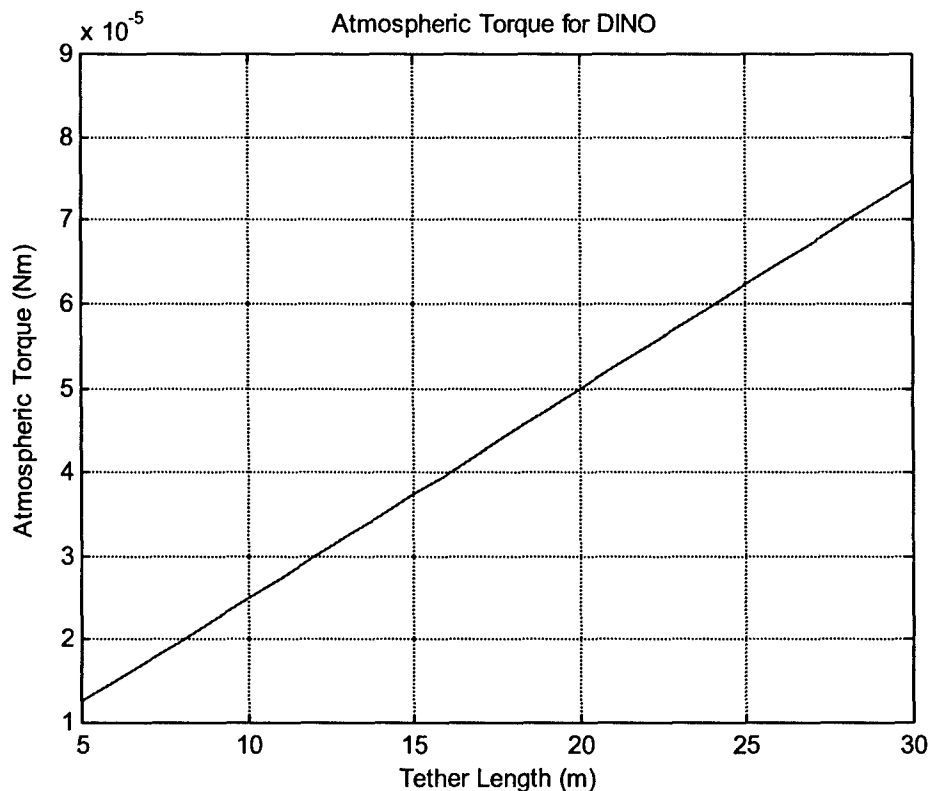


Figure 2-1

The general relationship for the magnitude of the atmospheric torque as a function of main satellite mass, tip-mass mass and tether length is the following:

$$\tau_{atm} = \left| (a_{Tip} - a_{Main}) \frac{m_{Main} m_{Tip}}{m_{Main} + m_{Tip}} L \right|$$

Eq. 2-3

We will define the following:

$$m^* = \frac{m_{Main} m_{Tip}}{m_{Main} + m_{Tip}}$$

Eq. 2-4

Thus:

$$\tau_{atm} = |a_{Tip} - a_{Main}| m^* L$$

Eq. 2-5

If we then go on to determine the length of tether we need to compensate for the atmospheric torque by way of a gravity-gradient torque...

The moment of inertia of DINO can be approximated by the following expression:

$$I \approx m_{Main} r_{Main}^2 + m_{Tip} r_{Tip}^2$$

Eq. 2-6

where, once again, r_{Main} is the distance between the main satellite and DINO's center of mass and r_{Tip} is the distance between the tip-mass and the CG. We also know that $m_{Main} r_{Main} = m_{Tip} r_{Tip}$ and $r_{Main} + r_{Tip} = L$, the length of the tether. Hence, we can infer the following expression:

$$I \approx m_{Main} \left(\frac{\frac{m_{Tip} L}{m_{Main}}}{1 + \frac{m_{Tip}}{m_{Main}}} \right)^2 + m_{Tip} \left(\frac{\frac{m_{Main} L}{m_{Tip}}}{1 + \frac{m_{Main}}{m_{Tip}}} \right)^2$$

Eq. 2-7

which simplifies to:

$$I \approx \frac{m_{Main} m_{Tip}^2 + m_{Tip} m_{Main}^2}{(m_{Main} + m_{Tip})^2} L^2$$

Eq. 2-8

and again to:

$$I \approx \frac{m_{Main} m_{Tip}}{m_{Main} + m_{Tip}} L^2$$

Eq. 2-9

finally:

$$I \approx m^* L^2$$

Eq. 2-10

Now, we want the gravity-gradient torque to fully compensate for the atm drag torque. Hence, $g_r > \tau_{atm}$. A simplification of the gravity-gradient torque can be represented as the following:

$$g_r \approx 3\omega^2 I$$

Eq. 2-11

where ω is the angular velocity of the spacecraft as it orbits the earth. DINO's angular velocity, assuming an ISS orbit, is roughly equal to:

$$\omega \approx \sqrt{\frac{\mu_e}{r^3}}$$

Eq. 2-12

where μ_e is the earth's gravitational parameter. Hence, ω is equal to about 1.157×10^{-3} rad/s. Thus we have the following:

$$g_r \approx 3 \frac{\mu_e}{r^3} I > \tau_{atm}$$

Eq. 2-13

or:

$$3 \frac{\mu_e}{r^3} (m^* L^2) > |a_{Tip} - a_{Main}| m^* L$$

Eq. 2-14

which simplifies to:

$$L > |a_{Tip} - a_{Main}| \frac{r^3}{3\mu_e}$$

Eq. 2-15

given our orbit and accelerations, we have the following:

$$L > 0.149 \text{ meters}$$

With this tether length, we would have a gravity-gradient torque equal to the maximum atmospheric torque we would expect, namely: 3.714×10^{-7} Nm

Figures 2-2 and 2-3, below, give a summary of the atmospheric and gravity-gradient torques that DINO would experience given the assumptions laid out in this document. The minimum tether length due to atmospheric disturbance torques occurs at the cross-over point.

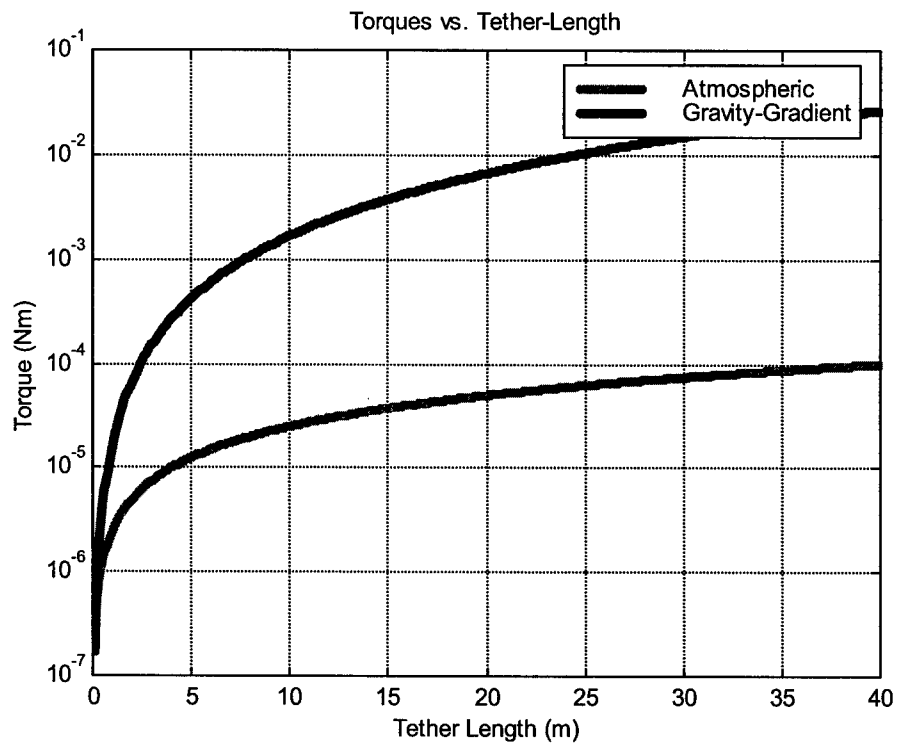


Figure 2-2

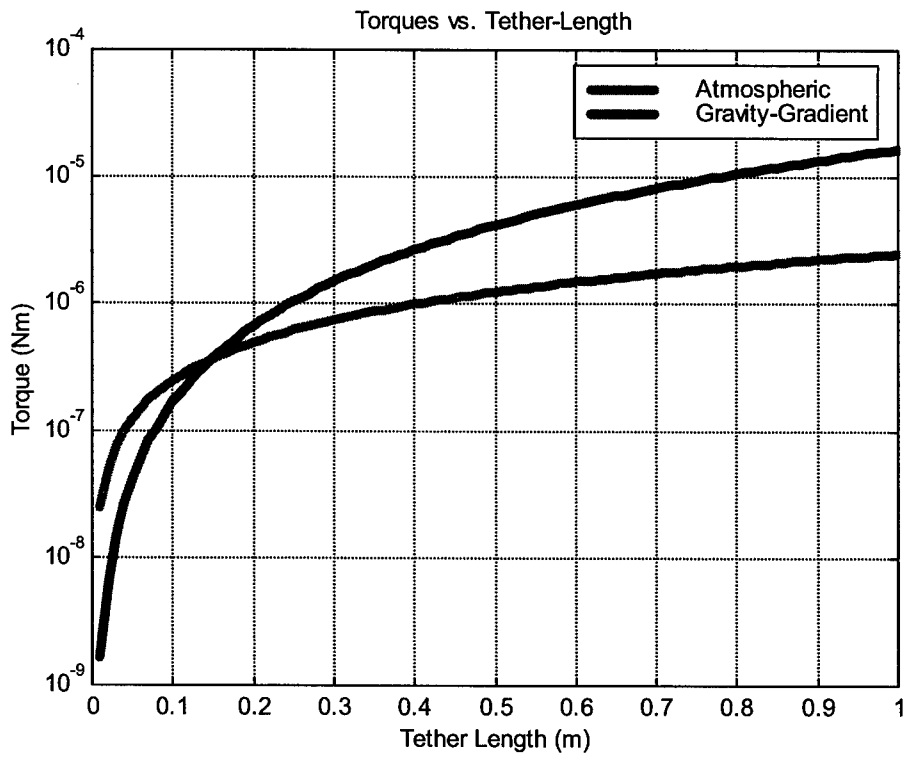


Figure 2-3



Torque Rod Size Report

DINO-ADCS-RPT-TQSIZE, Rev. A

Written by:
Stephen Stankevich

Prepared for:
Nanosat III

Table of Contents

1	Scope.....	4
1.1	Identification.....	4
1.2	Document Maintenance.....	4
1.3	Systems Overview.....	4
1.4	Document Overview.....	4
1.5	Referenced Documents.....	4
2	Background.....	4
3	Actuator Requirements.....	5
3.1	Disturbance Torques.....	5
3.2	Detumbling.....	5
4	Sizing Analysis.....	6
4.1	Torque Coils.....	6
4.2	Torque Rods.....	6
4.2.1	Design Options.....	10
	Appendix A – List of Acronyms.....	Error! Bookmark not defined.

1 Scope

1.1 Identification

This document applies to the DINO project, a project undertaken by the Colorado Space Grant Consortium at the University of Colorado at Boulder. This project is part of the Nanosatellite III Program sponsored by the Air Force Office of Scientific Research (AFOSR), Air Force Research Laboratory (AFRL), Association of Aeronautics and Astronautics (AIAA), and Goddard Space Flight Center (GSFC).

1.2 Document Maintenance

This document falls under the DINO document control requirements as specified under the DINO Configuration Management plan. All changes and updates must be made in accordance with the DINO CM plan.

1.3 Systems Overview

The purpose of the student-led Deployment and Intelligent Nanosatellite Operations (DINO) mission is to determine cloud heights from space, evaluate the performance of intelligent operations, and assess deployment technologies for nanosatellites including a gravity-gradient boom, memory composite hinges, and thin-film solar arrays.

1.4 Document Overview

The calculation of the required size for proper magnetic field generation and engineering analysis of the available area within the DINO spacecraft for torque rods is described in this document.

1.5 Referenced Documents

Makovec, Kristin L.: [A Nonlinear Magnetic Controller for Three Axis Stability of Nanosatellites](#); Virginia Polytechnic Institute and State University; July 23, 2001.

Radtke, Gregg: [Magnetic Torquer Overview Technical Note](#); University of Arizona; December 1, 1999.

2 Background

There are several primary industry standards used to control spacecraft attitude. These methods are the use of reaction wheels, propulsion systems, and magnetic torque devices. Of these options reaction wheels and magnetic torquers were originally studied for their applicability to the DINO spacecraft. Propulsion systems were not considered for obvious reasons, primarily safety concerns. Single axis reaction wheels control the spacecraft's attitude by either slowing down or speeding up their rotation rate and thereby exerting a change in angular momentum of the s/c. The main performance characteristics of reaction wheels are their ability to quickly

slew the s/c. The slew rates are based on the weight of the wheel and its rotation rate. One drawback to reaction wheels is the need to dump stored momentum in the wheel as the rotation rates become excessively high. This energy is usually released through the use of a single or multiple torque rods. The second control actuator considered was a magnetic torque rod. These are either wound loops of wire around air or around a ferromagnetic material such as iron. By passing a current through the loops of wire a magnetic dipole moment is produced. The moment interacts with the Earth's magnetic field to provide a torque on the s/c. Drawbacks of this system are the weight of the ferromagnetic material in the case of torque rods or the volume of the torque coils. By weighing the benefits and disadvantages of each system magnetic torque rods/coils have been selected as the primary actuator. The greatest benefit of this system is the ability to design and construct magnetic torquers at the University of Colorado.

3 Actuator Requirements

Several requirements may be placed on the actuators chosen for the DINO s/c. The attitude control subsystem has been initially allotted only 2.6 kg. However, project management has implied that as much as 4 kg could be allotted if needed. Secondly, the subsystem has been allotted only 4W for nominal operation. The 4W is not the maximum power usage for detumbling of the s/c. In nominal operation the control actuators must respond to disturbance torques by the environment and damp oscillations caused by the gravity gradient torques induced by the tethered boom.

3.1 Disturbance Torques

Several environmental factors will cause disturbance torques during orbit around the Earth. These factors are solar radiation pressure from the sun, aerodynamic drag from the Earth, and gravity gradient forces from the Earth. Since DINO will utilize a gravity gradient tether those forces will not be considered as a disturbance torque. Early analysis of solar pressure and drag forces discovered a maximum disturbance force of 1.1×10^{-4} N m. This assumes a 400km altitude, drag coefficient of 2.5 (sufficiently high), and cross-sectional area of 1m^2 . Dividing the maximum disturbance torque by the maximum magnetic field of 5×10^{-5} Tesla the required dipole moment output of the torquers is 2.2 Am^2 . However, smaller torquer outputs are acceptable with slower recovery rates. Therefore, the minimum torquer output shall be considered as 1 Am^2 for normal operations.

3.2 Detumbling

Prior to deploying the gravity gradient tether the spacecraft will have to be stabilized from a tumbling state. Exact rotational rates of the initial tumble will be unknown and may be relatively fast. Therefore, the minimum torquer output determined above will not be sufficient to efficiently detumble the s/c. A greater moment on the order of 10 to 20 Am^2 would be desired but requires much too many resources in power and weight. The recommendation of the ADCS team is that the torquers be designed to output the greatest possible output beyond the minimum of 1.0 Am^2 that is allowable per overall s/c resources. The greater the

output produced by the magnetic torquers the faster the s/c may be slowed or slewed to another orientation. Specific requirements for detumbling of the spacecraft will be discussed in document DINO-ADCS-RPT-DTUMBL. This document will be based on simulations for the detumbling of the s/c.

4 Sizing Analysis

4.1 Torque Coils

Torque coils are simply wound loops of wire, commonly copper wire, with current passed through. The current flowing in the loops acts similar to a solenoid and produces a magnetic dipole moment shown in equation 4-1.

$$\vec{M} = INA$$

Eq. 4-1

In equation 4-1, I is the input current, N is the number of wire loops, and A is the area of the torque coil. The torque on the s/c is then produced by the cross product of the magnetic dipole moment and the Earth's magnetic field vector.

$$T = M \times B$$

Eq. 4-2

Early studies into torque coils revealed several benefits. They produce a reliable and easily modeled dipole moment output. Early studies also revealed that a torque coil producing a large enough output would require a large volume. The dimensions of the coil would require a radius of near 6 inches. This large volume is a major drawback to the consideration of using torque coils.

4.2 Torque Rods

Torque rods behave in the same manner as torque coils except they utilize the effect of a ferromagnetic rod in the middle of the wound loops of wire. A common material such as iron has a magnetic permeability from 100 to 5000 times that of air. Thus magnifying the dipole moment output from the loops of wire themselves. The major drawback to this system is the heavy weight of iron (density of 4800 kg/m³ to 7874 kg/m³). A major trade study has been conducted into the sizing requirements for a magnetic torque rod.

Although a torque rod output moment of 2.2Am² is enough to counteract disturbance forces a larger torque output is preferential. Equation 3 shows an estimate of the required slew time for a given attitude error.

$$t = 2\sqrt{\frac{I_3\theta}{M \cdot B}}$$

Eq. 4-3

In equation 4-3, I₃ is the moment of inertia about the radial direction, theta is the initial attitude error, M is the maximum torque rod dipole moment output, and B is the maximum magnetic field strength¹. Figure 4-1 shows the relationship

between the dipole moment output and the estimated slew times for an initial position error of 2° in a single axis perpendicular to the magnetic field.

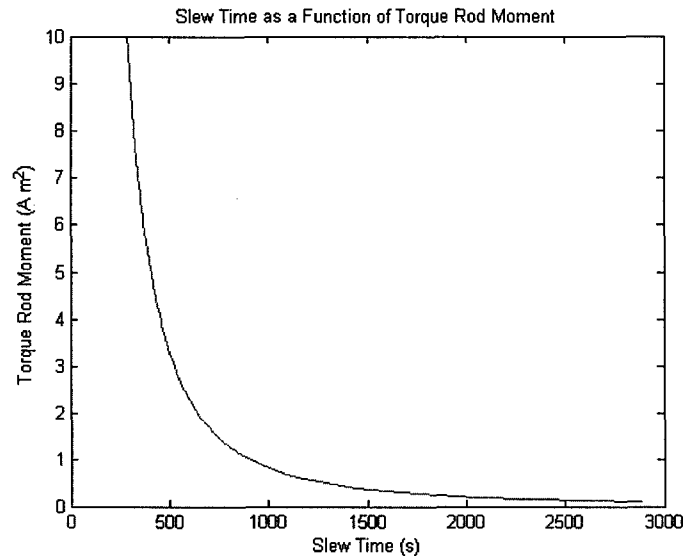


Figure 4-1: Slew time for 2 degree error

Due to the exponential form of the relationship it is more desirable to produce a maximum torque output of greater 5 Am^2 to stay above the knee in the curve.

Obtaining a torque output moment of over 5 Am^2 is not easy with the weight and power limitations put on the system by the s/c design. To analyze how this may be accomplished a MATLAB program was written based on several primary equations of power, weight, and output.

$$m = \pi r^2 (Ni + lM)$$

Eq. 4-4

Where m is the torque rod output moment, r is the radius of the iron core, N is the number of wire turns, i is the input current, l is the torque rod length, and M is the magnetization defined by $M = B/\mu_0$, B being the magnetic field strength and μ_0 being the permeability of air. This equation allows comparison of the output moment by varying the torque rod radius and length. Figure 4-2 shows the relationship between the physical size and the torque rod output moment for an input current of 300mA and material permeability of 500.

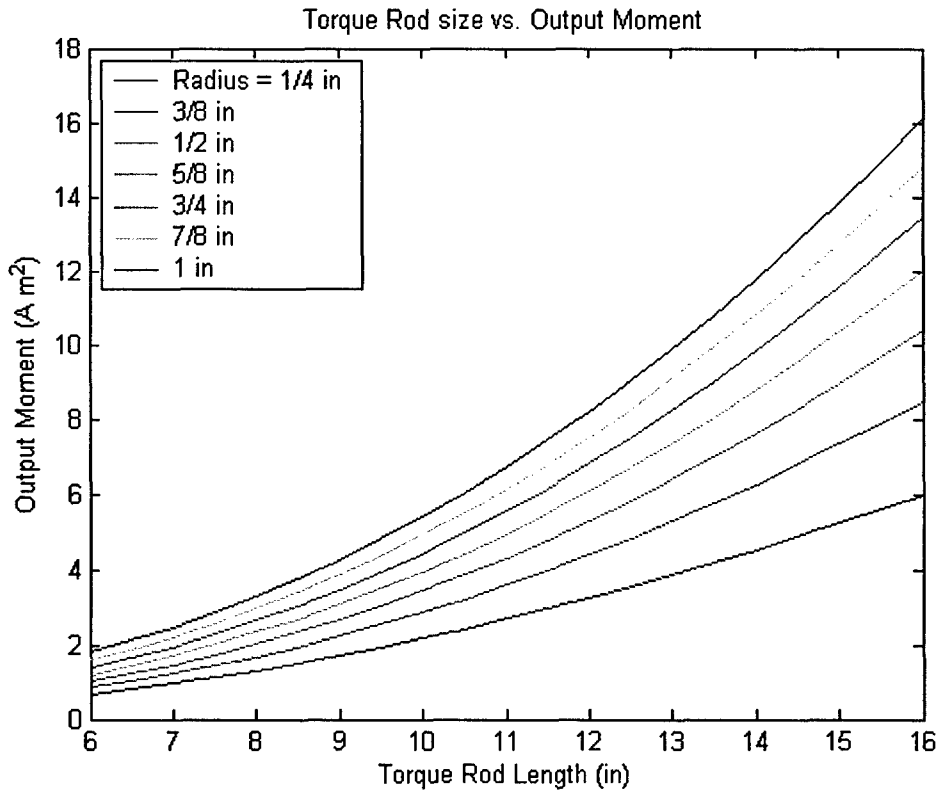


Figure 4-2: Sizing chart for 300mA current and mu = 500

Figure 4-2 shows an output moment of at least 5 Am² is obtainable at an input current of 300mA. Actually, the output moment is very obtainable at an input current of only 150mA. However, the torque rod size required to obtain the desired moment at lower currents is large and has tremendous weight on the order of several kilograms per torque rod. Equation 5 shows the relationship between the weight of the torque rod and the size.

$$W = \pi r^2 l \rho_{iron}$$

Eq. 4-5

Where ρ is the density of iron equal to 4800 kg/m³. Figure 4-3 shows the relationship between the torque rod size and actual weight.

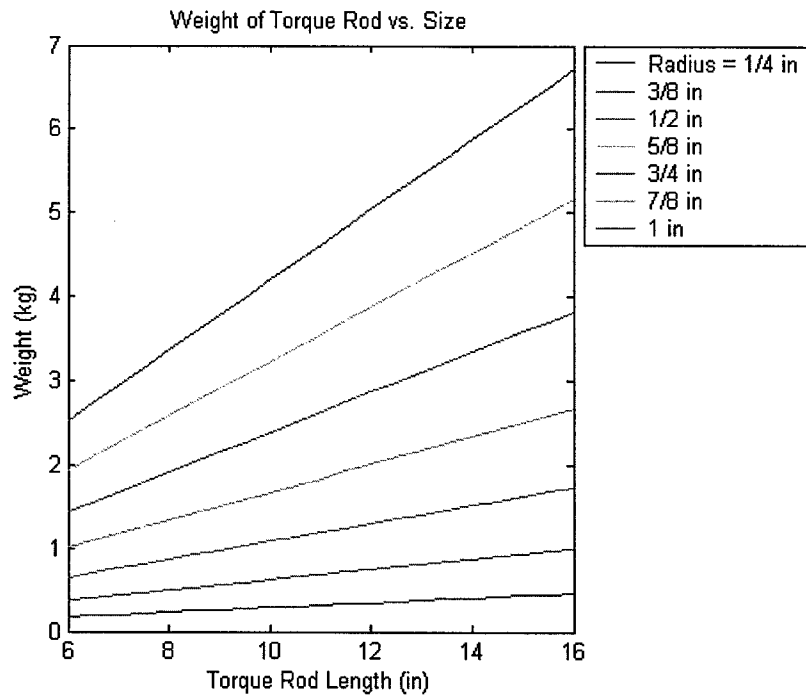


Figure 4-3: Torque rod weight including the weight of the wire

Figure 4-3 shows the only torque rod configuration that will maintain a weight of less than 2 kg for all three torque rods is of a long rod with radius of $\frac{1}{4}$ " or $\frac{3}{8}$ ". Because of the small inner radius required to keep the torque rods within weight constraints the input current must be the before mentioned 300mA or larger. Even at 300mA the torque rods will have to be an undesirable length of near 16 inches each. This can be accomplished by placing two 8 inch rods in each axis. This may require a more complicated control algorithm but is necessary in order to detumble the spacecraft upon mission start. The third concern with the currently suggested configuration is power concerns. Figure 4 shows the relationship between the power consumption in the wire around the torque rods.

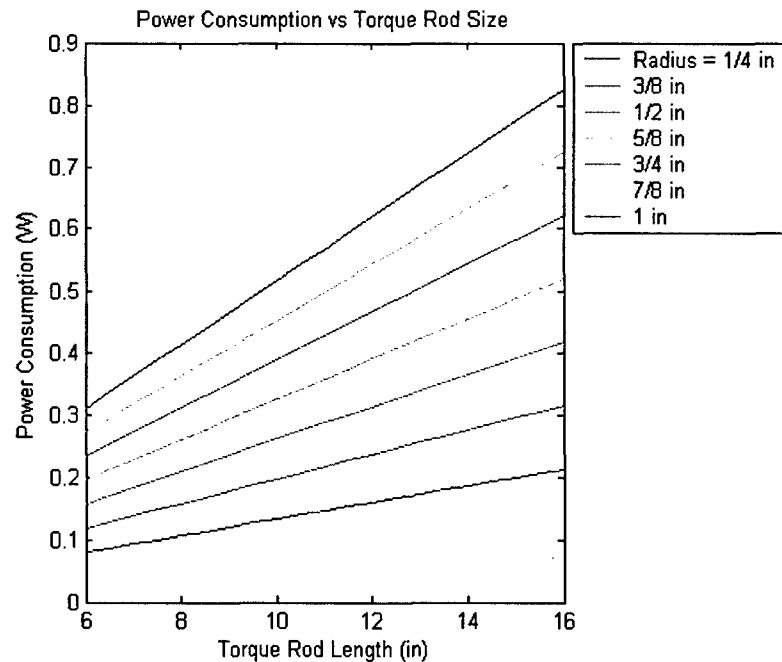


Figure 4-4: Power consumption of torque rod for 24 gauge wire

Figure 4-4 shows that for 24 gauge wire with a long torque rod and at most 3/8 inch radius the power consumption is below 300mW. This low power consumption is thus not a design concern. The maximum power usage by the torque rods will be while detumbling the spacecraft. After this time the torque rod use will be minimal and input currents may be kept at a maximum of 150mA minimizing power consumption further.

Due to the strict weight requirements and desired torque rod dipole moment output a minimum design has been made. The torque rods shall be made of an iron core with a minimum length of 10 inches and inner radius of 3/8 inches. The torque rods shall be wrapped with 24 gauge wire with an input current capable of 300mA for detumbling of the spacecraft. This configuration is approximately 0.4kg per torque rod for a total of 1.2kg. The power consumption is minimal at 200mW per torque rod at maximum output. The actual torque rod moment output for this design is 3.0 Am^2 . The design study for torque rod output, weight, and power was based on equation found in reference 2. Furthermore, iterative analysis beyond the graphs presented in this paper discovered a standard ferrite material with $\mu = 800$. This material is easily obtained and thus was used to reproduce the graphs presented.

4.2.1 Design Options

The previous section outlined some sizing options and minimum requirements based on several design decisions that have not been completed. The type of wire used in the design significantly alters the

characteristics of the torque rod. A smaller wire such as 30 gauge is smaller and allows more turns of wire for the same length of torque rod creating a larger output. The larger amount of wire will then consume significantly more power and wire temperature may also become a concern. Larger wire will consume less power, but have a small torquer output.

The actual iron used will alter the torquer output. An iron composition with a higher magnetic permeability will have a larger torque output. The design study was conducted for a material with only a $\mu = 800$ which is a standard ferrite material. This is one of the best ways to improve performance because it has no effect on other design decision, it simply increases output. Irons with higher values of μ may be more expensive. Another concern with the iron is finding material with a linear hysteresis curve. This means the torque rod output will be linear with increasing current. If this is not linear the controller theory will have to be more complex to account for the non-linear behavior. Microcosm or Ithaco may be able to provide insight as to where to obtain desirable iron cores.

Another design decision is the maximum current input allowable. The more input current allowable the higher the output moment per equation 4. For detumbling mode it may be possible to allow even more than 300mA to each torque rod. If this were the case the design may be made smaller. Figure 5 shows the torque rod output at only 150mA.

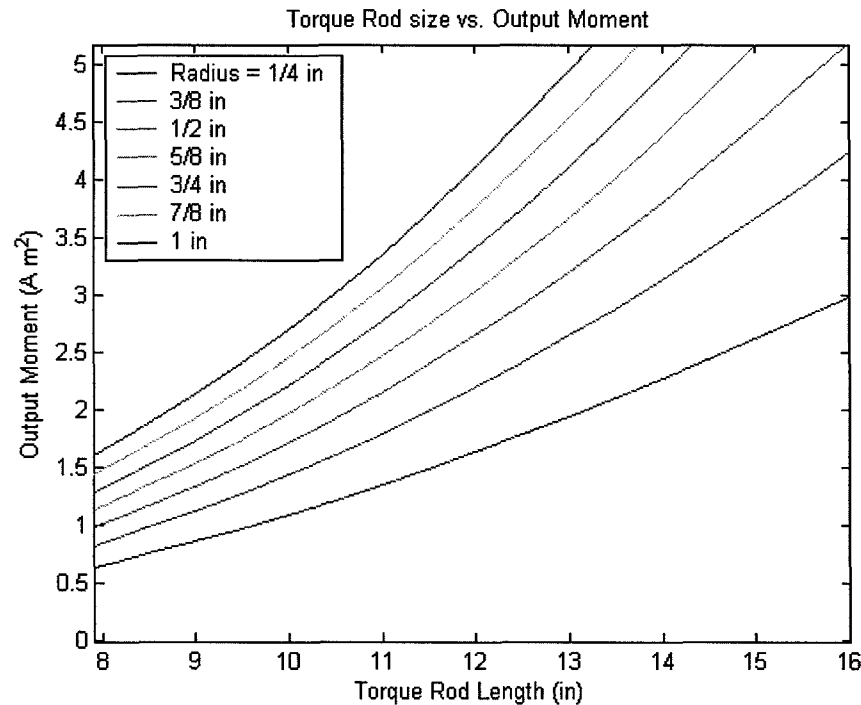


Figure 4-5: Torque Rod output for 150mA input current

The figure shows for a 10 in torque rod and a 150mA input current an output moment of 1.5 Am² may be obtained. This will suffice as a minimum requirement for normal operations.



DINO ADCS Report

DINO-ADCS-RPT-ADCS, Rev. A

Written by:
Brian Roberts

Prepared for:
Nanosat III

Table of Contents

1	Scope.....	4
1.1	Identification.....	4
1.2	Document Maintenance.....	4
1.3	Systems Overview.....	4
1.4	Document Overview.....	4
1.5	Referenced Documents.....	5
2	Sensors.....	5
2.1	Honeywell HMC2003 Magnetometer.....	5
2.2	Analog Devices ADXRS150 Rate Gyroscope.....	6
3	Actuators.....	7
3.1	Magnetic Torque Rod.....	7
4	ADCS Box.....	7
4.1	Rate Gyro.....	8
4.1.1	Circuit Design.....	8
4.1.2	Testing.....	9
4.2	Torque Rod Current Control.....	10
4.2.1	Circuit Design.....	10
4.2.2	Testing.....	11
4.3	Digital Conversion.....	12
4.3.1	Analog to Digital Conversion.....	12
4.3.2	Digital to Analog Conversion.....	12
4.3.3	Conversion Testing.....	12
5	ADC System Integration.....	13
5.1	Testing.....	13

1 Scope

1.1 Identification

This document applies to the DINO project, a project undertaken by the Colorado Space Grant Consortium at the University of Colorado at Boulder. This project is part of the Nanosatellite III Program sponsored by the Air Force Office of Scientific Research (AFOSR), Air Force Research Laboratory (AFRL), Association of Aeronautics and Astronautics (AIAA), and Goddard Space Flight Center (GSFC).

1.2 Document Maintenance

This document falls under the DINO document control requirements as specified under the DINO Configuration Management plan. All changes and updates must be made in accordance with the DINO CM plan.

1.3 Systems Overview

The purpose of the student-led Deployment and Intelligent Nanosatellite Operations (DINO) mission is to determine cloud heights from space, evaluate the performance of intelligent operations, and assess deployment technologies for nanosatellites including a gravity-gradient boom, memory composite hinges, and thin-film solar arrays.

1.4 Document Overview

Attitude determination and control has the primary objective of maintaining the spacecraft's orientation in order to obtain scientific data defined by the mission objectives. The primary mission objectives for the Deployable and Intelligent Nanosatellite Operations, DINO, satellite are mechanical deployments and stereoscopic imaging of cloud formations. An ADC system has been developed to enable these objectives to be met. The system is designed to provide a nominal orientation for deployment of first a gravity-gradient tethered boom followed by deployments of FITS and the CTD panel. The FITS and CTD panel consist of a secondary solar array and a sensor package, not attitude control devices. The system will then provide passive control in the roll and pitch axes through gravity-gradient stabilization and yaw control through a feedback control system. While the system will only be used for yaw control in nominal operations it has been designed to provide three-axis control for s/c detumbling after mission start, prior to the deployment of the gravity-gradient tether.

The ADC system has been designed to provide a simple and effective means of controlling s/c attitude to meet mission objectives. The system will consist of a magnetometer for measurement of the local magnetic field and three single-axis rate gyroscopes for measurement of the s/c rotational rates. These devices will be used with an onboard orbit propagator and magnetic field model yielding the expected local magnetic field. The attitude will be determined through software

algorithms comparing the local sensed magnetic field and expected magnetic field and directly incorporating the s/c rotation rates. The attitude will then be controlled by magnetic torque rods exerting a magnetic dipole moment that interacts with the Earth's magnetic field to provide a torque on the s/c. The torque rods will be controlled by electronics on the ADCS interface board which in turn are controlled by the software control algorithm.

1.5 Referenced Documents

Honeywell HMC2003 Datasheet
Analog Devices ADXRS150EB Datasheet
DINO-ADCS-DWG-SCBD1
DINO-ADCS-DWG-SCBD2
DINO-ADCS-DWG-SCBD3
DINO-ADCS-DWG-SCBD4
DINO-ADCS-DWG-SCBD5
DINO-ADCS-DWG-SCBD6
DINO-ADCS-ASM-TORROD
DINO-ADCS-RPT-MAG

2 Sensors

The sensors associated with the attitude determination are the Honeywell HMC2003 Magnetometer and the Analog Devices ADXRS150EB Rate Gyroscope.

2.1 Honeywell HMC2003 Magnetometer

The Honeywell magnetometer provides local magnetic field sensing data. The output of the magnetometer is three 0.5 – 4.5V analog signals for the x,y, and z components of the magnetic field. These components will be used in attitude determination and also to provide the optimal control of the magnetic torque rods for interaction with Earth's magnetic field sensed by the magnetometer. All other specifications for the Honeywell HMC2003 Magnetometer are shown in the referenced datasheet.

Due to the magnetometer's sensitivity to local magnetic fields it shall be isolated from other electronic equipment. For this reason it will not be located on the attitude board with the rest of the electronic components of the system. Figure 2-1 shows the electrical interface with the magnetometer that shall be built onto a small circuit board.

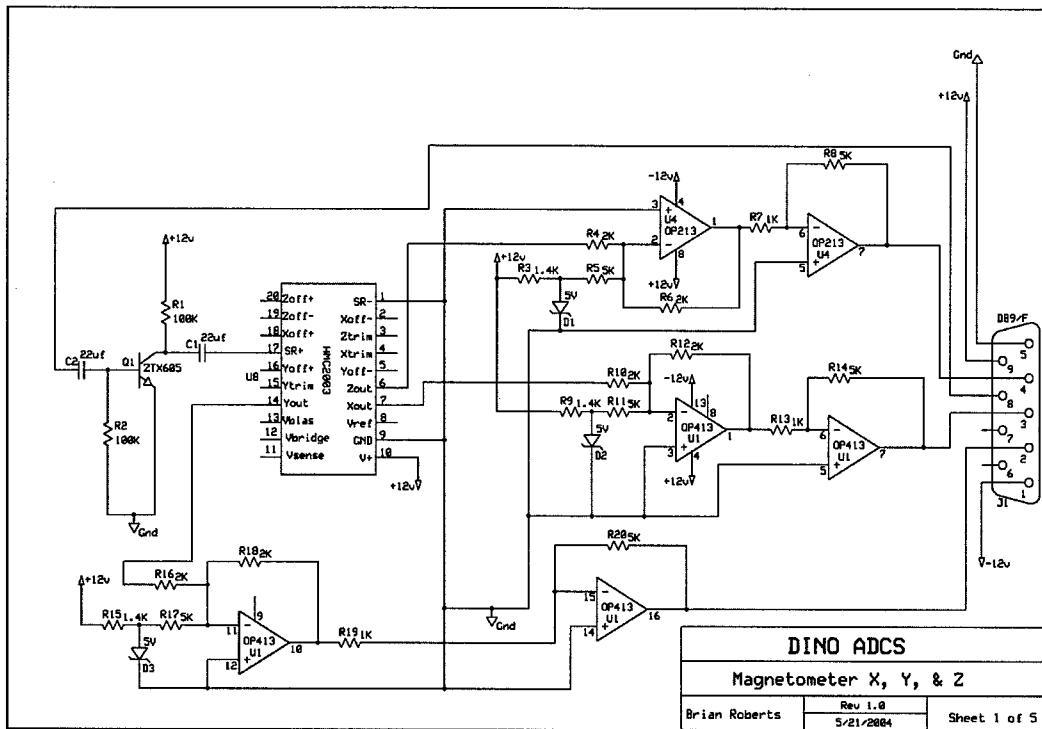


Figure 2-1: Schematic of Magnetometer Circuit.

The Honeywell magnetometer provides output for field ranges of ± 2 Gauss. However, this is significantly greater than the field that shall be sensed in flight. The maximum magnetic field of the Earth is near 0.3 Gauss in either the positive or negative direction depending on the orientation of the s/c. Therefore, a conditioning circuit has been built to focus on the output from 2V to 3V, corresponding to a field range of ± 0.5 Gauss from null field. With the A/D converters in ADC system the accuracy of the magnetometer becomes $244\mu\text{Gauss}$.

2.2 Analog Devices ADXRS150 Rate Gyroscope

The Analog Devices rate gyroscope provides rotation rate measurements along the z-axis of the IC chip. Therefore, three of these single-axis rate gyros are placed in an orthogonal alignment to provide full three-axis rate information. These sensors shall be placed on the attitude board discussed in detail later in the manual. The resolution of the gyro has been tested up to $0.004^\circ/\text{s}$ by the manufacturer. The output of each rate gyro chip is a $0.25\text{V} - 4.75\text{V}$ analog output that is converted to digital data on the interface board. The rate data is directly used by the attitude determination algorithms as s/c rates. All other specifications for the Analog Devices ADXRS150EB Rate Gyroscope are provided in the referenced datasheet.

As with the magnetometer the rate gyro provides output ranges much greater than needed for the system. To provide higher accuracy results a conditioning circuit has been designed to focus on the rate gyro output between 1.75V-3.25V. This yields a rotation range of +/- 60°/s. With the 12-bit A/D converters used by ADC system interface board the accuracy of the rate gyros are 0.0293°/s.

3 Actuators

The only actuators associated with the ADC system are three single-axis magnetic torque rods. The magnetic torque rods provide continuous two-axis control and periodic three-axis control. A full discussion of the magnetic torque rods is included in this section.

3.1 Magnetic Torque Rod

A separate document titled DINO-ADCS-RPT-TQSIZE outlines the methods used to design the magnetic torque rods. A final design was selected based on a large trade study, material availability, and analytical analysis. The magnetic torque rods will be built using a manganese zinc core with a magnetic permeability of 800. The density of the material is much less than that of iron. The cores are wrapped in 28AWG magnet wire. The torque rods will simply have an input of two power lines. The torque rod control circuitry will vary the amount and direction of current through the torque rods to vary the magnetic field produced by the torque rods.

The design calls for three torque rods in an orthogonal reference frame. The torque rods are placed in the s/c at locations most convenient for the structural layout of the s/c and to isolate them as much as possible from electrical equipment. They are placed in the s/c such that the ends of the torque rods are at the sides of the s/c. This will force the largest magnetic fields emanating from the torque rods outside of the s/c rather than into sensitive electronic equipment. The torque rods are built to the specifications of a approximately 12'' length with 1/2'' diameter. The effects upon circuitry within the DINO spacecraft was functionally tested by applying 500mA (160% of maximum current) to the torque rods with the flight computer, camera's, radios, and ADC systems running within 1'' of the torque rods. This configuration did not effect the operation of these circuits; therefore, the placement of the torque rods within the spacecraft is dependant upon the magnetometer only.

4 ADCS Box

The ADCS Box will be the primary center for electronics associated with the ADC system. The ADC system contains circuits for the magnetometer, rate gyros, and torque rod control. The ADCS Box will contain all the electrical circuits and sensors except that of the magnetometer. The magnetometer is isolated away from other electronics.

4.1 Rate Gyro

4.1.1 Circuit Design

The analog devices rate gyros are supplied in an easy to integrate evaluation board package. The package has 20 pins connected inline. **Error! Reference source not found.** 1 shows the circuit design for connection of the rate gyros.

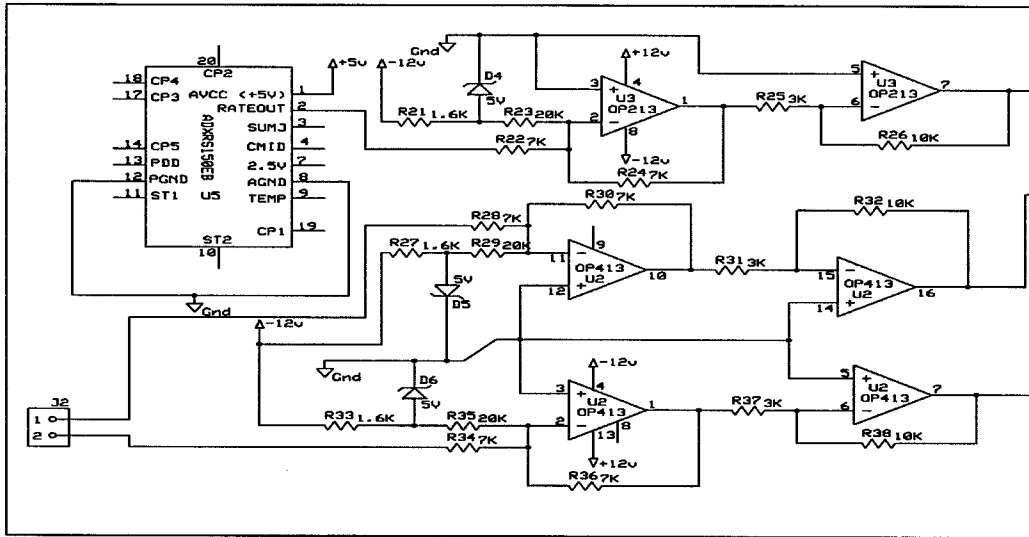


Figure 4-1: Schematic for Rate Gyro Electrical Interface.

The range of the raw rate gyro output with 0.004°/s of resolution allows for 75,000 points of discrete intervals. A 12-bit analog to digital (A/D) conversion allows 4096 discrete intervals which greatly reduces the possible resolution, thereby, reducing the sensing capability of the ADCS system. The expected rates in an orbit are highest at release from the launch vehicle and will most likely be less than 10°/s. Reducing the range of the output to ±60°/s will allow for a higher resolution in the A/D conversion. The number of discrete intervals for maximum resolution is reduced to 30,000 which are not within the range of a 12-bit signal, but does allow for much higher resolution of 0.0293°/s. The signal conditioning was designed such that a change in orbit requirements would allow for a change in the output of the rate gyro circuitry. This would be accomplished by changing the resistance values within the signal conditioning circuitry. The following equations (Eq. 4-1 thru 4-5) are utilized to perform the resistance calculations.

$$V_{out} = R_3 \left(\frac{V_{in}}{R_1} - \frac{5}{R_2} \right) \frac{R_5}{R_4}$$

Eq. 4-1

$$V_{out} = \frac{R_5}{R_4} \left(V_{in} - \frac{5R_3}{R_2} \right)$$

Eq. 4-2

$$I_2 = \frac{5V}{R_2} + 4mA$$

Eq. 4-3

$$R_0 = \frac{5V - 12V}{I_2}$$

Eq. 4-4

$$R_1 = R_3$$

Eq. 4-5

Table 4-1 allows the resistances in the equations to be correlated to the resistors in the actual circuitry for the magnetometer as depicted in the schematic DINO-ADCS-DWG-SCBD2

Table 4-1: Rate Gyro Resistor Matrix

Equation Nomenclature	Circuit Nomenclature	Current Resistance Value
R ₀	R ₂₁ , R ₂₇ , R ₃₃	1.6K
R ₁	R ₂₂ , R ₂₈ , R ₃₄	5.6K
R ₂	R ₂₃ , R ₂₉ , R ₃₅	16K
R ₃	R ₂₄ , R ₃₀ , R ₃₆	5.6K
R ₄	R ₂₅ , R ₃₁ , R ₃₇	3K
R ₅	R ₂₆ , R ₃₂ , R ₃₈	10K

4.1.2 Testing

The rate gyro circuitry was constructed on a "prototyping board" with the corresponding components. A voltmeter was placed in the output of the circuit. Variable power supplies were utilized to simulate the input voltages of the +12VDC, -12VDC, and +5VDC power supplies. The circuit was then rotated in each direction to verify correct response of the rate gyro. The rate gyro was also verified to have insignificant drift by placing it in a stable atmosphere (i.e. not rotating) and taking data for 48 hours. The following figure, Figure 4-2 displays the results of this test.

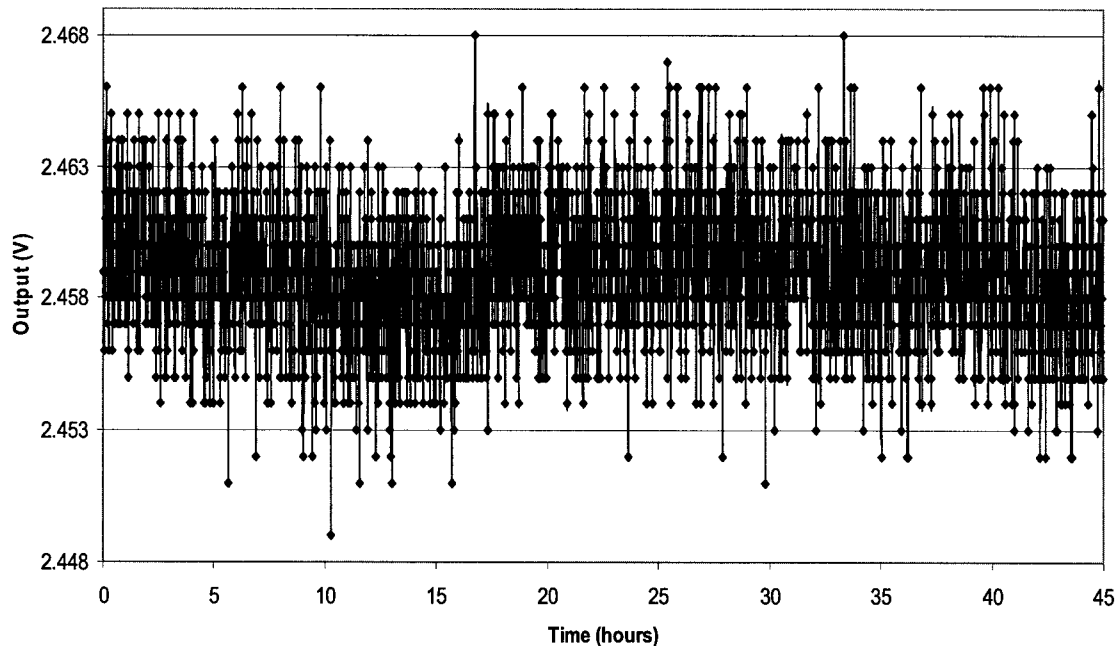


Figure 4-2: Rate Gyro 48hr Test Results

The rate gyro had no drift when average value of the output is taken. The null rate is approximately 2.5VDC and will have to be taken from the individual rate gyros before launch to verify the values in software. This value will also be affected by the signal conditioning circuitry. The circuits were tested individually in the same manner after they were manufactured and populated. After testing, the circuits were functionally tested with the completed ADCS electronics hardware which is addressed in later sections of this document.

4.2 Torque Rod Current Control

4.2.1 Circuit Design

Several requirements are placed upon the attitude electronics by the torque rods.

1. The input current must be supplied in proportional control between 0-300mA.
2. The input current must be capable of being supplied in either direction through the torque rod.
3. The amount and direction of current must be capable of being controlled by the flight computer.

These requirements led to a design shown in **Error! Reference source not found.** The input to the control circuit is an analog voltage and a directional signal. These signals shall be supplied through a Texas Instruments DAC8574 D/A converter from the flight computer.

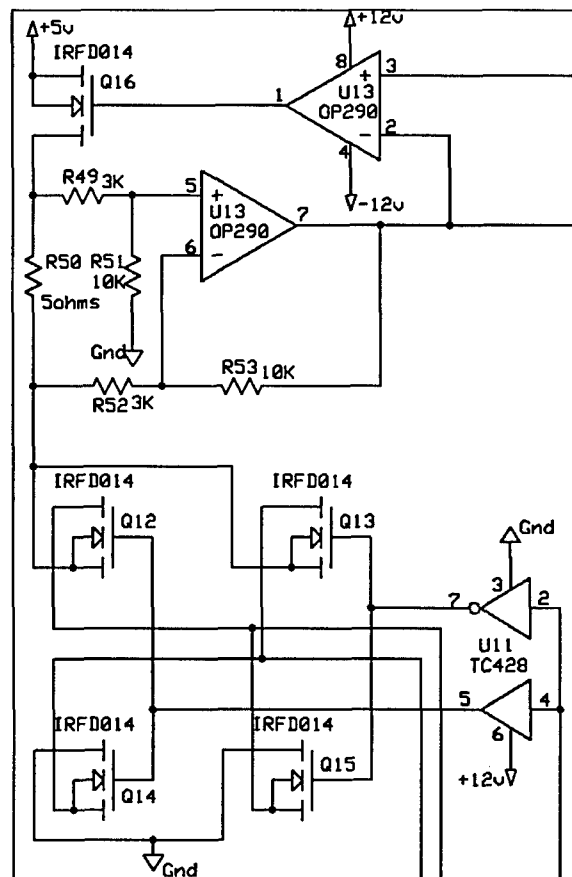


Figure 4-3: Schematic of torque rod control circuit.

The methodology of this circuit is fairly simple. The amount of current to the torque rod may be controlled by varying the input current ($V=IR$). Since there is a set resistance in the R_{bias} and the torque rod, $I=V/R$. Thus, a digital signal from the flight computer to a D/A can supply an output voltage. The output voltage is amplified through the op-amp and thereby supplies the desired current to the torque rods. The direction of current is controlled through the switching MOSFET's. By sending a TTL high/low one of two things occurs. Either both switches Q12 and Q14 are closed or both switches Q13 and Q15 are closed. When Q12 and Q14 are closed the current flows in a positive direction and when Q13 and Q15 are closed current flows in the negative direction. The gates are controlled by the high/low input to an inverting/non inverting amplifier.

4.2.2 Testing

The torque rod control circuitry was constructed on a "prototyping board" with the corresponding components. An ammeter replaced the torque rod in the output of the circuit. Variable power supplies were utilized to simulate the input voltages of the +12VDC, -12VDC, and +5VDC power supplies. An additional variable power supply was then

utilized to simulate the input voltage from the flight computer to control the torque rod current output. The directional input was simulated by connecting to ground and +5VDC on the +5VDC power supply. This test was successful and yielded the expected results of 0-300mA for a 0-5VDC input and the current direction changed with respect to the directional input. The circuits were tested individually in the same manner after they were manufactured and populated. After testing, the circuits were functionally tested with the completed ADCS electronics hardware which is addressed in later sections of this document.

4.3 Digital Conversion

The ADC system contains analog to digital and digital to analog conversion hardware which will enable the flight computer to access information from the sensors and control the actuators from an isolated I2C bus.

4.3.1 Analog to Digital Conversion

The analog to digital (A/D) conversion will be accomplished by the Texas Instruments ADS7828 A/D converter. This is a 12-bit converter with an I2C interface and capable of accepting 8 analog inputs. There are 2 ADS7828 chips in the ADCS Box which accept the rate gyro, torque rod current feedback, and magnetometer inputs. The magnetometer inputs are separated onto the second ADS7828 to enable it to be transferred into the Magnetometer Box if future testing reveals large noise spikes on the magnetometer analog lines from the Magnetometer Box to the ADCS Box. Each of the ADS7828 has the capability to have 4 addresses on the I2C bus enabling one I2C bus to be utilized, minimizing the amount of interface wiring required between the ADC and C&DH systems.

4.3.2 Digital to Analog Conversion

The digital to analog (D/A) conversion will be accomplished by the Texas Instruments DAC8574 D/A converter. This is a 16-bit converter with an I2C interface and capable of converting 4 analog outputs. There are 2 DAC8574 chips in the ADCS Box which output the torque rod current amount, torque rod current direction, and magnetometer reset signal. The DAC8574's each has the capability of 4 I2C addresses which do not correspond to the addresses of the ADS7828. This enables the two ADS7828 and the two DAC8574 to be on the same I2C bus, further minimizing the interface wiring between the ADC and C&DH systems.

4.3.3 Conversion Testing

Each of the A/D and D/A converters was tested individually with the flight computer through testing software. The software was able to access the converters and vary the outputs on the D/A converter and sense changes in input for the A/D converter. The original A/D

converter, ADS1112, was also tested individually. This A/D converter had addressing which corresponded to the addressing of the DAC8574, but had the ability to have 8 addresses. During functional testing of the conversion board it was found that the ADS1112 was not able to handle 3 inputs per chip from 0-5V as originally thought. The ADS1112 was able to handle 2 inputs from 0-5V and 3 inputs from 0-2V; therefore, a design change was made to the ADS7828, which can handle up to 8 inputs from 0 to 5V. The tradeoff was that the ADS1112 is a 16-bit converter whereas the ADS7828 is a 12-bit converter. The ADC system has since been tested as a complete unit and is explained in further sections of this document.

5 ADC System Integration

The ADCS electronics within the ADCS Box were integrated after individually testing each section of the ADC system. The magnetometer electronics were then integrated with the ADCS electronics to ensure the entire ADC system operated properly prior to integration into the DINO electronics.

5.1 Testing

The ADCS electronics were tested as a unit with testing software. The software was an open loop system which allowed the testing operators to change current and direction of the torque rods. The output of the rate gyros and torque rod current feedback were verified to be correct. The testing replaced the torque rods with an ammeter in the same fashion as the individual testing of the torque rod control circuit. All testing involved the connectors for the wiring harness to ensure continuity of the system. The functional test verified the torque rod current could be controlled through software and that the flight computer would be able to take readings from the rate gyros and magnetometer.



Magnetometer Report

DINO-ADCS-RPT-MAG, Rev. A

Written by:
Brian Roberts

Prepared for:
Nanosat III

Table of Contents

1	Scope.....	4
1.1	Identification.....	4
1.2	Document Maintenance.....	4
1.3	Systems Overview.....	4
1.4	Document Overview.....	4
1.5	Referenced Documents.....	4
2	Magnetometer Testing with Torque Rods OFF.....	5
2.1	Setup and Procedure.....	5
2.2	Results.....	5
3	Magnetometer Testing with Torque Rods ON.....	7
3.1	Setup and Procedure.....	7
3.2	Results.....	8
4	Magnetometer Operation.....	9
4.1	Magnetometer Output.....	9
4.1.1	Raw Output.....	10
4.1.2	Signal Conditioning.....	10
4.2	Magnetometer Attitude Sensing.....	11
4.2.1	Orbit Propagation and B-Field.....	11
	Appendix A – List of Acronyms.....	12

1 Scope

1.1 Identification

This document applies to the DINO project, a project undertaken by the Colorado Space Grant Consortium at the University of Colorado at Boulder. This project is part of the Nanosatellite III Program sponsored by the Air Force Office of Scientific Research (AFOSR), Air Force Research Laboratory (AFRL), Association of Aeronautics and Astronautics (AIAA), and Goddard Space Flight Center (GSFC).

1.2 Document Maintenance

This document falls under the DINO document control requirements as specified under the DINO Configuration Management plan. All changes and updates must be made in accordance with the DINO CM plan.

1.3 Systems Overview

The purpose of the student-led Deployment and Intelligent Nanosatellite Operations (DINO) mission is to determine cloud heights from space, evaluate the performance of intelligent operations, and assess deployment technologies for nanosatellites including a gravity-gradient boom, memory composite hinges, and thin-film solar arrays.

1.4 Document Overview

The magnetometers were tested with the torque rods to examine the effect of the torque rods on the sensing ability of the magnetometer. Research into the effects of magnetic material on magnetometer operation revealed that the magnetometer should be placed a minimum of 12in from any magnetic device. This configuration is not possible with the DINO spacecraft; therefore, testing was needed to examine the effect of the torque rods on the magnetometer for placement of the torque rods and magnetometer in the spacecraft. This document describes the procedures used for testing including results and analysis. A requirement for placement of the torque rods 9in away from the magnetometer was created from this testing. The magnetometer signal is conditioned to increase the resolution of the circuitry to that of the actual sensing device. The correlation of this signal to Earth's magnetic field is then utilized for attitude sensing.

1.5 Referenced Documents

HMC2003 Magnetometer Datasheet
DINO-ADCS-PROC-MAGTST
AFRL Internal Cargo Unit Users Guide
DINO-ADCS-DWG-SCBD1
DINO-ADCS-DWG-BLBD1
Geopack-2003

NPSAT1 Magnetic Attitude Control System
 Spacetrack Report No. 3

2 Magnetometer Testing with Torque Rods OFF

2.1 Setup and Procedure

The magnetometer and torque rods were setup per DINO-ADCS-PROC-MAGTST. The outputs were saved in a Microsoft Excel format for data analysis.

2.2 Results

The following figures and tables (figure 2-1, 2, & 3 and table 2-1, 2, & 3) graph the average output of the magnetometer over a period of 0.5-2 seconds for each test: X, Y, Z.

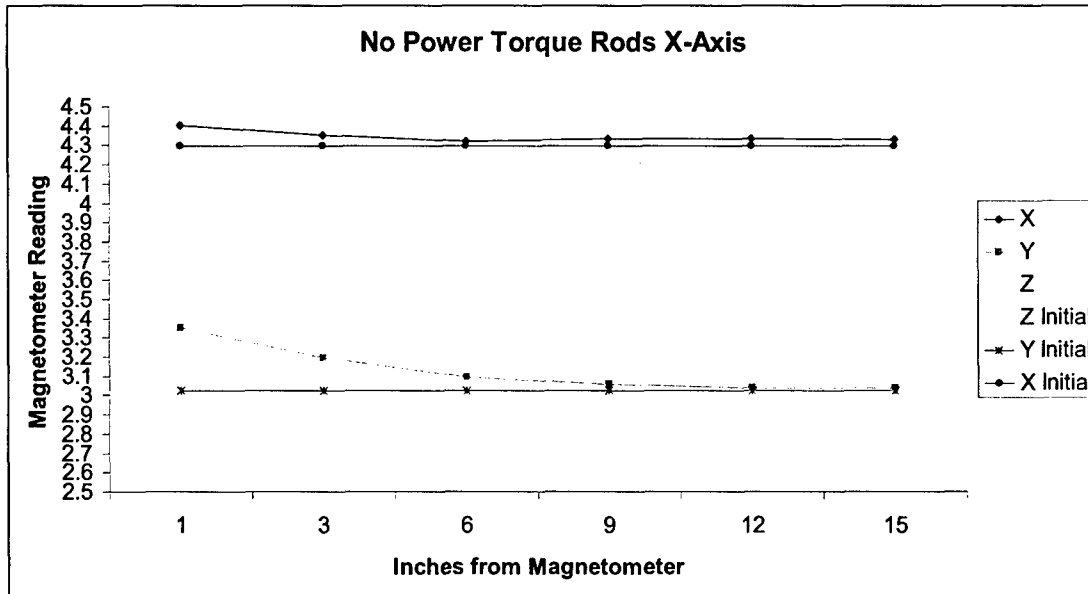


Figure 2-1: Torque Rod in X-Axis

Table 2-1: Torque Rod in X-Axis

Inches	X	Y	Z	Z Initial	Y Initial	X Initial
1	4.402052	3.35285	4.220316	4.209123	3.027012	4.296351
3	4.352215	3.196078	4.215541	4.209123	3.027012	4.296351
6	4.318976	3.095682	4.223722	4.209123	3.027012	4.296351
9	4.333718	3.058824	4.225298	4.209123	3.027012	4.296351
12	4.333333	3.041394	4.22358	4.209123	3.027012	4.296351
15	4.331118	3.039326	4.217791	4.209123	3.027012	4.296351

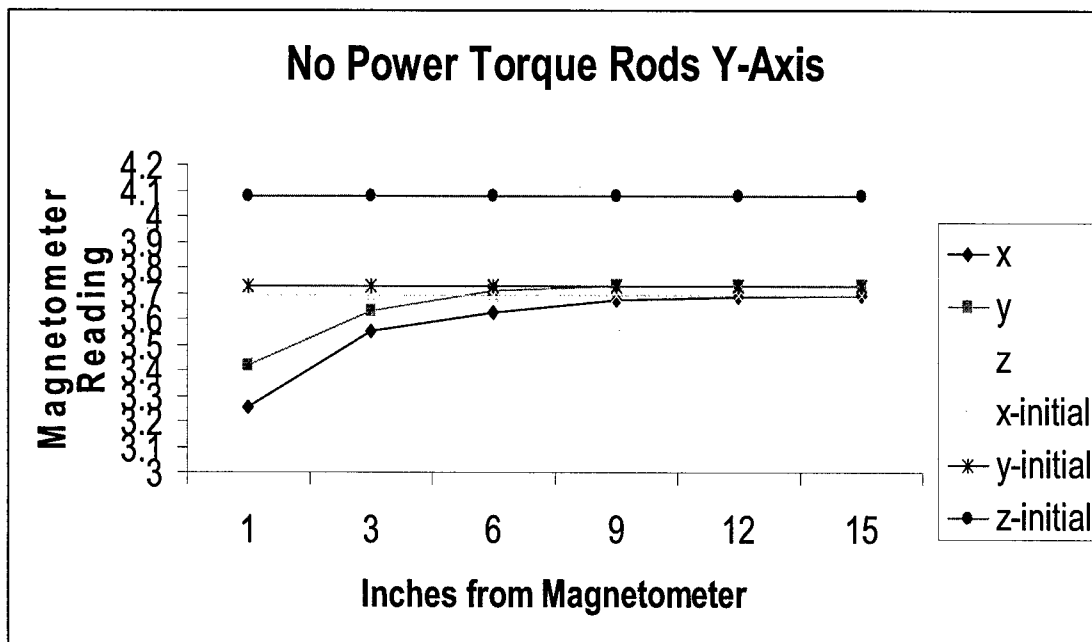


Figure 2-2: Torque Rod in Y-Axis

Table 2-2: Torque Rod in Y-Axis

Inches	x	y	z	x-initial	y-initial	z-initial
1	3.251946	3.418341	4.033967	3.691477	3.725624	4.078165
3	3.54902	3.627451	4.094268	3.691477	3.725624	4.078165
6	3.6257	3.707866	4.107026	3.691477	3.725624	4.078165
9	3.67224	3.726286	4.11277	3.691477	3.725624	4.078165
12	3.686084	3.725681	4.109842	3.691477	3.725624	4.078165
15	3.689387	3.726424	4.099129	3.691477	3.725624	4.078165

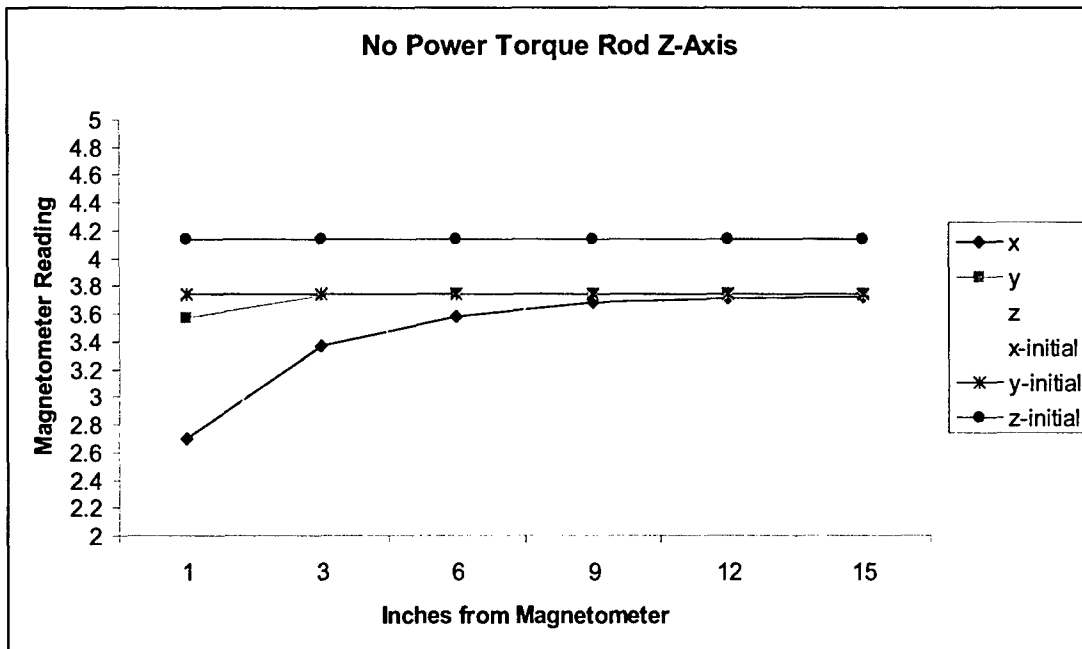


Figure 2-3: Torque Rod in Z-Axis

Table 2-3: Torque Rod in Z-Axis

	x	y	z	x-initial	y-initial	z-initial
1	2.697965	3.572819	2.38885	3.731575	3.744591	4.137931
3	3.366149	3.731073	3.801471	3.731575	3.744591	4.137931
6	3.580599	3.748269	3.120624	3.731575	3.744591	4.137931
9	3.680822	3.745937	4.13348	3.731575	3.744591	4.137931
12	3.708483	3.746699	4.141056	3.731575	3.744591	4.137931
15	3.725267	3.744764	4.143717	3.731575	3.744591	4.137931

The effects of the un-powered torque rod on the magnetometer’s output do not become apparent until the torque rod is 9 inches from the magnetometer. This observation leads to a requirement where the torque rods must be placed a minimum of 9 inches from the magnetometer.

3 Magnetometer Testing with Torque Rods ON

3.1 Setup and Procedure

The magnetometer and torque rods were setup per DINO-ADCS-PROC-MAGTST. The outputs were saved in a Microsoft Excel format for data analysis.

3.2 Results

The following figures and tables (figure 3-1 & 2 and table 3-1 & 2) graph the average output of the magnetometer over a period of 0.5-2 seconds for each test: X & Y.

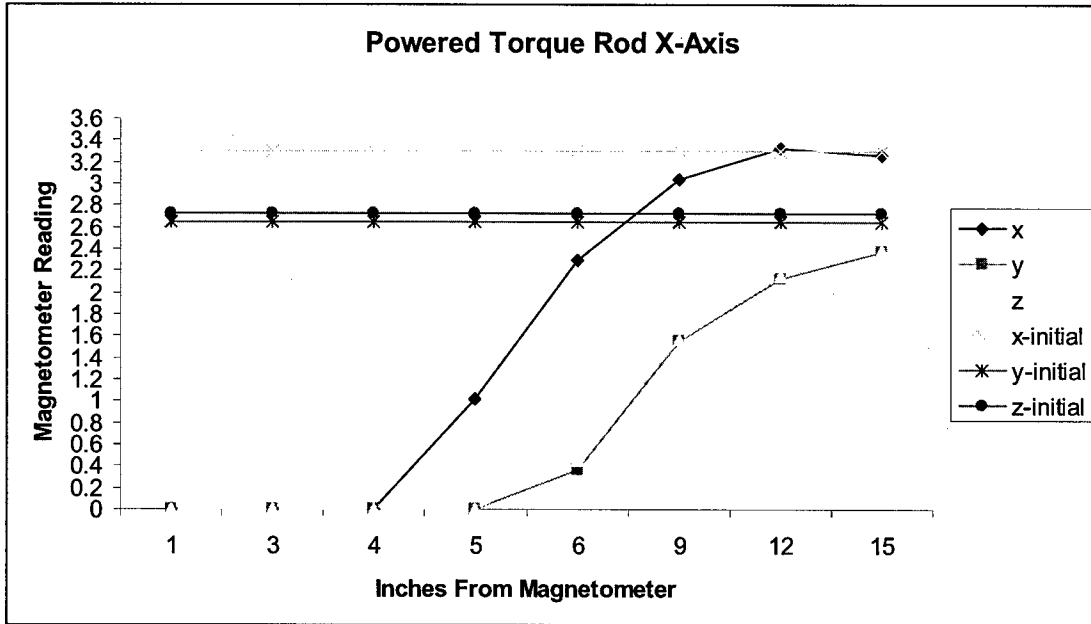


Figure 3-1: Torque Rod in X-Axis

Table 3-1: Torque Rod in X-Axis

Inches	x	y	z	x-initial	y-initial	z-initial
1	0	0	0	3.300135	2.646748	2.73213
3	0	0	0	3.300135	2.646748	2.73213
4	0	0	0	3.300135	2.646748	2.73213
5	1.019876	0	0	3.300135	2.646748	2.73213
6	2.297013	0.371365	0.457297	3.300135	2.646748	2.73213
9	3.04504	1.549117	1.56591	3.300135	2.646748	2.73213
12	3.324673	2.123203	2.158333	3.300135	2.646748	2.73213
15	3.255508	2.37265	2.390237	3.300135	2.646748	2.73213

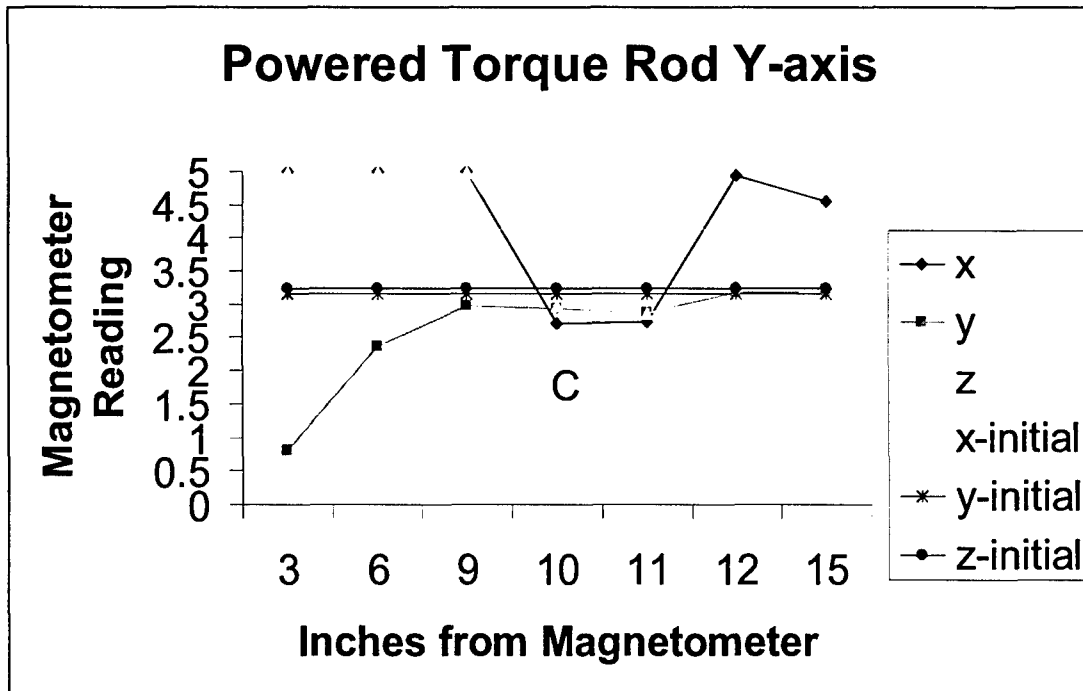


Figure 3-2: Torque Rod in Y-Axis

Table 3-2: Torque Rod in Y-Axis

Inches	x	y	z	x-initial	y-initial	z-initial
3	5	0.801879	5	4.119786	3.155674	3.240404
6	5	2.367195	5	4.119786	3.155674	3.240404
9	5	2.982353	5	4.119786	3.155674	3.240404
10	2.707701	2.927419	2.978495	4.119786	3.155674	3.240404
11	2.734559	2.873652	2.855882	4.119786	3.155674	3.240404
12	4.931373	3.171443	3.269859	4.119786	3.155674	3.240404
15	4.559971	3.192144	3.292609	4.119786	3.155674	3.240404

The magnetometer became saturated in the X and Y Axes very quickly which is seen in the figures and tables above. The effect of the powered torque rods is extremely detrimental to the ability of the magnetometer to detect accurately. This factor will require the software to ignore readings from the magnetometer during torque rod operation, effectively setting a duty cycle requirement for the torque rods. The Z-Axis was not tested due to time requirements and the expected results being confirmed by the X-axis and Y-axis tests, therefore, the Z-axis was not required.

4 Magnetometer Operation

4.1 Magnetometer Output

4.1.1 Raw Output

The Honeywell HMC2003 magnetometer outputs in 3-axes. The output is a range of 0.5-4.5VDC which corresponds to ± 2 gauss. The resolution of the magnetometer is $40\mu\text{gauss}$ with a field sensitivity of 1V/gauss .

4.1.2 Signal Conditioning

The range of the raw magnetometer output with $40\mu\text{gauss}$ of resolution allows for 100,000 points of discrete intervals. A 12-bit analog to digital (A/D) conversion allows 4096 discrete intervals which do not give the highest resolution possible, thereby, reducing the sensing capability of the ADCS system. The expected field in an orbit, which conforms to the specifications given in the *AFRL Internal Cargo Unit Users Guide* section 4.1, is within $\pm 0.5\text{gauss}$ allowing for the signal to be amplified prior to A/D conversion. This reduces the number of discrete intervals for maximum resolution to 25,000 which is not within the range of a 12-bit signal, but greatly increases the resolution of the final signal to $244\mu\text{gauss}$. The signal conditioning was designed such that a change in orbit requirements would allow for a change in the output of the magnetometer circuitry. This would be accomplished by changing the resistance values within the signal conditioning circuitry. The following equations (Eq. 4-1 thru 4-5) are utilized to perform the resistance calculations.

$$V_{out} = R_3 \left(\frac{V_{in}}{R_1} - \frac{5}{R_2} \right) \frac{R_5}{R_4}$$

Eq. 4-1

$$V_{out} = \frac{R_5}{R_4} \left(V_{in} - \frac{5R_3}{R_2} \right)$$

Eq. 4-2

$$I_2 = \frac{5V}{R_2} + 4mA$$

Eq. 4-3

$$R_0 = \frac{5V - 12V}{I_2}$$

Eq. 4-4

$$R_1 = R_3$$

Eq. 4-5

Table 4-1 allows the resistances in the equations to be correlated to the resistors in the actual circuitry for the magnetometer as depicted in the schematic DINO-ADCS-DWG-SCBD1

Table 4-1: Magnetometer Resistor Matrix

Equation Nomenclature	Circuit Nomenclature	Current Resistance Value
R ₀	R ₃ , R ₉ , R ₁₅	1.2K
R ₁	R ₄ , R ₁₀ , R ₁₆	1.2K
R ₂	R ₅ , R ₁₁ , R ₁₇	3K
R ₃	R ₆ , R ₁₂ , R ₁₈	1.2K
R ₄	R ₇ , R ₁₃ , R ₁₉	1.5K
R ₅	R ₈ , R ₁₄ , R ₂₀	7.5K

4.2 Magnetometer Attitude Sensing

4.2.1 Orbit Propagation and B-Field

In order to properly sense the attitude of DINO within the orbit the spacecraft must know its location and the magnetic field in that location. The orbit propagator used on the spacecraft is the SGP4 orbit propagation software. The 3-axis sensing of the magnetometer allows a vector the B-field of the Earth to be sensed. Geopack 2003 then can be utilized with the orbit propagator to compare the actual B-field vector with the expected B-field vector to create an attitude error. Testing of this software architecture was researched in the referenced documentation.



The Workings of the Entire Command and Data Handling System

DINO-CDH-RPT-CDH, Rev. A

Written by:
Martin Winkelman

Prepared for:
Nanosat III

Table of Contents

1	Scope.....	4
1.1	Identification.....	4
1.2	Document Maintenance.....	4
1.3	Systems Overview.....	4
1.4	Document Overview.....	4
1.5	Referenced Documents.....	4
2	System Description.....	4
3	Interfaces.....	4
3.1	Connections to Power System.....	4
3.2	Connections to Tip Mass.....	5
3.3	Connections to Communication System.....	5
3.4	Connections to Thermal Sensors.....	5
3.5	Connections to Mechanisms.....	5
3.6	Connections to Science.....	5
3.7	Connections to Attitude Determination and Control.....	5
4	Hardware.....	5
4.1	Flight Computer.....	5
4.1.1	Arcom Viper	5
4.1.2	Arcom Mercury	5
4.2	Interface Board.....	6
4.3	USB Hub.....	6
5	Testing.....	6
6	Appendix A – List of Acronyms.....	7

1 Scope

1.1 Identification

This document applies to the DINO project, a project undertaken by the Colorado Space Grant Consortium at the University of Colorado at Boulder. This project is part of the Nanosatellite III Program sponsored by the Air Force Office of Scientific Research (AFOSR), Air Force Research Laboratory (AFRL), Association of Aeronautics and Astronautics (AIAA), and Goddard Space Flight Center (GSFC).

1.2 Document Maintenance

This document falls under the DINO document control requirements as specified under the DINO Configuration Management plan. All changes and updates must be made in accordance with the DINO CM plan.

1.3 Systems Overview

The purpose of the student-led Deployment and Intelligent Nanosatellite Operations (DINO) mission is to determine cloud heights from space, evaluate the performance of intelligent operations, and assess deployment technologies for nanosatellites including a gravity-gradient boom, memory composite hinges, and thin-film solar arrays.

1.4 Document Overview

This document describes all the hardware of the Command and Data Handling subsystem.

1.5 Referenced Documents

Command and Data Handling Interface Board – DINO-CDH-RPT-INTBRD
Command and Data Handling USB Hub – DINO-CDH-RPT-HUB
Command and Data Handling Flight Computer – DINO-CDH-RPT-FCOMP
Command and Data Handling Wiring Details – DINO-CDH-RPT-WIRING

2 System Description

The command and data handling subsystem is responsible for storing and running all of the spacecraft's software and controlling all of the other subsystems.

3 Interfaces

Full details for internal wiring and connections to the wiring harness are in the Command and Data Handling Wiring Details (DINO-CDH-RPT-WIRING) document.

3.1 Connections to Power System

- RS-422 to send commands/receive status

- digital output to watchdog timer on power board
- 4 analog inputs from battery thermal sensors
- 5V C&DH power provided by power board

3.2 Connections to Tip Mass

- RS-232 serial connection

3.3 Connections to Communication System

- RS-232 serial to transmit radio
- RS-232 serial to receive radio
- USB to TNC microcontroller

3.4 Connections to Thermal Sensors

- 4 I2C buses

3.5 Connections to Mechanisms

- I2C bus
- 5 digital inputs to monitor deployment status

3.6 Connections to Science

- 2 USB cameras

3.7 Connections to Attitude Determination and Control

- I2C bus

4 Hardware

4.1 Flight Computer

The flight computer is a PC/104 form factor single board computer based on the Intel Xscale CPU. Implementations of the C&DH system are being tested using 2 different computers: the Arcom Viper and the Arcom Mercury. More details on these 2 computers are in the Command and Data Handling Flight Computer (DINO-CDH-RPT-FCOMP) document.

4.1.1 Arcom Viper

The Viper was the first choice for the flight computer before the Mercury became available and has been used in developing hardware and software for the C&DH system. Because this computer has only 2 USB ports, the use of a USB hub will be necessary to connect the Viper to the 4 USB devices used in the satellite.

4.1.2 Arcom Mercury

The Mercury is a new computer from Arcom that features a faster CPU and some upgraded I/O options. It has 4 USB ports, so the USB hub is not needed if this computer is used in the C&DH system. This computer

is the preferred choice for the mission and will be used if it succeeds in testing.

4.2 Interface Board

The Interface Board is used to provide I2C, digital I/O, and analog inputs for the C&DH system and is controlled by digital outputs and a USB connection from the flight computer. It also is used to turn power to the USB hub on and off. More details on the Interface board are in the Command and Data Handling Interface Board (DINO-CDH-RPT-INTBRD) document.

4.3 USB Hub

A modified off the shelf USB hub will be used to provide enough USB ports for the C&DH system if the Arcom Viper is used as the flight computer. This is a powered hub that only operates when it is turned on, and power to this hub can be switched on and off by controls sent to the Interface Board. More details on the hub are in the Command and Data Handling USB Hub (DINO-CDH-RPT-HUB) document.

5 Testing

Initial testing running software on the flight computers with connections to other subsystems, the Interface Board, and the USB hub has been successful. Both flight hardware designs using the Viper and Mercury computers will be built and tested for hardware integration testing.

6 Appendix A – List of Acronyms

CPU Central Processing Unit, the main integrated circuit in a computer system.

C&DH The Command and Data Handling subsystem

GPIO General-purpose input/output.

I2C Inter-Integrated Circuit, a two-wire bidirectional synchronous serial protocol invented by Philips Semiconductors. I2C is used by many small and inexpensive D/A converters, A/D converters, memories, and I/O expansion chips

I/O Input/Output

RAM Random Access Memory

RS-232 A full-duplex asynchronous serial protocol characterized by single wires for receive, transmit, and each flow control signal. Signal values swing between approximately -15 and +15 Volts.

RS-422 A full-duplex asynchronous serial protocol using one twisted pair for transmit and one twisted pair for receive. Signaling is via 5V differential-drive.

USB Universal Serial Bus, the same popular serial interface used by modern personal computers



Command and Data Handling Flight Computer

DINO-CDH-RPT-FCOMP, Rev. A

Written by:
Martin Winkelman

Prepared for:
Nanosat III

Table of Contents

1	Scope.....	4
1.1	Identification.....	4
1.2	Document Maintenance.....	4
1.3	Systems Overview.....	4
1.4	Document Overview.....	4
1.5	Referenced Documents.....	4
2	Description of Flight Computer.....	4
3	Arcom Viper.....	4
3.1	General Description.....	4
3.2	Hardware Specifications.....	5
4	Arcom Mercury.....	6
4.1	General Description.....	6
4.2	Hardware Specifications.....	6
5	Testing.....	7
6	Appendix A – List of Acronyms.....	8

1 Scope

1.1 Identification

This document applies to the DINO project, a project undertaken by the Colorado Space Grant Consortium at the University of Colorado at Boulder. This project is part of the Nanosatellite III Program sponsored by the Air Force Office of Scientific Research (AFOSR), Air Force Research Laboratory (AFRL), Association of Aeronautics and Astronautics (AIAA), and Goddard Space Flight Center (GSFC).

1.2 Document Maintenance

This document falls under the DINO document control requirements as specified under the DINO Configuration Management plan. All changes and updates must be made in accordance with the DINO CM plan.

1.3 Systems Overview

The purpose of the student-led Deployment and Intelligent Nanosatellite Operations (DINO) mission is to determine cloud heights from space, evaluate the performance of intelligent operations, and assess deployment technologies for nanosatellites including a gravity-gradient boom, memory composite hinges, and thin-film solar arrays.

1.4 Document Overview

This document covers the computers used in the Command and Data Handling subsystem that will run the flight software used to control the satellite.

1.5 Referenced Documents

No other documents are referenced.

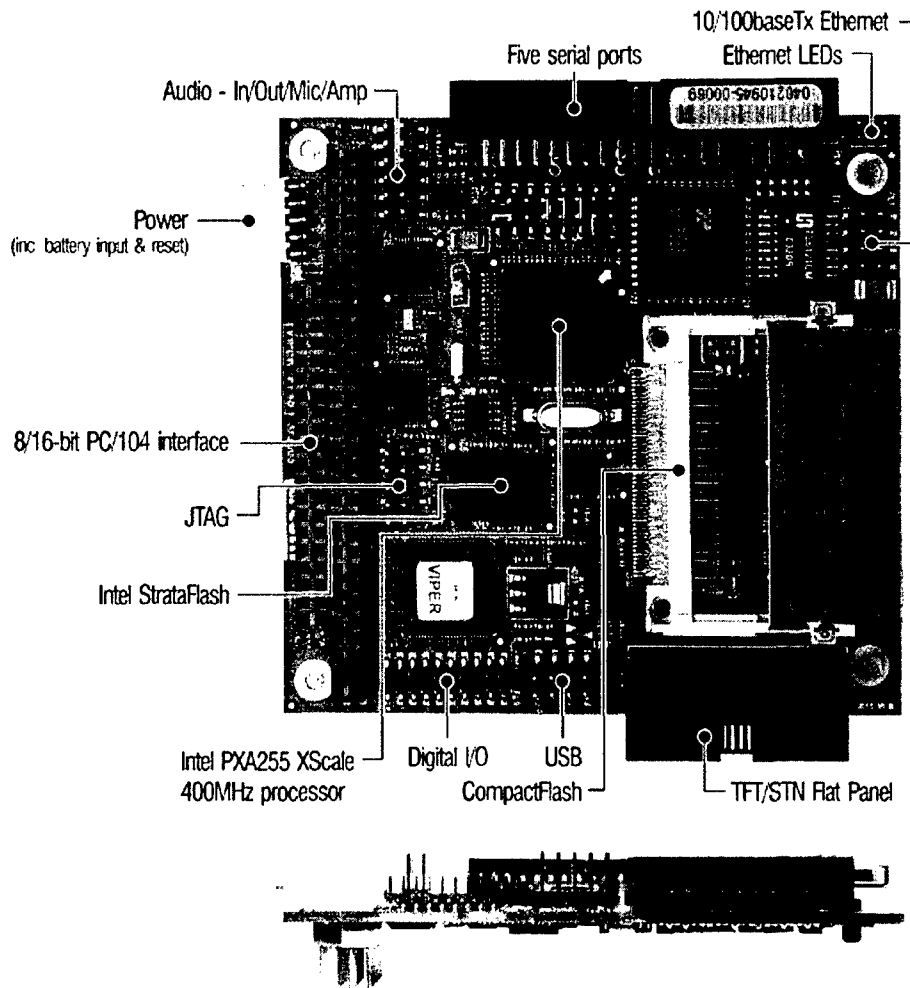
2 Description of Flight Computer

The flight computer has an Intel Xscale CPU running a Linux kernel and the flight software. It interfaces with other hardware in the Command and Data Handling system and other subsystems using RS-232, RS-422, USB, and digital I/O interfaces. There are 2 computers that are being configured and tested for use as the flight computer: the Viper and Mercury, both of which are manufactured by Arcom.

3 Arcom Viper

3.1 General Description

This is a single board computer with a PC/104 form factor based around an Intel Xscale CPU. This computer was the first choice for use as the flight computer before the Mercury became available.



3.2 Hardware Specifications

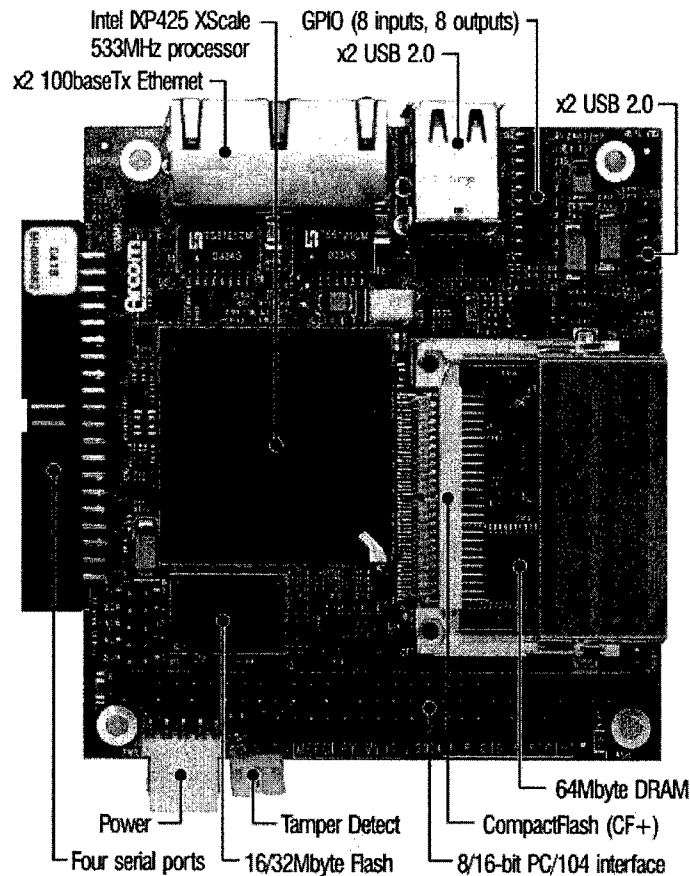
- 400MHz Intel PXA255 XScale CPU
- Redboot firmware with Linux support
- 64 Megabytes of RAM
- 16 Megabytes of Flash memory
- CompactFlash socket
- 2 USB ports
- 100 megabit Ethernet interface
- 4 RS-232 serial ports
- 1 RS-422/RS-485 serial port
- 8 GPIO digital inputs/ 8 GPIO digital outputs

Additional information on this computer can be found at the manufacturer's web site at <http://www.arcom.com/pc104-xscale-viper.htm>

4 Arcom Mercury

4.1 General Description

This is a new PC/104 form factor XScale based computer that was recently introduced by Arcom, and is very similar to the Viper in many ways. It has a faster CPU, and more USB ports. It will be used as the flight computer if all testing using it is successful.



4.2 Hardware Specifications

- 533MHz Intel IXP425 XScale CPU
- Redboot firmware with Linux support
- 64 Megabytes of RAM
- 16 Megabytes of flash memory
- CompactFlash socket
- 4 USB ports
- 2 100 megabit Ethernet interfaces
- 3 RS-232 serial ports
- 1 RS-422/RS-485 serial port
- 8 GPIO digital inputs/ 8 GPIO digital outputs

Additional information on this computer can be found at the manufacturer's web site at <http://www.arcom.com/pc104-ixp425-mercury.htm>

5 Testing

Both computers have run test versions of the flight software, and are being tested for electrical integration. The Viper has been tested more than the Mercury at this point, so it will be used if problems with the Mercury are discovered. If both computers test successfully, the Mercury will be used.

6 Appendix A – List of Acronyms

CPU Central Processing Unit, the main integrated circuit in a computer system.

GPIO General-purpose input/output.

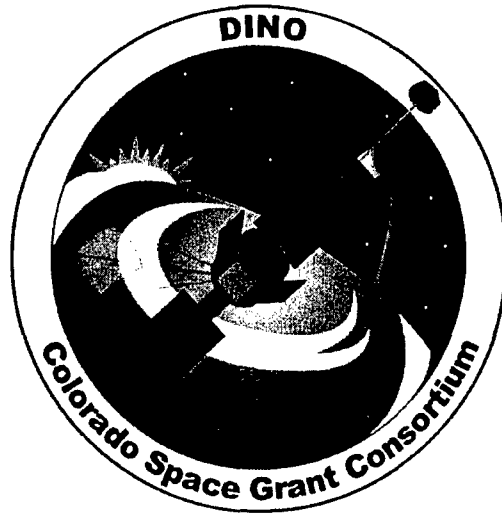
I/O Input/Output

RAM Random Access Memory

RS-232 A full-duplex asynchronous serial protocol characterized by single wires for receive, transmit, and each flow control signal. Signal values swing between approximately -15 and +15 Volts.

RS-422 A full-duplex asynchronous serial protocol using one twisted pair for transmit and one twisted pair for receive. Signaling is via 5V differential-drive.

USB Universal Serial Bus, the same popular serial interface used by modern personal computers



Command and Data Handling USB Hub

DINO-CDH-RPT-HUB, Rev. A

Written by:
Martin Winkelman
Henry Au- \AA ng

Prepared for:
Nanosat III

Table of Contents

1	Scope.....	4
1.1	Identification.....	4
1.2	Document Maintenance.....	4
1.3	Systems Overview.....	4
1.4	Document Overview.....	4
1.5	Referenced Documents.....	4
2	USB Hub Description.....	4
3	USB Hub Modification Procedure.....	4
3.1	Parts and Requirements.....	4
3.2	Warnings.....	5
3.3	Procedure.....	5
3.4	Diagrams.....	6
4	Testing the Modified USB Hub.....	7
	Appendix A – List of Acronyms.....	8
	Appendix B – Top view of USB Hub Connectors.....	9

1 Scope

1.1 Identification

This document applies to the DINO project, a project undertaken by the Colorado Space Grant Consortium at the University of Colorado at Boulder. This project is part of the Nanosatellite III Program sponsored by the Air Force Office of Scientific Research (AFOSR), Air Force Research Laboratory (AFRL), Association of Aeronautics and Astronautics (AIAA), and Goddard Space Flight Center (GSFC).

1.2 Document Maintenance

This document falls under the DINO document control requirements as specified under the DINO Configuration Management plan. All changes and updates must be made in accordance with the DINO CM plan.

1.3 Systems Overview

The purpose of the student-led Deployment and Intelligent Nanosatellite Operations (DINO) mission is to determine cloud heights from space, evaluate the performance of intelligent operations, and assess deployment technologies for nanosatellites including a gravity-gradient boom, memory composite hinges, and thin-film solar arrays.

1.4 Document Overview

This document describes the modification, use and testing of the USB hub used by the Command and Data Handling subsystem.

1.5 Referenced Documents

No other documents are referenced.

2 USB Hub Description

A modified commercial off the shelf USB hub is used with the Arcom Viper flight computer because this computer has 2 USB ports, and the total number of USB devices that need to interface with the computer is 4.

3 USB Hub Modification Procedure

3.1 Parts and Requirements

Parts:	Model Number:
1 Linksys USB 2.0 4-Port Hub	USB2HUB4
2 120F Solid Tantalum Capacitors SMD – min 10V rating	---
5 4.7F Solid Tantalum Capacitors SMD – min 10V rating	---
4 120F Solid Tantalum Capacitors SMD – min 10V rating	---
20 Header Pins	---

Requires:

DC 5V, 2.4A for the power connector
DC 5V, 500mA max for the USB ports

Tools Needed:

Fine flathead Screwdriver
Needle nose Pliers
Cutting Tool (small in size, but can cut through metal)
Soldering iron with conic tip
Solder

3.2 Warnings

1. Work in a static-area environment.
2. When modifying board, be extra careful as the other components of the board may be easily knocked off.

3.3 Procedure

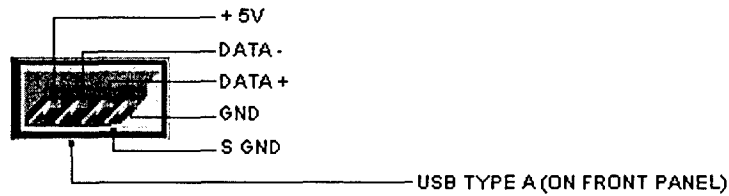
1. Acquire the USB Hub and pry off the sticker that reads "ProConnect ® USB 4-Port Hub USB 2.0."
2. Remove the front piece of black plastic that covers the LEDs with the words: POWER 4 3 2 1."
3. Use the fine flathead screwdriver and wedge it into the slit on the side of the cover. It is recommended to place the screwdriver closer to the front of the hub as the bracket is there.
4. Apply enough upward force until the side breaks open. Do the same to the other side.
5. Remove the hub from its housing.
6. Use the pliers and grab onto the housing of the green LEDs. Apply a rocking left and right motion until the LEDs and its housing are detached.
7. When looking at the left half of the USB connector, it has a "C" shaped metal housing. Take the pliers and grab onto the bottom portion of the "C" and bend it to create a "S." Do the same for the other half.
8. Lift the metal upward so that it is perpendicular to the board and using the pliers on the metal, apply a rocking motion on it until the metal snaps off the board.
9. Repeat steps 7 and 8 for the rest of the USB connectors.
10. After the metal housing has been removed, use the pliers and grab onto the plastic portion of the USB connector. Raise this plastic upwards until it is perpendicular to the board and use the cutting tool and cut into the plastic until it is removed. Repeat for the other 3 connectors.
11. Use the cutting tool and remove the Type-B USB connector.
12. Use the cutting tool and remove the power housing.
13. To remove the capacitors: use the pliers and grab onto the casing on the electrolytic capacitor and keep twisting it while forcing it up until it comes off.

14. Using a soldering iron, remove the extra metal in the PCB for the 4 USB pins. Do this for the 5 USB ports.
15. Replace with 4 headers each and solder them in with the long end facing up.
16. On the bottom of the board, solder the tantalum capacitors to the extra wire sticking out of the PCB.
 C18, C19 – 100µF
 C14, C37, C23, C31, C20 – 4.7µF
 C11, C15, C9, C7 – 120µF
17. Clip off any excess pins and wires if exists.

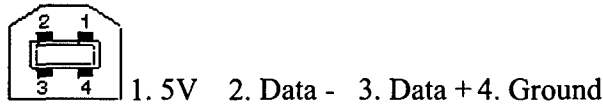
3.4 Diagrams

USB Pin assignment:

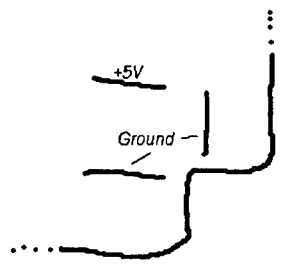
Type A:



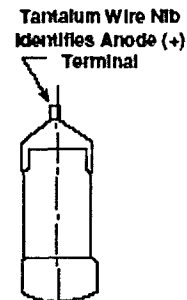
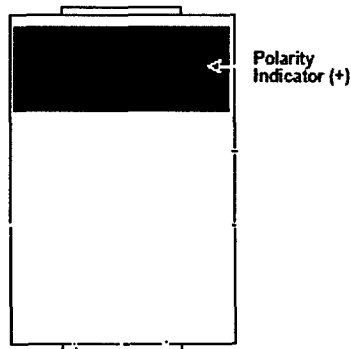
Type B:



Power:



Capacitors:



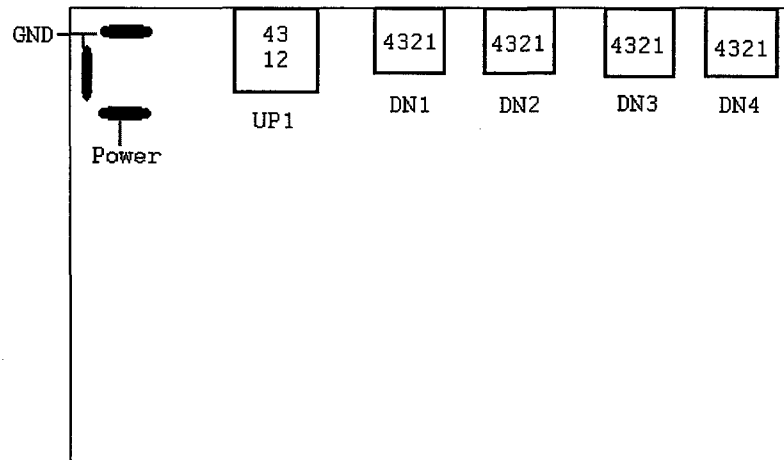
4 Testing the Modified USB Hub

The modified hub has been tested with various USB devices (such as the cameras from the Science system) using connections where power is drawn from the hub, and also when power is provided to USB devices from a separate source, and will work either way. This hub is not self powered and will only work when 5 volts is supplied to the power connector.

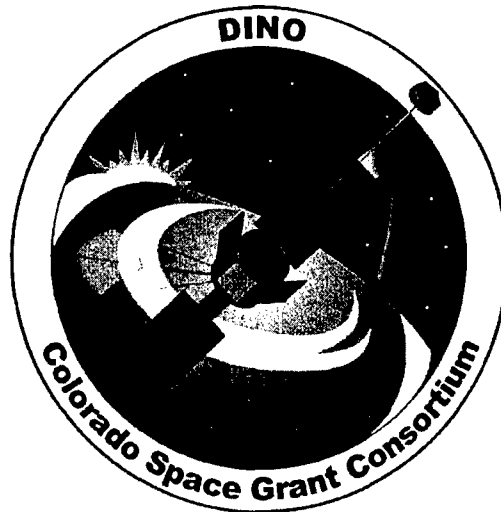
Appendix A – List of Acronyms

USB Universal Serial Bus, the same popular serial interface used by modern personal computers

Appendix B – Top view of USB Hub Connectors



USB Hub top view



Command and Data Handling Interface Board

DINO-CDH-RPT-INTBRD, Rev. A

Written by:
Martin Winkelman

Prepared for:
Nanosat III

Table of Contents

1	Scope.....	4
1.1	Identification.....	4
1.2	Document Maintenance.....	4
1.3	Systems Overview.....	4
1.4	Document Overview.....	4
1.5	Referenced Documents.....	4
2	Reasons for Interface Board Design.....	5
2.1	The Need for Additional Interfaces.....	5
2.2	Off the Shelf Hardware vs. Custom Designed Hardware.....	5
3	Hardware on the Interface Board.....	6
3.1	PIC Microcontroller.....	6
3.2	Digital Line Driver.....	6
3.3	Thermal Sensor.....	6
3.4	Power Regulators.....	6
3.5	Power Switch.....	7
	Appendix A – List of Acronyms.....	8
	Appendix B – Schematic of Interface Board.....	9

1 Scope

1.1 Identification

This document applies to the DINO project, a project undertaken by the Colorado Space Grant Consortium at the University of Colorado at Boulder. This project is part of the Nanosatellite III Program sponsored by the Air Force Office of Scientific Research (AFOSR), Air Force Research Laboratory (AFRL), Association of Aeronautics and Astronautics (AIAA), and Goddard Space Flight Center (GSFC).

1.2 Document Maintenance

This document falls under the DINO document control requirements as specified under the DINO Configuration Management plan. All changes and updates must be made in accordance with the DINO CM plan.

1.3 Systems Overview

The purpose of the student-led Deployment and Intelligent Nanosatellite Operations (DINO) mission is to determine cloud heights from space, evaluate the performance of intelligent operations, and assess deployment technologies for nanosatellites including a gravity-gradient boom, memory composite hinges, and thin-film solar arrays.

1.4 Document Overview

This document describes the Interface Board, which is connected to the flight computer to provide additional analog and digital inputs and outputs used to interface with other subsystems.

1.5 Referenced Documents

The Report on Microcontrollers (DINO-SW-RPT-MICROS) is referenced in this document.

2 Reasons for Interface Board Design

2.1 The Need for Additional Interfaces

The flight computer has multiple serial ports, USB ports and digital GPIO lines, but all of this is not enough to interface with all other subsystems on the satellite without adding additional hardware. An early version of the interface requirements list demonstrates this:

System	Digital Out	Digital In	Analog Out	Analog In
ADCS	3	0	3	9
Comm	0	0	0	0
Power	1	0	0	0
Mech	0	2	0	11 or 17
Science	1	1	0	0 + 2x USB
Thermal	0	0	0	30
Tip Mass	0	0	0	0
TOTALS	4	3	3	50 or 56

2.2 Off the Shelf Hardware vs. Custom Designed Hardware

Earlier revisions of the C&DH subsystem design involved use of a commercial off the shelf interface board connected to the flight computer using the PC/104 bus. This approach had to be abandoned when it was determined that a custom design would be simpler to implement for multiple reasons.

The primary reason use of an off the shelf interface board was abandoned is the limited support for these commercial boards for the CPU and Operating System used on the flight computer. The flight computer uses an Intel Xscale CPU and runs the Linux Operating System. Some vendors only released binary Linux drivers for their boards and did not make source code available, with no support for the Xscale CPU. Even with source code available, attempts to port x86 based drivers to work with the Xscale based flight computer were not initially successful. It became apparent that it would be simpler to implement a custom hardware solution than to writing or porting a driver for a commercial board.

The interface board is based on the RCPOD design, which had been used successfully in previous projects by members of the Software team. This design uses a Microchip PIC16C765 microcontroller which interfaces to the flight computer using USB and provides several analog and digital inputs and outputs. The RCPOD firmware also allows the digital I/O to be configured to be used as I2C bus connections through its driver software. Use of the I2C bus drastically reduces the total number of wires needed to interface with other systems when compared with earlier designs that used discrete analog and digital lines. More details on the RCPOD hardware and software features are in the Report on Microcontrollers (DINO-SW-RPT-MICROS) document.

3 Hardware on the Interface Board

The PIC16C765 microcontroller is not the only integrated circuit on this board. There is also a thermal sensor, a digital line driver, 2 power regulators, and a power switch.

3.1 PIC Microcontroller

The PIC16C765 microcontroller using RCPOD firmware is controlled and powered by its USB connection to the flight computer. It provides digital GPIO and I2C interfaces, as well as 8 bit analog inputs. The reset line for the microcontroller is connected to digital output 5 from the flight computer and must be driven high to enable the microcontroller. This line is connected to a pulldown resistor going to ground so the microcontroller will be held in a reset state if the digital output from the flight computer is not enabled and being driven high.

3.2 Digital Line Driver

A 74HCT244 line driver is used to expand the I2C clock output from pin RB6 (labeled SCL in the schematic) on the PIC16C765 to be used as the clock for all I2C buses. Using a line driver keeps more digital I/O pins on the PIC available, while preventing a short on one of the I2C clock lines from disabling all I2C buses. To enable the outputs for the line driver, pin RB7 on the PIC16C765 (labeled SCL_{EN} in the schematic) must be driven low. A pullup resistor is connected to the output enable lines, so output is disabled by default if the output from the PIC is not enabled and driven low.

3.3 Thermal Sensor

A surface mount Microchip TC74 I2C thermal sensor is soldered to the Interface Board and provides temperature readings for the C&DH subsystem. It is connected to I2C Thermal Bus 4.

3.4 Power Regulators

A pair of Maxim 8867 power regulators are used to switch power to the analog and I2C thermal sensors on and off. They also limit the amount of current that would be drawn from the I/O board if there is a short circuit on these power buses. The enable inputs for these power regulators are connected to pulldown resistors so that the power outputs are disabled unless the digital outputs from the flight computer are enabled and driven high. The power to the analog thermal sensors is controlled by digital output 7 from the flight computer, and the power to the I2C thermal sensors is controlled by digital output 6 from the flight computer.

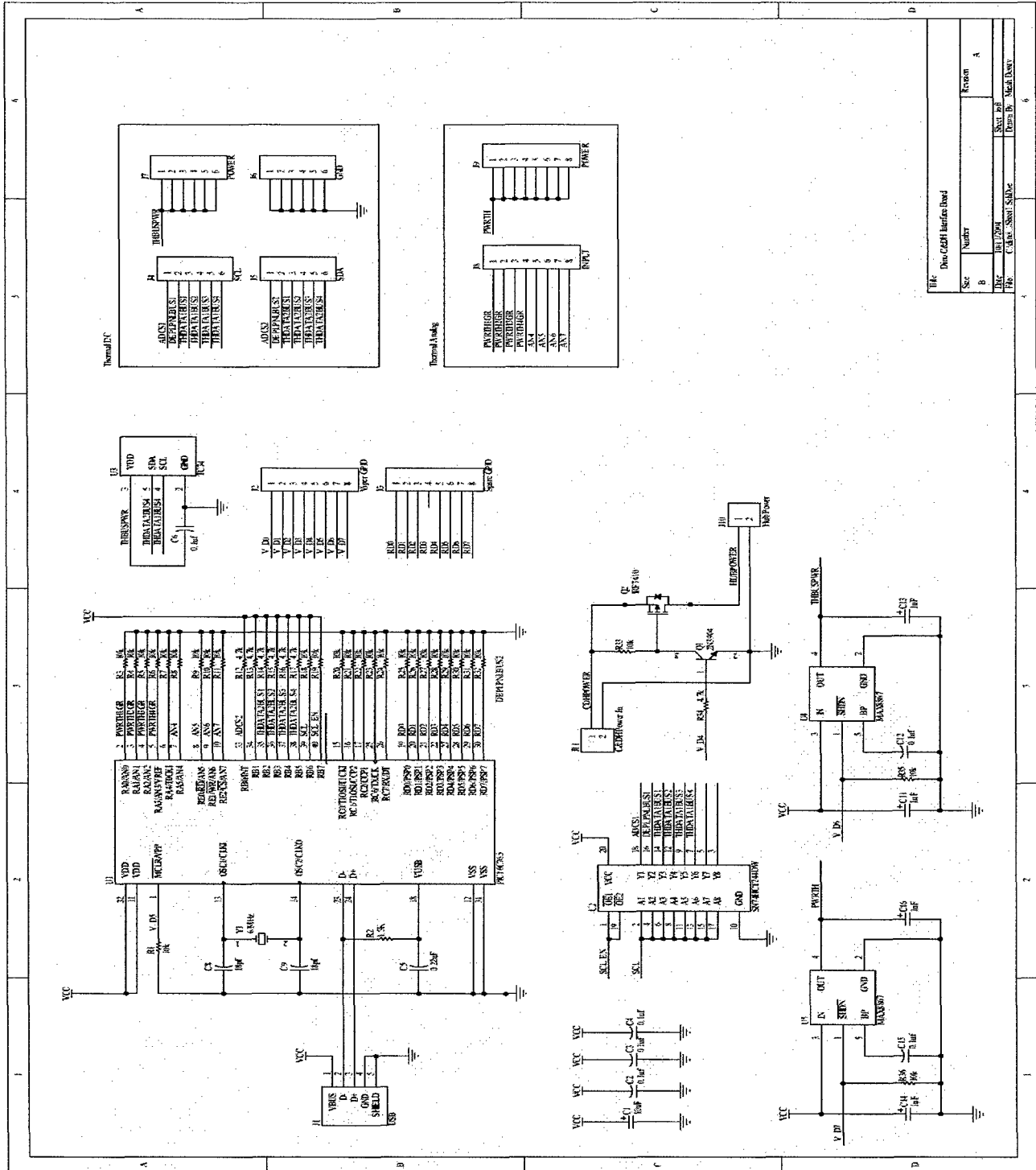
3.5 Power Switch

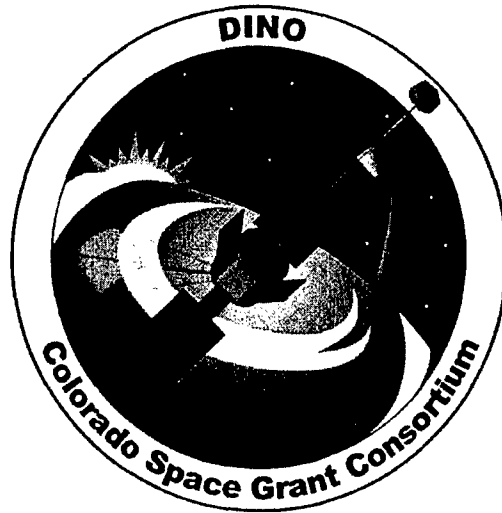
An IRF7410 MOSFET and a 2N3904 BT act as a high current power switch that can be used to switch power to a device connected to the C&DH power bus on and off. This switch circuit is connected to digital output 4 of the flight computer, and must be driven high to turn power on.

Appendix A – List of Acronyms

BJT	Bipolar Junction Transistor, a popular category of transistors that act as current amplifiers
C&DH	The Command and Data Handling subsystem
CPU	Central Processing Unit, the main integrated circuit in a computer system.
GPIO	General-purpose input/output.
I2C	Inter-Integrated Circuit, a two-wire bidirectional synchronous serial protocol invented by Philips Semiconductors. I2C is used by many small and inexpensive D/A converters, A/D converters, memories, and I/O expansion chips
I/O	Input/Output
MOSFET	Metal Oxide Semiconductor Field Effect Transistor, a transistor technology that performs much better at power switching applications than typical BJTs.
USB	Universal Serial Bus, the same popular serial interface used by modern personal computers

Appendix B – Schematic of Interface Board





Terminal Node Controller

DINO-COMM-RPT-TNC, Rev. A

Written by:
Matt Freeman
Bill Bixler

Prepared for:
DINO

Table of Contents

1	Scope.....	4
1.1	Identification.....	4
1.2	Document Maintenance.....	4
1.3	Systems Overview.....	4
1.4	Document Overview.....	4
1.5	Referenced Documents.....	4
2	TNC Specification.....	4
3	TNC Modifications.....	5
4	TNC Interface.....	5
5	TNC Testing.....	5
	Appendix A – List of Acronyms.....	6

1 Scope

1.1 Identification

This document applies to the DINO project, a project undertaken by the Colorado Space Grant Consortium at the University of Colorado at Boulder. This project is part of the Nanosatellite III Program sponsored by the Air Force Office of Scientific Research (AFOSR), Air Force Research Laboratory (AFRL), Association of Aeronautics and Astronautics (AIAA), and Goddard Space Flight Center (GSFC).

1.2 Document Maintenance

This document falls under the DINO document control requirements as specified under the DINO Configuration Management plan. All changes and updates must be made in accordance with the DINO CM plan.

1.3 Systems Overview

The purpose of the student-led Deployment and Intelligent Nanosatellite Operations (DINO) mission is to determine cloud heights from space, evaluate the performance of intelligent operations, and assess deployment technologies for nanosatellites including a gravity-gradient boom, memory composite hinges, and thin-film solar arrays.

1.4 Document Overview

This document covers the reason for choosing the BP-96A packet modem for DINO's communication system, and how we integrated it to the radios and flight computer.

1.5 Referenced Documents

BayPac of Tigertronics (1997). *BayPac BP-96A Packet Modem* 12-03-04
<http://www.tigertronics.com/files/bp96aman.pdf>

Micro Controller Documentation (2004). DINO-SW-RPT-MICROS

2 TNC Specification

The TNC specifications :

Compatibility: G3RUH 9600 baud DFM

PAR9600 / PICPAR / BP-96

Computer Interface: Centronics Parallel Port

Power: Computer Parallel Port (5ma) or external power source of 8 to 14 volts @0m a

Signals: PTT (active low) 75ma @2v (MAX).

Rx Input 300mv p-p (nom)

Tx Output 0 - 3v p-p

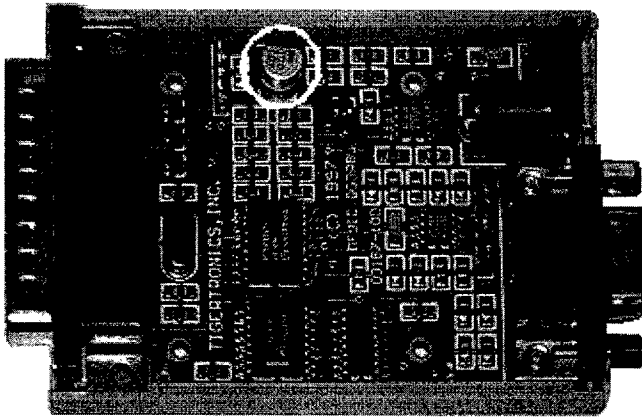
Connectors: Parallel Port - DB-25M

Radio Port - DB-9F
Power - 5.5 x 2.1 mm (Center)
Size: 7/8" H x 2-1/4" W x 3" D
Case: Molded ABS - Gray/White
Construction: Surface Mount Technology (SMT)

3 TNC Modifications

TNC modifications:

Replace the only electrolytic capacitor on the TNC with a tantalum capacitor (82E).



4 TNC Interface

See the Micro Controller Documentation (DINO-SW-RPT-MICROS).

5 TNC Testing

The TNC's have tested to be fully functional with the microcontroller board. For information about testing the TNC/Microcontroller board unit, refer to the Micro Controller Documentation (DINO-SW-RPT-MICROS).

Appendix A – List of Acronyms

TNC – Terminal Node Controller



The Boom Braking Box/Slowdown Mechanism

DINO-MECH-RPT-BOOM, Rev. A

Written by:
M. Wilson

Prepared for:
Nanosat III

Table of Contents

1	Scope.....	4
1.1	Identification.....	4
1.2	Document Maintenance.....	4
1.3	Systems Overview.....	4
1.4	Document Overview.....	4
1.5	Referenced Documents.....	4
2	Boom Components.....	5
3	Boom Assembly and Mounting Procedures.....	6
3.1	Gear Sub-assembly.....	6
3.2	Box assembly.....	6
3.3	Mounting Procedures.....	7
	Appendix A – List of Acronyms.....	8

1 Scope

1.1 Identification

This document applies to the DINO project, a project undertaken by the Colorado Space Grant Consortium at the University of Colorado at Boulder. This project is part of the Nanosatellite III Program sponsored by the Air Force Office of Scientific Research (AFOSR), Air Force Research Laboratory (AFRL), Association of Aeronautics and Astronautics (AIAA), and Goddard Space Flight Center (GSFC).

1.2 Document Maintenance

This document falls under the DINO document control requirements as specified under the DINO Configuration Management plan. All changes and updates must be made in accordance with the DINO CM plan.

1.3 Systems Overview

The purpose of the student-led Deployment and Intelligent Nanosatellite Operations (DINO) mission is to determine cloud heights from space, evaluate the performance of intelligent operations, and assess deployment technologies for nanosatellites including a gravity-gradient boom, memory composite hinges, and thin-film solar arrays.

1.4 Document Overview

This document pertains to the boom braking box which is intended to be a slowdown mechanism for the deployed Tip Mass. The boom braking box is partially housed within the Tip Mass, and pieces of tape measure material are wound inside the box – specifically, clamped between two mated spindles. The boom braking box is supposed to be set in motion by the activation of the Lightband. Sheer momentum keeps the Tip Mass moving and the interaction between gears housed within the box give it the ability to slowly wind down which should adequately decelerate the whole structure.

1.5 Referenced Documents

The following is a list of all documents related to the boom braking box design and construction. Please note: the nomenclature is of the form MissionName-MissionSubsystem(Mechanisms)-DocumentType(Drawing)-ComponentName.

DINO-MECH-DWG-CNTPAN
DINO-MECH-DWG-BXSIDE
DINO-MECH-DWG-INSPIN
DINO-MECH-DWG-OUTSPIN
DINO-MECH-DWG-LGGEAR
DINO-MECH-DWG-GSPOOL
DINO-MECH-DWG-DRSHFT

DINO-MECH-DWG-SHFTMT
DINO-MECH-DWG-RATCHET
DINO-MECH-DWG-SPROD
DINO-MECH-DWG-RPAWL
DINO-MECH-DWG-LPAWL
DINO-MECH-DWG-PINGUI
DINO-MECH-DWG-RODGUI
DINO-MECH-DWG-ADBK
DINO-MECH-DWG-SCRSR
DINO-MECH-DWG-OUTPAN
DINO-MECH-DWG-TGUIDEL
DINO-MECH-DWG-TGUIDER
DINO-MECH-DWG-SPACER
DINO-MECH-DWG-CENTGUI
DINO-MECH-DWG-INNGUI
DINO-MECH-DWG-OUTGUI
DINO-MECH-DWG-ROLLER
DINO-MECH-ASM-BBBOX
DINO-MECH-ASM-GSETR
DINO-MECH-ASM-GSETL

2 Boom Components

The following is a list of all parts encompassing the boom braking box assembly and mounting components

DINO-MECH-DWG-CNTPAN: Central panel
DINO-MECH-DWG-BXSIDE: Open box side panel (2)
DINO-MECH-DWG-INSPIN: Inner spindle (2)
DINO-MECH-DWG-OUTSPIN: Outer spindle (2)
DINO-MECH-DWG-LGGEAR: Large gear (2)
DINO-MECH-DWG-GSPOOL: Gear mount spool (4)
DINO-MECH-DWG-DRSHFT: Drive shaft (2)
DINO-MECH-DWG-SHFTMT: Shaft mount (2)
DINO-MECH-DWG-RATCHET: Ratchet gear (2)
DINO-MECH-DWG-SPROD: Spring rod (2)
DINO-MECH-DWG-RPAWL: "Right" pawl
DINO-MECH-DWG-LPAWL: "Left" pawl
DINO-MECH-DWG-PINGUI: Right side rod guide for right pawl
DINO-MECH-DWG-RODGUI: Left side rod guide for left pawl
DINO-MECH-DWG-ADBK: Sp ring adjustment bracket
DINO-MECH-DWG-SCRSR: Screw for spring adjustment
DINO-MECH-DWG-OUTPAN: Outer panel for Boom breaking box
DINO-MECH-DWG-TGUIDEL: Left tape measure guide
DINO-MECH-DWG-TGUIDER: Right tape measure guide
DINO-MECH-DWG-SPACER: Outer panel spacer
DINO-MECH-DWG-CENTGUI: Center tape measure guide

DINO-MECH-DWG-INNGUI: Inner tape measure guide (center)
DINO-MECH-DWG-OUTGUI: Outer tape measure guide (center)
DINO-MECH-DWG-ROLLER: Tape measure roller (4)

3 Boom Assembly and Mounting Procedures

3.1 Gear Sub-assembly

The mounting of the gears to each other requires that the inner spindle and the outer spindle be mated to each other via two #4-40 1/2" socket head screws. The screws fit into the outer spindle and down into the inner. On both sides of this assembly go two spools. The spools fit over the spindle assembly, the spindles fitting into 0.05" pockets in the sides of the gear spools. The large gear on the backside of the screw mates to the spools and spindles both by way of three #4-40 3/16" counter-sunk screws. Through all of the parts fits a 1/4" rod 2 3/4" long; there is a notch on the rod that fits the shaft mount. To the shaft mount fits a ratchet gear connected with three #4-40 3/16" counter-sunk screws. The drive shaft fits through the hole in the central panel and the outer panel on the backside. There are two drive shafts as there are two gear assemblies. The gear assemblies should be mounted so that the teeth of the ratchet gears appear to move away from the interior of the box. The spindles have exactly the opposite formation – that is, towards the center guide.

3.2 Box assembly

The central panel of the boom braking box fits two measure guides to it by four #4-40 7/16" screws. Also, the central panel in front mounts the tape measure guide that runs up through the main body of the box. First, to the central panel is mated an elliptical spacer via two #4-40 3/4". The screws also run through the outer guide and into the center tape measure guide. On the backside of this central guide piece is another guide cover that fits to the center guide with a single #4-40 1/4" socket head screw. Between the inner and outer guides, four rollers are fitted concentrically to the four pertinent holes in the guides pieces, and they can be secured by two 1/2" dowels held in place by lock washers and nuts. To the central panel fits two side box panels; view the document DINO-MECH-ASM-BBBOX to verify the proper orientation of the boxes. Each side panel fits to the central panel by three #4-40 3/16" socket head screws. Once the shafts are put into place, the outer panel can be attached. It also mates to the side box panels by three #4-40 3/16" screws on either side. To the 1/8" holes in the side of the outer panel, two rods run through to give mount to the two pawls. The pawls should be situated 0.1" from the inside wall of the outer panel. Above each are the rod guides – one being designated a "pin guide" – to hold the spring rod. The spring rod continually pushes down on each pawl which themselves push down on the ratchet. The geometry of the ratchet ensures that the movement of that gear and the drive shaft that it is attached to are impeded. There is an adjustment bracket above the larger of the two pawls. Its purpose is

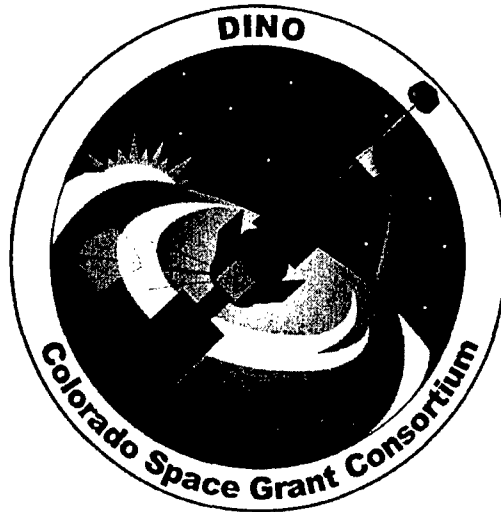
to provide resistance as necessary to increase the ratcheting power of the deployment.

3.3 Mounting Procedures

There are holes in the base of the side panels, and those holes fit under the Tip Mass box structure. With two #8-32 screws, the boom braking box can be held in place. The center guide piece must be facing downwards on the satellite, towards the nadir plate.

Appendix A – List of Acronyms

DINO – Deployable and Intelligent Nanosatellite Operations, referring to the Colorado Space Grant mission entry for Nanosat III.



Deployment of the CTD Experiment Panel

DINO-MECH-RPT-CTD, Rev. A

Written by:
M. Wilson

Prepared for:
Nanosat III

Table of Contents

1	Scope.....	4
1.1	Identification.....	4
1.2	Document Maintenance.....	4
1.3	Systems Overview.....	4
1.4	Document Overview.....	4
1.5	Referenced Documents.....	4
2	CTD Components.....	5
3	CTD Assembly and Mounting Procedures.....	6
3.1	Panel Sub-assembly.....	6
3.2	Mounting Procedures.....	6
4	CTD Deployment and Performance.....	7
4.1	Experiment Panel Deployment.....	7
4.2	Performance Metrology.....	7
5	FrangiBolt Components.....	7
6	FrangiBolt Assembly and Mounting Procedures.....	7
6.1	FrangiBolt Assembly.....	7
6.2	Mounting Procedures.....	8
7	FrangiBolt Deployment.....	9
7.1	Deployment.....	9
	Appendix A – List of Acronyms.....	10

1 Scope

1.1 Identification

This document applies to the DINO project, a project undertaken by the Colorado Space Grant Consortium at the University of Colorado at Boulder. This project is part of the Nanosatellite III Program sponsored by the Air Force Office of Scientific Research (AFOSR), Air Force Research Laboratory (AFRL), Association of Aeronautics and Astronautics (AIAA), and Goddard Space Flight Center (GSFC).

1.2 Document Maintenance

This document falls under the DINO document control requirements as specified under the DINO Configuration Management plan. All changes and updates must be made in accordance with the DINO CM plan.

1.3 Systems Overview

The purpose of the student-led Deployment and Intelligent Nanosatellite Operations (DINO) mission is to determine cloud heights from space, evaluate the performance of intelligent operations, and assess deployment technologies for nanosatellites including a gravity-gradient boom, memory composite hinges, and thin-film solar arrays.

1.4 Document Overview

This document pertains to the deployment of the CTD experiment panel onboard the DINO satellite. The panel is connected to and deployed by shape-memory composite hinges courtesy of Composite Technology Development, Inc. The CTD experiment panel is one of the various deployable mechanisms for the DINO mission. In order that CTD, Inc. may have quantitative data determining the performance of its composite hinges, the CTD experiment panel will mount a rate gyro sensor board to test relative acceleration. The CTD experiment panel will be successfully deployed so long as the appropriate Wattage is supplied to the composite hinges, and so long as the FrangiBolt restraint is successfully released. The FrangiBolt is a device supplied to Colorado Space Grant Consortium by the TiNi Aerospace company. Inside this device is a composite material that, when heated, expands in such a way so as to stress the release bolt and break it in two. This document will elaborate on the processes that will ensure a successful deployment of the CTD experiment panel.

1.5 Referenced Documents

The following is a list of all documents related to the CTD experiment panel design and construction. Please note: the nomenclature is of the form MissionName-MissionSubsystem(Mechanisms)-DocumentType(Drawing)-ComponentName.

DINO-MECH-DWG-EXPPAN
DINO-MECH-DWG-CPCONE
DINO-MECH-DWG-PANMNT
DINO-MECH-DWG-RELEASE
DINO-MECH-DWG-SBOARD
DINO-MECH-DWG-CTDHNG
DINO-MECH-DWG-ISOMNT
DINO-MECH-ASM-PANEL
DINO-MECH-ASM-CTDPAN1
DINO-MECH-ASM-CTDPAN2
DINO-MECH-DWG-FRACT
DINO-MECH-DWG-FHOUSE
DINO-MECH-DWG-CPLATE
DINO-MECH-DWG-CSLIDE
DINO-MECH-DWG-OUTSPR
DINO-MECH-DWG-INNSPR
DINO-MECH-DWG-FRBOLT
DINO-MECH-DWG-SPRWASH
DINO-MECH-DWG-FRMNT
DINO-MECH-ASM-WASHERS
DINO-MECH-ASM-FSLIDE
DINO-MECH-ASM-FRANGI

2 CTD Components

The following is a list of all parts encompassing the CTD experiment panel assembly and mounting components

DINO-MECH-DWG-EXPPAN – Experiment panel (1)
DINO-MECH-DWG-CPCONE – Cup cones (3)
DINO-MECH-DWG-PANMNT – Panel-side hinge mounts (2)
DINO-MECH-DWG-RELEASE – Panel release eye (1)
DINO-MECH-DWG-SBOARD – Panel mounted sensor board (1)
DINO-MECH-DWG-CTDHNG – Shape-memory composite hinges (2)
DINO-MECH-DWG-ISOMNT – Isogrid-side hinge mounts (2)

3 CTD Assembly and Mounting Procedures

3.1 Panel Sub-assembly

To begin the assembly of the deployable CTD panel, start with the experiment panel itself designated "EXPPAN." There is a link to that part above, saved as a drawing file, as well as a link to all other parts listed in this document. The nomenclature is consistent throughout. Various parts are attached to the panel and they are:

PANMNT – Two hinge mounts for the CTD shape-memory composite hinges. Each mount is mated to the panel by two #8-32 3/4" socket head screws.

CPCONE – Three half cylindrical "cones" mate to the pocketed side of the experiment panel by two #4-40 5/8" socket head screws.

SBOARD – The rate gyro sensor board fits onto the experiment panel by three #6-32 3/4" socket head screws. The sensor board is at the bottom of one of the material pockets on the experiment panel. It is mounted on stand-offs, however, being 1/4" tall each.

RELEASE – The release eye is a component that is also attached to the FrangiBolt assembly which is the release mechanism for the panel deployment. The release eye is mated to the experiment panel by two #2-56 3/16" socket head screws.

3.2 Mounting Procedures

To mount the CTD experiment panel assembly to the DINO satellite, the isogrid-side hinge mounts need to be mated to the main structure. Those hinge mounts are designated "ISOMNT" and are attached to the satellite by three #10-32 1/2" socket head screws. The mounts in turn fit two #6-32 1/2" socket head screws. The screws in question go through the CTD hinge anchors to mate with the panel-side hinge mounts and the isogrid-side hinge mounts both in the same way. Once the panel is attached to the main structure via the composite hinges, it can be locked into place with the release eye component and the FrangiBolt. In order to prepare the panel for stowing, the hinges must first be supplied with the appropriate electrical power. With the supply of 0.6 V at 1 A, the composite hinges should become pliable enough to bend into formation. A 1" round dowel (over which the hinges bend) should be used to get the specified curvature for the hinges. Once the release eye is in its position relative to the isogrid, the FrangiBolt can be put in place through the opening of the release eye. Each cup cone should fit snugly into the grooves located alongside the isogrid panel. A view of the isogrid in question can be found in the "CTDPAN" assemblies, but also in documentation from the Structures subsystem team. The experiment panel can be locked into place with clamps and Belleville washers, the latter being for accurate tightening. The pre-tensioned force in place can be determined from the compression displacement of the washers.

4 CTD Deployment and Performance

4.1 Experiment Panel Deployment

Successful deployment of the experiment panel will occur if the proper power supply is provided to the composite hinges, and if the FrangiBolt successfully releases. If 0.6 V at 1 A is supplied to the hinges as is planned, the hinges should be fully prepared to unfold. When the hinges reach their temperature limit, power supply is supposed to shut off. At around the same time, the FrangiBolt is supposed to be actuated. This actuation causes the FrangiBolt bolt to break in two thus freeing the CTD panel from restraint.

4.2 Performance Metrology

The kinematics of the panel deployment can be measured from the rate gyro sensors mounted onboard the experiment panel itself. The specifics of this measurement should be detailed in the appropriate documentation.

5 FrangiBolt Components

The following is a list of all parts encompassing the FrangiBolt assembly and mounting components

- DINO-MECH-DWG-FRACT – FrangiBolt actuator (1)
- DINO-MECH-DWG-FHOUSE – FrangiBolt actuator housing (1)
- DINO-MECH-DWG-CPLATE – Slide cover plate (1)
- DINO-MECH-DWG-CSLIDE – Sliding component inside cover plate (1)
- DINO-MECH-DWG-OUTSPR – Outer spring with greater diameter (1)
- DINO-MECH-DWG-INNSPR – Inner spring with smaller diameter (1)
- DINO-MECH-DWG-FRBOLT – FrangiBolt bolt #8 (1)
- DINO-MECH-DWG-SPRWASH – Spring washers (10)
- DINO-MECH-DWG-FRMNT – FrangiBolt mount (1)

6 FrangiBolt Assembly and Mounting Procedures

6.1 FrangiBolt Assembly

The FrangiBolt assembly has a few components associated with it. Firstly, the outer housing consists of the FrangiBolt housing (FHOUSE) and the cover slide plate (CPLATE). The assembly procedures for these two parts will be elaborated below, but first, here are the individual component parts:

CSLIDE – This part fits within the cover slide plate. The face is oriented in the same way as the pocketed face of the cover slide plate. Its position within the

cover slide plate is determinate upon the final tightness of the two portions of the outer FrangiBolt housing.

OUTSPR – This spring fits around the inner spring and it also fits behind the cover slide. The cover slide is supposed to back up into the pocket of the cover slide plate with both springs behind it. As the cover slide plate and the FrangiBolt housing are screwed together, the cover slide should move slightly backwards into the pocket of the cover slide plate. This is because the FrangiBolt bolt will be pressed up against it on one side, and the springs on the other side.

INNSPR – The inner spring will fit inside the outer spring, and, in the same way, it will buttress the cover slide.

FRACT – The FrangiBolt actuator sits upright in the pocket on the side of the FrangiBolt housing. It's held in place by the bolt that runs through it and on through to the pocketed face of the FrangiBolt housing. The bolt has washers stacked below the bolt head which keep it in place until the point of breaking.

SPRWASH – There are 10 washers behind the bolt head that prevent the bolt from moving prior to actuation, and also keep the bolt from reentering the hole that would prevent the release of the CTD experiment panel. The washers fit around the bolt and are paired so that every two have their concave faces towards each other.

FRBOLT – The FrangiBolt bolt goes through the length of the FrangiBolt housing. The ten washers buttress it on the backside of the dually pocketed face of the housing. Further, the bolt runs through the actuator.

FRMNT – The FrangiBolt mount mates to the CTD isogrid panel and it fits the whole FrangiBolt housing in the raised pocket of the material.

6.2 Mounting Procedures

To begin, the FrangiBolt mount can first be attached to the isogrid structure, on the CTD isogrid panel and towards the interior of the structure. The elevated pocket on top of the FrangiBolt mount should face towards the center of the DINO structure. For the full mounting geometry, review documents DINO-MECH-ASM-CTDPAN1 and DINO-MECH-ASM-CTDPAN2. The FrangiBolt mount is attached to the isogrid panel by four #10-32 1/2" socket head screws and lock washers for each. The FrangiBolt bolt can first be fitted into the FrangiBolt housing, FHOUSE. Behind the head should be the 10 spring washers that can be seen in their proper formation in the document DINO-MECH-ASM-WASHERS. These washers further fit into the pocketed face at the end of the FrangiBolt housing. The bolt should be slid through the hole in the FrangiBolt housing, and should be passed through the release eye DINO-MECH-DWG-RELEASE which extends into the depth cut in the FrangiBolt housing. The release eye can be mated to the CTD experiment panel from that point. Aside from fitting through the release eye, the bolt should fit through the FrangiBolt actuator. The actuator fits in a pocketed side of the FrangiBolt housing with all wiring being oriented towards the opening cut in the bottom of the FrangiBolt mount. Now, the components of the sliding device should be

fitted into the pocket of the cover slide. The smaller diameter spring fits through the larger diameter spring, and both go behind the slide cover. The cover slide and the springs should be compressed into the pocketed face of the cover plate with the cover slide facing outward. The cover plate and the FrangiBolt housing (bolt included) must be pressed together and mated with 4 #6-32 1 1/2" socket head screws. This is the FrangiBolt housing in total. It is, in turn, mounted to the FrangiBolt mount by four #4-40 3/8" socket head screws. The document DINO-MECH-ASM-FRANGI displays the proper orientation of the assembly itself.

7 FrangiBolt Deployment

7.1 Deployment

The FrangiBolt actuator requires only the proper power supply to operate successfully. The actuator uses 25 W at 28 V and should be controlled by input from the thermal sensors attached. Once the device reaches its expected temperature power is cut off.

Appendix A – List of Acronyms

DINO – Deployable and Intelligent Nanosatellite Operations, referring to the Colorado Space Grant mission entry for Nanosat III.

CTD – Composite Technology Development, Inc.; the company supplying the unique shape-memory composite hinges for the DINO program.



Mission Operations Plan

DINO-MOPS-PLN-OPS, Rev. B

Written by:
James Burkert

Prepared for:
Nanosat III

Table of Contents

1	Scope.....	4
1.1	Identification.....	4
1.2	Document Maintenance.....	4
1.3	Systems Overview.....	4
1.4	Document Overview.....	4
1.5	Referenced Documents.....	4
2	Introduction.....	4
3	Mission Concept.....	4
4	Mission Objectives and Success Criteria.....	5
4.1	Flight Segment Objectives and Criteria.....	5
4.1.1	Assess Deployment Technologies	5
4.1.2	Demonstrate Stereo Imaging	5
4.1.3	Demonstrate Intelligent Operations	5
4.2	Ground Segment Objectives and Criteria.....	5
4.2.1	Demonstrate two-way communication with DINO	5
4.2.2	Display Telemetry	6
4.2.3	Download and Distribute Science Data	6
5	Operations Systems Overview.....	6
5.1	Ground Software System.....	6
5.1.1	Software Simulator	6
5.1.2	Graphical User Interface	7
5.1.3	Communications Software	9
5.1.4	Data Management and Distribution Software	9
5.2	Flight Software System.....	9
6	Mission Operations Functions.....	11
6.1	Operations Planning.....	11
6.2	Activity Scheduling and Development.....	12
6.3	Mission Control.....	12
6.4	Data Services.....	13
6.5	Navigation and Attitude Control.....	14
6.6	Spacecraft and Payload Operations.....	14
6.7	Mission Assurance and Risk Mitigation.....	15
6.8	Operator Training and Certification.....	15
7	Mission Timeline.....	17
7.1	Beginning of Life.....	18
7.2	Nominal Operations.....	19
7.3	Standby.....	20
7.4	End of Life.....	20
	Appendix A – List of Acronyms.....	21
	Appendix B – Glossary.....	22

1 Scope

1.1 Identification

This document applies to the DINO project, a project undertaken by the Colorado Space Grant Consortium at the University of Colorado at Boulder. This project is part of the Nanosatellite III Program sponsored by the Air Force Office of Scientific Research (AFOSR), Air Force Research Laboratory (AFRL), Association of Aeronautics and Astronautics (AIAA), and Goddard Space Flight Center (GSFC).

1.2 Document Maintenance

This document falls under the DINO document control requirements as specified under the DINO Configuration Management plan. All changes and updates must be made in accordance with the DINO CM plan.

1.3 Systems Overview

The purpose of the student-led Deployment and Intelligent Nanosatellite Operations (DINO) mission is to determine cloud heights from space, evaluate the performance of intelligent operations, and assess deployment technologies for nanosatellites including a gravity-gradient boom, memory composite hinges, and thin-film solar arrays.

1.4 Document Overview

This document details the mission operations plan for the DINO mission. The phases of the mission and the tools used to plan for the mission are outlined.

1.5 Referenced Documents

Space Mission Analysis and Design 3rd Edition by Wertz and Larson
DINO-ADCS-RPT-ADCS
DINO-SW-RPT-SW

2 Introduction

The DINO Mission Operations Plan (MOP) describes the operational characteristics of the flight and ground-based elements of the DINO command and data systems and the roles of operations personnel.

3 Mission Concept

DINO is a student-designed and -built low-earth orbit satellite with the mission of measuring cloud topography from space, performing on-board data analysis, and evaluating three deployment technologies. The first experiment evaluates the Foldable Integrated Thin-Film Stiffened Solar Array (FITS Solar Array) from MicroSat. The second experiment is the demonstration of Elastic Memory Composite (EMC) Hinges, donated by Composite Technologies Development (CTD), which will deploy a panel on the spacecraft. Hinge performance during the initial deployment

and then during attitude maneuvers and thermal events will be evaluated. Third, the slow-down mechanism of the gravity-gradient boom, an in-house design, will be tested. The slow-down mechanism will be evaluated with data sent wirelessly from the tip mass accelerometers and magnetometer to the body of the satellite.

4 Mission Objectives and Success Criteria

The Mission Objectives and their success criteria are defined below. Fulfilling these in-flight objectives is the direct responsibility of the Mission Operations Team. The MOPS Team methodology for achieving these objectives is outlined in section 6.

4.1 Flight Segment Objectives and Criteria

4.1.1 Assess Deployment Technologies

The objective is to deploy all five mechanisms – the gravity gradient boom, the Foldable Integrated Thin-Film Stiffened Solar Array (FITS), the two antennas and the Composite Technologies Development panel.

The criteria for success are the full deployment of the gravity gradient boom, FITS panel, and the CTD panel, approximately 75% of the on-board deployables. The antennas constitute the remaining 25%, and are considered less mission-critical because they will still function if they are not deployed.

4.1.2 Demonstrate Stereo Imaging

The objective is to create stereo images and calculate the altitude above the ground of the leading and trailing edge of clouds, and a topographical map of the cloud's interior.

The success criterion is to complete one correct topographical map. This must be verified by downloading the appropriate pictures and confirming that the correct altitude of the cloud edges was calculated within ± 500 meters.

4.1.3 Demonstrate Intelligent Operations

The objective is to demonstrate that the satellite can evaluate its environment and respond accordingly.

The criterion for success is that the satellite reacts properly and autonomously at least one time. This will be proven by examining downloaded spacecraft logs.

4.2 Ground Segment Objectives and Criteria

4.2.1 Demonstrate two-way communication with DINO

The objective is to successfully transmit and receive information from the spacecraft.

The criterion for success is that 95% of data sent by either the ground station or DINO is received by the other system.

4.2.2 Display Telemetry

The objective is to graphically show health and status information. The data will be graphed over time, and easily compared to simulated telemetry. The comparison between the actual and simulated telemetry is particularly critical, to identify potential problems with the Mission Module (MM).

The criterion for success is the GUI sending commands to the spacecraft and displaying Health and Status (H&S) data.

4.2.3 Download and Distribute Science Data

The ground software must automatically handle incoming science data from the satellite. It will downlink the data, make it available to the Science Team for confirmation and further analysis, and then post the data in an online database for public access.

The instrumentation readings of the various onboard experimental mechanisms will similarly be obtained and evaluated, then distributed to the experiment's primary investigators via a secure online database.

The criterion for success is the successful distribution of raw and analyzed data to the appropriate people and databases.

5 Operations Systems Overview

5.1 Ground Software System

The software simulator, the graphical users interface (GUI), the communications software, and the data management and distribution software (DMDS) collectively composes the Ground Software System.

5.1.1 Software Simulator

The software simulator provides accurate simulation of the satellite on the ground. This simulation capability allows the Mission Operations Team to validate new procedures, Mission Modules, software upgrades, and train new Mission Operators on the behavior of the satellite. Like most simulators, it is composed of a number of software tools. The interaction of these elements is displayed in Figure 1.

The Simulator uses the Flight Software, the Mission Module, and a separate Python-based Simulation Module, and finally Satellite Tool Kit (STK) from Analytical Graphics, Inc. (AGI). The Simulation Module contains the algorithms to simulate most of the telemetry of the spacecraft, and STK

supplies some environmental information, such as simulated magnetometer readings.

The Flight Software and Mission Module are identical to the flight versions; however newer versions of either the Flight Software or Mission Module can be inserted for testing. The Simulation Module is a Python-based program that returns varying values to the Flight Software. These values are based on the predicted conditions in space, such as temperature, and the normal hardware status like voltage and current monitors. Some specific values are delivered to the Simulation Module from Satellite Tool Kit, such as magnetometer readings for the spacecraft's current position, and updated Two-Line Elements (TLE). Additionally, STK will provide a three dimensional view of the spacecraft's position and attitude, based on the ADCS module within the Flight Software. STK's graphical display capability is designed to give the Mission Operators an instinctive feel for DINO's current state.

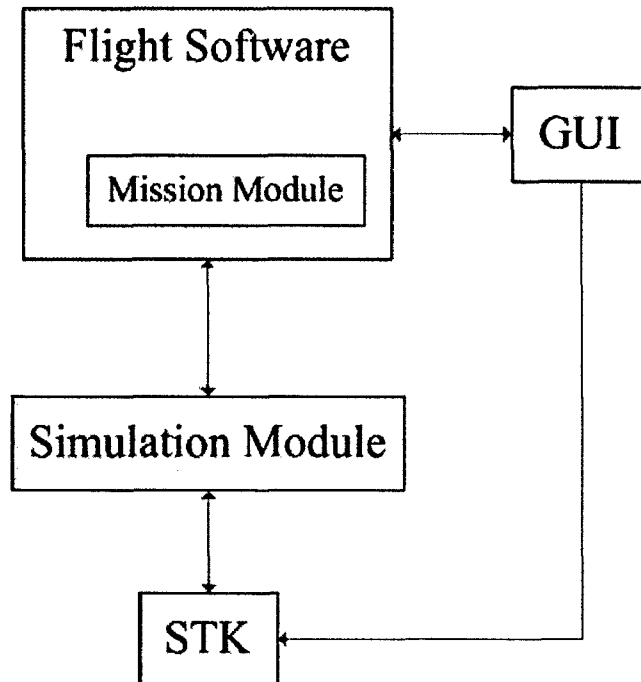


Figure 1: Simulator Flow Chart

5.1.2 Graphical User Interface

The Graphical User Interface, developed by DINO's Software Team, allows Mission Operators a fast and intuitive way to display telemetry and transmit commands to the spacecraft. The GUI is written in Python, to ease integration with the rest of the software components. Notably, the GUI can accept telemetry from the actual spacecraft, and any number of simulators. Although the GUI is termed an interface, it contains all the functionality associated with the user interface. The GUI alone can send commands to the satellite and the other parts of the Ground Software System. For a screenshot of the GUI, see

Figure 2. It should be noted that Figure 2 represents the most basic functionality implemented thus far.

Telemetry is displayed in graphical and tabular forms for the operator. Graphs can have several data sets overlaid on each other from any running simulators and the telemetry transmitted from the satellite. Additionally, by clicking on the graph, the user is presented with the exact value at that time, and the option to list commands executed before and after that time, within a user-specified boundary. The GUI functionality allows the operator to compare commands with associated sensor values. Combined with the 3D representation in STK, the operator should have an intuitive grasp whether or not the telemetry is reasonable. For example, if a temperature sensor spikes, the command log and the 3D representation can be examined quickly to determine either a cause for the spike or to conclude that it was a suspect sensor reading.

The GUI allows the operator to command the spacecraft. Each subsystem has its own display containing current status and a list of commands and activities. Activities are higher-level functions that the operator can perform, and each activity is composed of a list of detailed commands that will accomplish that activity. For example, an operator might want to disable the automatic ADCS system in the case of an error. That would constitute an activity, and the GUI would provide a time-ordered list of low-level commands needed to accomplish the activity. The operator can choose activities to send to the satellite, and the GUI will display a more detailed list of actual commands that will be sent to the spacecraft. The GUI does have an error-checking capability in which it inspects actions and commands requested by the user for validity, and informs the user if there is a potential problem with that command or activity.

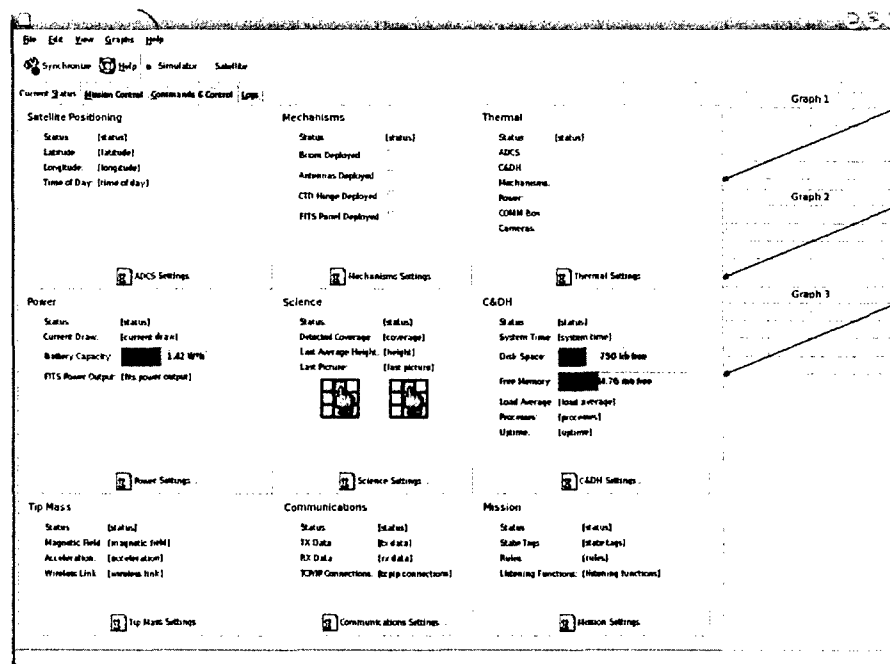


Figure 2: Screenshot of GUI

5.1.3 Communications Software

The communication software bridges the gap between the rest of the ground software and the satellite through the ground communications hardware. It controls and manages the radio link from the ground to the spacecraft, and performs the initial data management.

Radio link management consists of setting or changing uplink and downlink frequencies on the ground, monitoring signal strength, and informing the user of acquisition and loss of signal (AOS and LOS, respectively).

Data management in the Communications Software is strictly concerned with assembling packets, resolving packet errors, and assembling data from multiple ground stations into one consistent data set.

5.1.4 Data Management and Distribution Software

The Data Management and Distribution Software (DMDS) distributes telemetry into the appropriate databases and informs operators and users of telemetry availability. For example, it routes health and status data to the health and status database, deployable technology data to the secured online database, and stereo imaging data first to the Imaging Team for release, then to the public online database.

5.2 Flight Software System

The Flight Software System, FSS, is primarily the responsibility of the Software Team, so its functionality will only be discussed here as it is relevant to Mission Operations. (See DINO-SW-RPT-SW)

There are four primary segments of the FSS (See Figure 3). First, there is the Linux-based operating system, which provides the interface between commands and the actual hardware. Second, there is the Error Detection and Correction (EDC) module which is run by the operating system to check for errors, particularly bit flips from radiation. Third, there is the spacecraft-unique flight software, a module written in Python that contains the detailed information about the spacecraft systems, and contains the algorithms to run the Mission Module. Fourth, there is the Mission Module (MM) itself. The MM contains all the information necessary for the spacecraft's autonomous operations, and is the responsibility of Mission Operations. It will be discussed in depth below.

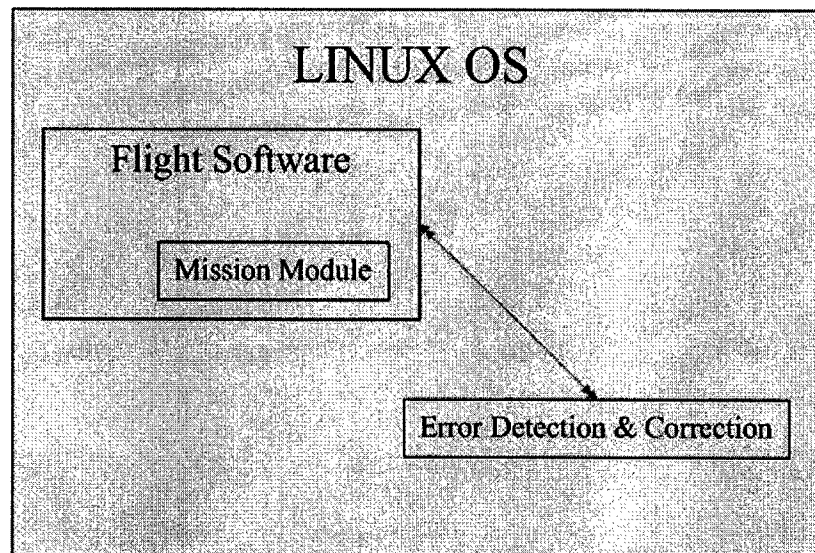


Figure 3: Flight Software System Architecture

The Mission Module (Figure 4) is based around *Observable Values*, *Rules*, and *Scripts*. Observable Values are variables that describe the state of a particular part of the spacecraft, for example the current, voltage, and thermocouple sensors. Rules are objects that monitor a particular observable value for changes. When the observable value changes, the rule executes a script to react to that changing value. A script is a set of commands to the Flight Software to respond to the current situation. These scripts can activate or deactivate rules, create or remove observable values, and scripts can command spacecraft hardware. See DINO-SW-RPT-SW for more information.

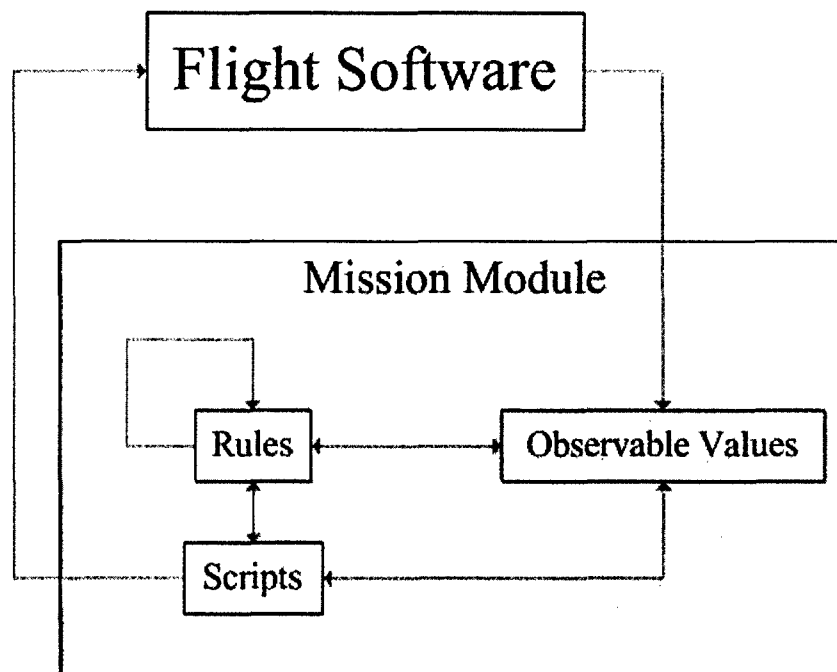


Figure 4: Mission Module Architecture

6 Mission Operations Functions

The Mission Operations Team has many functions to perform before, during, and after the mission. These are given in detail in sections 6.1-6.8, and summarized in Table 1, below. Each function is detailed, with the party responsible for the supervision of each function given last.

6.1 Operations Planning

Operations Planning consists of the pre-launch activities that define how Mission Operations will function during flight. This requires a thorough understanding of the spacecraft mission, systems, and objectives. The Operations Planning function provides a Mission Timeline before the launch that outlines what activities and objectives are part of each mission phase. See Section 7 for more information on the Mission Timeline.

There are a number of decisions that must be made before launch, with regard to Operations. Resources must be identified, scheduled, and managed to ensure the right people and equipment are available when needed. The level of spacecraft automation must be decided. The post-launch spacecraft functions must be identified, and responsibility for each function clearly delineated. Finally any needed software must be created and tested with the spacecraft hardware, and personnel trained in its use.

For DINO, pre-launch Operations Planning consists of extensive simulation to characterize the day-to-day activities of the satellite. These simulations are called Day In The Life (DITL) Tests. DITL Tests incrementally evaluate the software

and hardware interactivity, culminating in several week-long tests that simulate the actual spacecraft operations. The longest tests draw together all the flight and ground elements together for the first time, ensuring that all of them function well independently and together.

Operations Planning is performed by the MOPS Team, and is the responsibility of the MOPS Team Lead.

6.2 Activity Scheduling and Development

Prior to launch, Activity Scheduling and Development (ASD) is responsible for formulating the standard procedures to be used throughout the mission lifetime. The procedures must be verified through simulation with the entire set of ground and flight components. ASD assists Operations Planning in formulating the details of procedures.

During Flight, ASD further refines existing procedures and creates new procedures to accomplish unforeseen activities or objectives. All procedures are to be simulated prior to use, and inspected and approved by the Systems Team Lead, the Mission Operations Team Lead, and the Team Lead(s) of the system(s) involved with each procedure. Each modification of an existing procedure is likewise subjected to further review.

This function is performed by the Mission Operations Team, and is personally supervised by the MOPS Team Lead.

6.3 Mission Control

Mission Control is the day-to-day maintenance and operation of the satellite. Mission Control is responsible for executing the various procedures needed to keep the spacecraft operational, monitor the spacecraft for errors and anomalies, and instigate other MOPS functions as needed.

Mission Control for the DINO mission will be staffed by undergraduate or graduate students, trained on the satellite and ground software. The student pool will be separated into teams of three each, called Mission Control Teams (MCT), assembled with regard to similar scheduling availability. Each team will be composed of a Supervisor, an Analyst, and a Communications Engineer (CE).

The supervisor is responsible for maintaining the proficiency of the team, ensuring each member is on time for shifts, planning activities during pass times, and identifying anomalies, with the help of the other team members. The supervisor is required to have an in-depth knowledge about the satellite and ground systems.

The Analyst operates the Graphical User Interface in the Ground Software System to identify anomalies in the operation of the satellite, identify if possible the

causes of any anomalies, and alerts the supervisor to any potential problems. The Analyst sends commands to the spacecraft via the GUI.

The Communications Engineer (CE) starts and monitors the entire chain required to successfully communicate with the satellite. The CE predicts pass times and durations, and alerts the supervisor to each pass. During the pass the CE provides the team a countdown of the remaining time. The Communications Engineer additionally monitors the connectivity from the satellite to the ground stations, along with the link to each database and to the GUI.

During the mission, the Mission Operations Center (MOC) will be staffed by a MCT for each pass. The MOC will have a graphic representation of the satellite state, shown from STK, projected onto a screen. Basic spacecraft health and status information will be displayed here as well, to increase the overall situational awareness of the MCT.

This function is performed by the Mission Operations Team, and is the responsibility of the MOPS Team Lead to supervise.

6.4 Data Services

Data Services is strictly concerned with assembling, verifying, and routing data from the satellite to the eventual data user. As data is downloaded from the satellite, whether it is health and status data, science data and imagery, or experiment data, Data Services is responsible for archiving the data in the appropriate database, and informing interested parties of the data delivery and content.

Assembly and verification of the data involves receiving the data from one or more ground stations, assembling the multiple data streams into one coherent data set, and then verifying the contents of the data is not corrupted or incomplete.

Data routing is essentially archiving the data, then providing that data to whomever needs it. Each type of information is treated differently. Health and Status data must be archived in a database, and made available to the Ground Software for display.

Science data must similarly be archived, and forwarded to the Science Team for inspection and eventual release to the public. DINO's determination of cloud altitude may be potentially useful for meteorologists, giving this particular type of data an added delivery time requirement. To meet this delivery time constraint, the results of DINO's onboard analysis will be automatically made available to the public, after the system's initial verification. Continued verification of the onboard analysis is made by the Science Team, by comparing DINO's analysis with the images used in the analysis, essentially the Science Team will spot-check the process.

Experiment data, from the EMC Hinges, the FITS Solar Array, and the Ball power system design must be archived in a secure database, and the appropriate primary investigators informed of its availability. This data may be made publicly available, at the discretion of the primary investigators.

This function is performed by the automated ground software, and is the responsibility of the MOPS Team Lead to supervise, with the help of CSGC Network System Administrators.

6.5 Navigation and Attitude Control

DINO's Attitude Determination and Control System (ADCS) is designed to operate autonomously. To maintain the necessary accuracy with the magnetometer, the on-board propagator must be given updated Two-Line Elements approximately every two weeks. (See DINO-ADCS-RPT-ADCS)

If the closed-loop autonomous ADCS system above fails, it becomes the responsibility of the Mission Operation Team to handle Attitude Control. This will be done via an open-loop form of the ADCS system, implemented in the Mission Module. This option gives some degraded performance, and is considered a temporary alternative until the closed-loop system is operational.

This function is performed by the Mission Operations Team, and is the responsibility of the Mission Operations Team Lead, and additionally is supervised by the ADCS Team Lead.

6.6 Spacecraft and Payload Operations

Spacecraft and Payload Operations is the function that is responsible for responding to serious operational problems with either the spacecraft or payload. These types of problems are generally outside the knowledge, training and procedures of the Mission Operations Team, and require a more detailed knowledge of the satellite systems.

The process associated with Spacecraft and Payload Operations is initiated when the MCT Supervisor on duty recognizes a potentially serious problem with the satellite and contacts the MOPS Team Lead. If the MOPS Team Lead determines that the problem needs more information than the MOPS Team has, then the Team Lead contacts the designated Systems Team personnel, and the involved subsystem Team Leads, or associated experts. This group assembles, diagnoses the problem, and recommends the appropriate course of action. Once the proper action has been decided, it is the responsibility of the Mission Operations Team Lead to ensure that it is carried out.

This function is performed by the Mission Operations Team, the requisite system experts, and is supervised by the Mission Operations Team Lead.

6.7 Mission Assurance and Risk Mitigation

Mission Assurance and Risk Mitigation (MARM) is the function that ensures the satellite will continue to function. Mission Assurance focuses on achieving the mission objectives, and Risk Mitigation is how those objectives are achieved with minimum risk to the spacecraft.

Part of this effort is the spacecraft's autonomous control system, the Mission Module. The MM relies on the interaction of its components to guide the activity of the satellite. The combinations of rules and sensors allow the flexibility for basic autonomy, but the dangers are that the Mission Module may behave in an unpredictable or improper way and that the reaction to a particular situation could exacerbate a problem rather than resolve it. The solution to this is two-fold, first the Mission Module must be rigorously tested in a simulated environment, and the rest of the Flight Software must impose some limited oversight on the Mission Module's activities, much the same as inhibitors prevent hardware from doing certain activities.

Another part of the process for MARM is the certification of operations personnel and the validation of procedures. Certification is outlined in section 6.8 below. Procedure validation ensures that any commands sent to the spacecraft are valid, without relying on the ground software to catch potential errors.

This function is performed by the various Team Leads, and is the responsibility of the Mission Operations Team Lead, with supervision by the Project Manager and Systems Team Lead.

6.8 Operator Training and Certification

The Mission Operations Team is largely responsible for recruiting, training and certifying its personnel. Several teams must be formed to ensure staffing of the Mission Operations Center during pass times and around school scheduling. The personnel pool for Mission Operations consists of students at the University of Colorado, and is untrained in the specifics of operating a satellite, for the most part. This requires an intensive training period of several months to bring each person up to speed on the fundamentals of the DINO mission, and then further training in each of the specialties needed for each team.

The training coursework, materials, and certification requirements are outlined during Day In The Life Testing. Simulation is integrated into the training course, with an emphasis on performing basic operations, and trouble-shooting the satellite through sufficiently detailed technical knowledge.

The certification process is two-fold. First, an individual receives the Basic Certification, which introduces them to DINO as a whole system and prepares them for any position within the MCT. Once someone has the Basic Certification, they can become certified for any or all of the three positions within the MCT.

Each of these positions requires detailed knowledge of a particular part of the DINO mission.

The Basic Certification requires the individual to be able to recall with reasonable accuracy a functional block diagram of the Flight and Ground Systems. The individual must demonstrate familiarity with;

1. The responsibilities of each specialty position
2. The set up and verification of each specialty's station
3. The Ground Software System GUI
4. The basic day to day operations of the satellite
5. The various procedures used to control the spacecraft.

The second level, Specialty Certification, specifies that the individual is qualified to run a particular position in the MCT, whether it is Supervisor, Analyst, or CE (See 6.3). Each specialty requires a unique understanding of DINO, and each are outlined briefly below;

The Supervisor must be able to:

1. Plan activities and objectives for each pass opportunity
2. Operate either of the other positions with reasonable proficiency
3. Lead the MCT effectively
4. Communicate information clearly to the MOPS Team Lead and Project Manager.
5. Demonstrate a deep understanding of the satellite systems
6. Demonstrate proficiency in trouble-shooting problems through technical knowledge

The Analyst must be able to:

1. Demonstrate proficiency with the Ground Software GUI
2. Demonstrate a working knowledge of the Mission Module.
3. Demonstrate proficiency in spotting spacecraft anomalies.
4. Demonstrate fundamental understanding of the procedures used to operate the satellite.

The Communications Engineer must be able to:

1. Demonstrate understanding of the subtleties of the Ground Software System
2. Demonstrate proficiency in trouble-shooting problems with the Ground Software System
3. Demonstrate a working knowledge of the capabilities and limitations of the Software Simulators.
4. Demonstrates sufficient knowledge of STK to accurately predict pass Acquisition of Signal times and pass durations.
5. Demonstrate sufficient knowledge of Data Services to ensure it is working properly
6. Demonstrate the ability to trouble-shoot problems in Data Services.

These are the most basic areas that training and certification covers for the DINO Mission Operations Team. Care must be taken in designing the particulars of the training schedule and content to allow for the inexperience of student operators.

Table 1: Mission Operations Functions

MOPS Function	Responsibilities	Inputs	Outputs	Where Accomplished	
				On-Board S/C	Ground
Mission Planning	Deployables and science mission planning	Deployables requirements	Deployables schedule, Mission Timeline, Training Materials, Operations Plan, DITL Testing, Software Requirements		Operator with automated software support
Activity Planning & Development	Ground and S/C scheduling	Ground and S/C requirements	Procedures, schedules and objectives		Operator with automated software support
Mission Control	Monitor S/C health and status, perform maintenance	Telemetry and command requests, TLEs	Pass reports, real-time commands		Operator with automated software support
Data Services	Gathering, managing, and distributing mission data	S/C H&S, science payload and experiments data	Accessible database of historical H&S, science & experiment data	Data gathered and packaged	Recv. from S/C, stored in DB distributed via internet to users
Navigation & Attitude Control	ADCS duties	Orbit TLEs	ADCS control outputs	ADCS / MM	Acquire TLEs and update on S/C
Spacecraft & Payload Operations	Analyze anomalies, payload and system engineering calibrations	S/C and Payload engineering data	Anomaly responses, command requests		S/C design team
Mission Assurance & Risk Mitigation	Validation of procedures, MM & FSW upgrades	Proposed improvements and activities	Approval or recommendations		Subsystem Specialists and Team Leads
Operator Training & Certification	Obtaining, Training, & Certifying Operators	Untrained Personnel	Certified DINO Mission Operators		Mission Operations Team

7 Mission Timeline

The DINO Mission Timeline outlines the sequence of major events for each phase of operation. The schedule is objective-driven, rather than a strict schedule. In other

words, the objectives are accomplished when it is reasonably possible, rather than as soon as possible.

There are four phases to the mission; Beginning of Life (BOL), Nominal Operations (NOMOPS), Standby, and End of Life (EOL). Each phase represents a substantial step forward in the progression of the mission. Each step has its own version of the Mission Module, to focus the autonomous operations of the satellite safely and appropriately.

In each section below, the flight and ground objectives are discussed and presented in a table, and the Mission Module functionality at this point is outlined.

7.1 Beginning of Life

The Beginning of Life (BOL) phase starts at launch, and continues until all systems in both the flight and ground segments are verified and certified for nominal operations.

The flight objectives for this phase are largely deploying the various mechanisms as possible, establishing radio contact with the satellite, and verifying spacecraft health and status. Every subsystem of the spacecraft will have its own verification checklist that details the functionality to be tested, and the satellite will run a series of ground-initiated exercises to test the overall system capabilities. See Table 2 for a summary of the objectives.

The Mission Module at this phase of the mission does comparatively little, polling and logging sensor values at a slightly faster pace than normal to obtain coverage across the orbit. Science functionality is limited to allowing the ground to verify that the onboard algorithms are functioning properly. It will contain the verification exercises discussed above, and will run these upon command from the ground.

The ground objectives consist of the overall ground segment verification, continuing operator training, and updating the simulators. The update of the spacecraft simulators is a particularly critical objective. This activity involves reprogramming the ground simulation software to more closely match the nominal conditions in space. The BOL phase gives us the chance to determine what "nominal" really means for DINO. The update allows the Mission Modules to be better tested and rewritten and makes it considerably easier for Mission Operators to use those simulation values to spot potential anomalies on the spacecraft. Finally, with a more realistically tested Mission Module, the next phase of the mission can safely continue, to the Nominal Phase.

Table 2: Beginning of Life Activities

	Objective Type	Objective	Timing (Mission Start Time/Duration)
1	FLT	Antenna Deployment	Post Separation or ~1000 sec / ~30 sec
2	FLT	ADCS Detumble	~1500 sec / ~2000 sec
3	FLT / GND	Establish Communications	First Pass / ~7 minute pass
4	FLT/GND	Determine S/C Health	First Opportunity / NA
5	FLT/GND	Verify S/C Systems	First Opp. / Unknown
6	FLT	Boom Deployment	First Opportunity / Unknown
7	FLT	FITS Deployment	First Opp. / Unknown
8	FLT	CTD Deployment	First Opp. / Unknown
9	GND	S/C Sensor Calibration	Multiple Passes / Unknown
10	GND	Update S/C Simulators	Unknown / Unknown
11	GND	Operator Training	Continuous

7.2 Nominal Operations

The Nominal Operations phase of DINO's mission is the day-to-day standard operation of the satellite. In this phase, all satellite systems have been verified, and any problems within the flight or ground segments of the mission have been solved. See Table 3 for a list of objectives in this phase.

There are fairly few nominal objectives, but each has a broad scope. Science and Experiment investigations constitute the bulk of the work. The onboard analysis of images will continue to be updated as possible. The FITS Solar Array, the Shape Memory Composite Hinges, and the gravity gradient boom will all be constantly monitored and evaluated. In the case of the boom, the battery life on the tip mass will limit the availability of this data to a short window. In particular the FITS Solar Array and the EMC Hinges are targeted for testing during thermal snaps and attitude maneuvers.

The Intelligent Operations aspect of the mission will be explored with increasingly complex Mission Modules, designed to maximize the autonomy of DINO. The Modules will continue to be developed in-house, with the aid of software experts.

As a housekeeping duty, the onboard propagator will be periodically updated with new Two Line Elements (TLE) that allows the propagator to better predict the current position of the satellite, and increase the accuracy of the ADCS system.

In keeping with the spirit of the CSGC, DINO will be increasingly visible and open to the public, with frequent tours of the facility, demonstrations and presentations. These activities are designed to show the next generation of

students the possibilities and challenges of engineering for space applications, and encourage all ages to further explore science and mathematics.

Table 3: Nominal Operations

	Objective Type	Objective	Timing (Mission Start Time/Duration)
1	FLT	Science	Continuous
2	FLT/GND	MM/FSW Upgrades	Continuous
3	FLT	Experiment Investigations	Continuous / Maneuvers
4	FLT	ADCS TLE Updates	Continuous / ~Every 2 weeks
5	GND	Increased Public Outreach	Continuous

7.3 Standby

The Standby Phase is a type of operations where the spacecraft is set up to survive as long as possible at a very basic level. This stage will occur in the event that the spacecraft has experienced a serious onboard anomaly, or may be ordered into this state to preserve battery life.

Standby is characterized by no science activity, the minimum attitude control, and minimum communications with the ground.

7.4 End of Life

The End of Life (EOL) phase occurs when the satellite is no longer capable of sustained nominal operations. Depending on the circumstances, DINO will eventually burn up in Earth's atmosphere. If the satellite is alive during this time, the ADCS system will take as many readings as possible, to characterize the final time of the satellite. On the ground, the mission will be followed by the Post Mission Review, where the entire mission is scrutinized with hindsight to determine what went well, what needed improvement, and what future applications DINO's systems could support.

Table 4: End of Life

	Objective Type	Objective	Timing (Mission Start Time/Duration)
1	FLT	Increased ADCS Readings	EOL
2	FLT	S/C Destruction in Atmosphere	Unknown
3	GND	Post-Mission Evaluation	EOL

Appendix A – List of Acronyms

BOL: Beginning of Life
CSGC: Colorado Space Grant Consortium
CTD: Composite Technologies Development
DINO: Deployed Intelligent Nanosat Operations
EOL: End of Life
EMC: Elastic Memory Composite
FITS: Foldable Integrated Thin-Film Stiffened
FLT: Flight
FSS: Flight Software System
GND: Ground
H&S: Health and Status Telemetry
MARM: Mission Assurance and Risk Mitigation
MCT: Mission Control Team
MM: Mission Module
MOC: Mission Operations Center
MOP: Mission Operations Plan
MOPS: Mission OPERATIONs Team
S/C: Spacecraft
STK: Satellite Tool Kit

Appendix B – Glossary

Mission Control Team: A team composed of a Supervisor, Data Analyst, and Communications Engineer. The MCT mans the Mission Operations Center during passes with the satellite, and is responsible for sending and receiving commands and data with the satellite.

Mission Module: An operator-written set of rules and responses that govern the autonomous operation of the satellite. This plugs directly into the flight software, where it interacts with hardware input and produces the appropriate commands for the flight software to execute.

Python: A high-level open-source programming language. DINO uses Python because of its ease of use, fast development time, and compatibility with Linux. See DINO-FSW-RPT-FSW and www.python.org for more information.



People Involved in DINO

DINO-PM-RPT-PEOPLE, Rev. A

Written by:
Jennifer Michels
Josh Stamps

Prepared for:
Nanosat III

Table of Contents

1	Scope.....	4
1.1	Identification.....	4
1.2	Document Maintenance.....	4
1.3	Systems Overview.....	4
1.4	Document Overview.....	4
1.5	Referenced Documents.....	4
2	Student Involvement.....	4
2.1	Wide Spectrum of Majors	5
2.2	Subsystems	5
2.3	Paid vs. Credit Students	6
2.4	Start Dates for People	7
3	Industry Involvement.....	8
3.1	Ball Aerospace	8
3.2	Composite Technologies Development	9
3.3	MicroSat	10
3.4	TiNi & Starsys	11
3.5	Planetary Systems Corporation	11
3.6	Lockheed Martin	11
4	K-12 Outreach.....	12
	Appendix A – List of Acronyms.....	14

1 Scope

1.1 Identification

This document applies to the DINO project, a project undertaken by the Colorado Space Grant Consortium at the University of Colorado at Boulder. This project is part of the Nanosatellite III Program sponsored by the Air Force Office of Scientific Research (AFOSR), Air Force Research Laboratory (AFRL), Association of Aeronautics and Astronautics (AIAA), and Goddard Space Flight Center (GSFC).

1.2 Document Maintenance

This document falls under the DINO document control requirements as specified under the DINO Configuration Management plan. All changes and updates must be made in accordance with the DINO CM plan.

1.3 Systems Overview

The purpose of the student-led Deployment and Intelligent Nanosatellite Operations (DINO) mission is to determine cloud heights from space, evaluate the performance of intelligent operations, and assess deployment technologies for nanosatellites including a gravity-gradient boom, memory composite hinges, and thin-film solar arrays.

1.4 Document Overview

Since January 2003, people have learned, taught, and been inspired through the DINO program. This program has become a place where students at the University of Colorado can work together and learn. Industry has used this spacecraft as a platform to test new technologies but in the process teach the students involved. Finally, university students have brought concepts of this program and space to K-12 students around the state.

This document will highlight the involvement of people over the last two years in the DINO project.

1.5 Referenced Documents

None

2 Student Involvement

A total of 102 undergraduate and graduate students at the University of Colorado as well as two high school students from Boulder High School have been involved with the DINO project since January 2003. The majority of students that begin working with Space Grant do so as credit students or volunteers. The University of Colorado offers three levels of independent study credit to students including both upper and lower level undergraduate credit as well as graduate credit. Alternatively, students

can apply for paid positions. There is limited availability for these positions and so they are reserved for students who offer exceptional technical or leadership skills. Furthermore, these positions offer only about half the salary of a normal engineering internship. However, internships do not offer students the opportunity to experience the same high-level technical challenges and leadership responsibilities as Space Grant can offer. In summary, Space Grant attracts students who value a hands-on education and real-world engineering experience beyond what the classroom or industry can offer them.

Space Grant does not keep detailed records of volunteer students. All of the numbers below revolve around students who were paid or have earned credit. The majority of the data has been taken from an online database that was created in the fall of 2003. Because of this, student involvement previous to the fall of 2003 is not completely accounted for.

2.1 Wide Spectrum of Majors

Students from seven different majors have been involved with the DINO project. Those majors are aerospace engineering, applied math, civil engineering, computer science, electrical and computer engineering, engineering physics, and mechanical engineering. Additionally, four of the students have not reported their majors to Space Grant. Figure 1 below is a graph showing the percentage of students in each major.

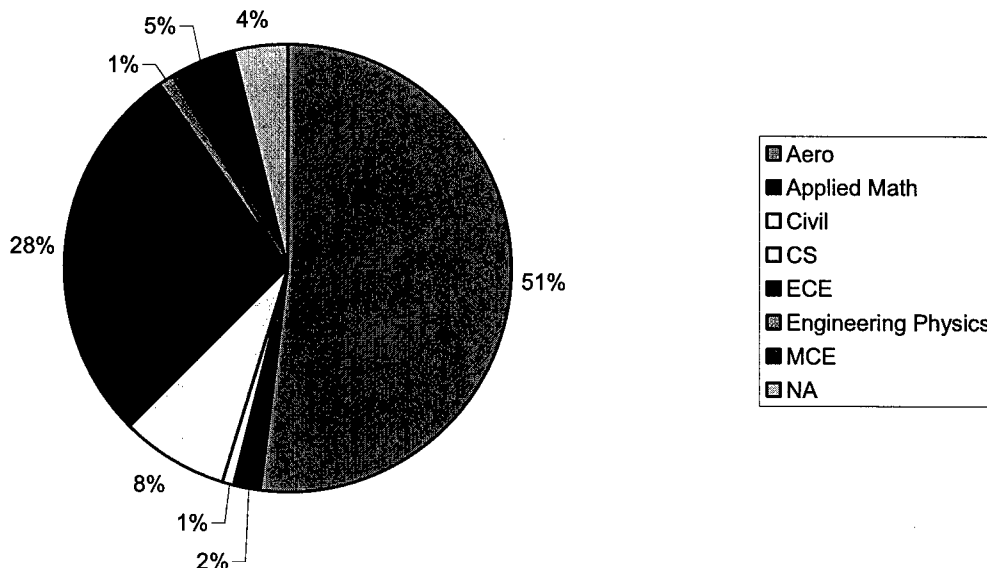


Figure 1: Percentage of Majors

2.2 Subsystems

There are 14 different subsystems on DINO. Below, in Figure 2, is a graph showing the percentage of the DINO team contributing to each subsystem.

Several students have worked on more than one subsystem. Each student was included each subsystem that they participated in.

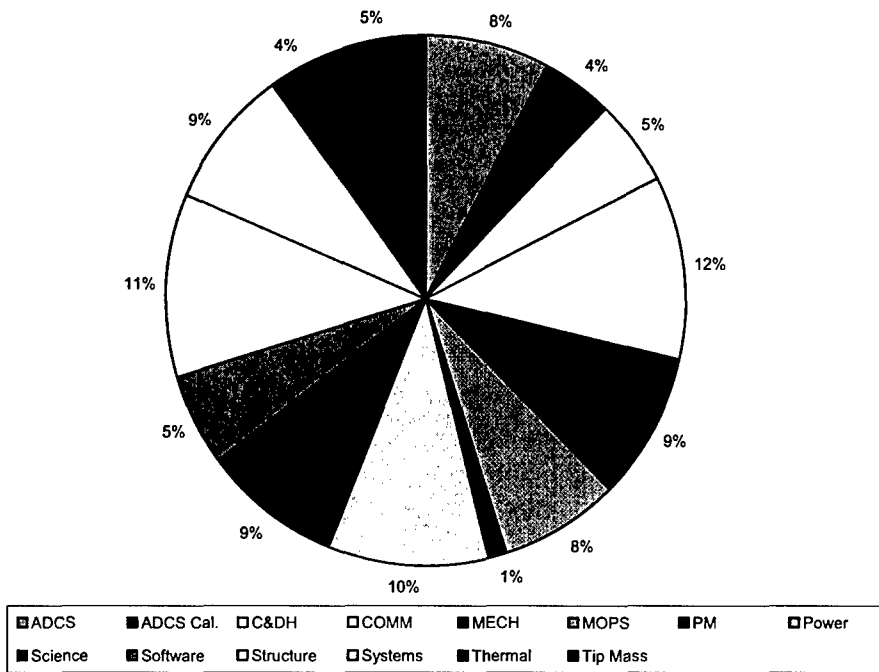


Figure 2: Subsystem Percentages

2.3 Paid vs. Credit Students

Below, in Figure 3, is a graph depicting how many paid students there are versus how many credit students.

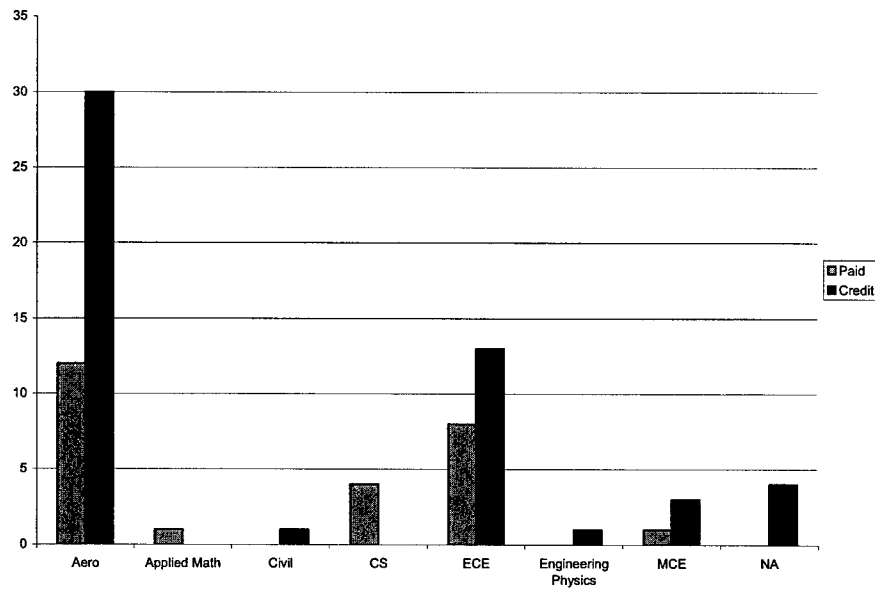


Figure 3: Number of Paid vs. Credit Students

2.4 Start Dates for People

As expected there is significant turnover at the transition between each semester. Most of the time, this is a result of students graduating and/or obtaining jobs. This shows that Space Grant is accomplishing its main objective, which is to prepare students for their careers. One trend that the project was pleased with is that most students involved in the completion of the DINO project started in the fall of 2003. This means that DINO was able to obtain a large number of students at the beginning of the project maintain their interest and enthusiasm until its completion.

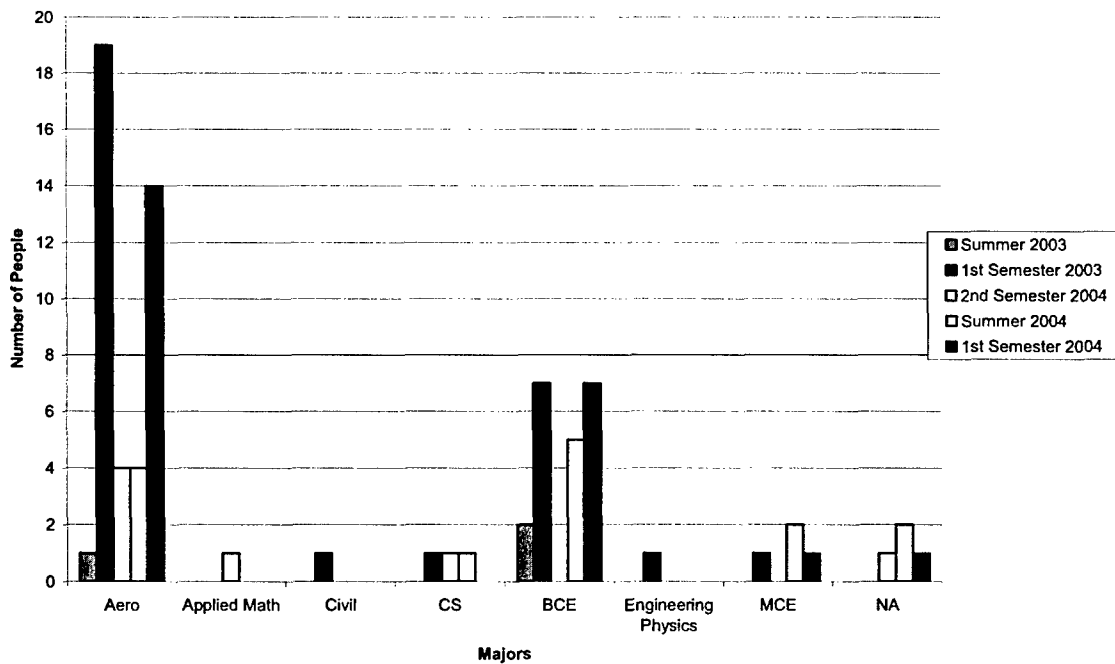


Figure 4: People's Start Date

3 Industry Involvement

DINO has been very fortunate in the amount of industry involvement with the project. Support from industry has ranged from hardware donations, monetary donations, real world training, and in many cases employment opportunities. Perhaps the most valuable donation is the mentorship that comes with each of these generousities. The industrial relationships have proven to be mutually beneficial to both Space Grant and the donating companies. This is made evident by the fact that several companies have elected to support Space Grant in every way mentioned above.

Ball Aerospace, Composites Technology Development, and MicroSat were three such companies that contributed in a variety of ways. Each of these companies donated hardware while also providing advising and employment opportunities. In the design of DINO, several components were also required that were beyond the financial scope of the project. In these cases, other companies were contacted for donations. Many were more than happy to contribute hardware and advising such as TiNi, Starsys, Planetary Systems Corporation, and Lockheed Martin. The contributions of each company are expanded on below, as well as descriptions of the relationship between each of them and Space Grant.

3.1 Ball Aerospace

Ball Aerospace is working in conjunction with the DINO team on the power subsystem. The power team at Ball Aerospace is currently developing an innovative method for packaging power systems in satellites. Ball engineers determined that working with students to develop this concept would be a more cost-friendly idea than pursuing the same development process at Ball. The

original concept for the physical portion of the power system was developed entirely by Ball engineers. Students however, accomplished the majority of the electrical design. During the design process, the Ball engineers took an advisory role to the Space Grant students responsible for procuring parts, building, and testing the system. Ball was happy enough with the project that many of the Space Grant students involved with it were offered employment as they approached graduation. In result, many students had the unique opportunity to work on the power subsystem from both the Space Grant and the Ball perspective.

Ball Aerospace was very generous to the program by donating hardware, money for hardware and student salaries, vibration and thermal vacuum testing, and mentorship. Out of everything that Ball has done for DINO, the mentorship has been the most valuable. Once a week two to four Ball engineers would come to the Space Grant offices. The original purpose of these meetings was to go over the status of the power system exclusively, but the meetings evolved into much more as the Ball engineers would always make time to answer the questions of other DINO subsystems. In fact many of these 'other' subsystems inherited advisors as a result. For example, the thermal team was in need of advising and so inherited the mentorship of at least three thermal engineers at Ball in the areas of radiation heat transfer analysis, thermal modeling, and MLI blanket design. A similar situation occurred with the DINO wiring harness team. Ball engineers have also provided consistent advice with scheduling and presentations.

The engineers at Ball have helped guide the DINO project over the last two years. They have been patient and understanding with the small mistakes sometimes committed by undergraduate students, as they are primarily interested in the learning experience of the student, but have also helped prevent large mistakes from occurring. The hardware and monetary donations have assisted DINO significantly but has been nothing in comparison with the time donation that engineers have given to the students.

3.2 Composite Technologies Development

Composite Technologies Development, CTD, is another company that has invested a considerable amount of resources into Space Grant in the form of hardware, funding, and mentorship. CTD is an emerging company that is developing around composite technologies. Since this company is new, it is currently working to obtain flight heritage. For this reason, CTD has selected DINO as an inexpensive way to demonstrate the performance of their EMC hinges.

CTD engineers designed and fabricated the hinges while Space Grant students conducted several functional and performance tests on them as well as designed the supporting hardware and electrical interfaces. Space Grant students

determined how the hinges would be utilized and completed the final assembly and integration of them.

The challenge for Space Grant was then to determine the best way to utilize this technology. Originally the EMC hinges were intended to deploy two aerofins from the side of the spacecraft in order to help with attitude control. After some analysis, the DINO team determined that the aerofins would actually lend minimal benefit with significant costs in mass. During the Nanosat III Subsystem Design Review a reviewer suggested putting an experiment on a deployable panel that would allow the spacecraft to measure the performance of the EMC hinges. After considering a few other options, this became the ideal alternative as it provides Space Grant with the opportunity to produce a detailed analysis of the hinge performance to CTD. In order to do so, the hinges have been mounted so as to deploy a panel 180°. This panel has a rate gyro mounted to it that will provide data indicating the performance of the hinges that deploy it.

Most of the work with CTD occurred during the summer of 2004. During this time the DINO team worked with two CTD employees. One of the two employees was another student from the University of Colorado. He was working at CTD on a summer internship. This allowed the DINO team to work with another student in a different setting.

3.3 MicroSat

MicroSat Systems, Inc. has contributed to DINO by donating their Foldable Integrated Thin-Film Stiffened (FITS) Solar Arrays. FITS was developed so as to provide maximum surface area with minimal stowage area. FITS can be folded and stowed up against a structure. By using their FITS Solar Arrays, DINO will reduce the solar array mass needed by 50%.

The efficiency of thin-film solar arrays is less than the efficiency of triple junction body mount solar arrays. Currently body-mount solar arrays can provide up to 28% efficiency where thin-film arrays can only provide around 8% efficiency. What the thin-film arrays lack in efficiency they make up for with maximum surface area and minimum mass. FITS will provide DINO with 90W of power at a cost in mass of 4kg. DINO is not only demonstrating this technology but is also depending on it as its primary source for power. The flight-data that DINO will then provide MicroSat will characterize the FITS solar array's performance in a space environment. This data will also benefit AFRL's Roadrunner project, for which application of the FITS system is intended.

The cells were entirely designed by MicroSat engineers, while Space Grant students designed the supporting hardware and electrical interfaces. Space Grant students also participated in the final assembly of the FITS engineering design unit as well as its final integration onto DINO.

3.4 TiNi & Starsys

The hardware donated by Ball, CTD, and MicroSat will help DINO accomplish its mission. However, these generous donations created new design challenges, as each component requires both mechanical and electrical interface designs. Furthermore, the CTD hinges and the FITS system are intended for deployment and so a method for stowing and releasing each component is also necessary. The same must also be designed for the antennas, as both will be stowed initially and will be deployed after orbit insertion. Enough actuators must be obtained so as to release the CTD panel, FITS system, and each antenna. These actuators must not only be appropriate for the deployment itself but also must have minimal costs to mass, power, and the budget. Most low mass, low power actuators come with a high price tag so Space Grant students explored several design alternatives and approached each respective company with donation requests. Two companies responded: TiNi and Starsys.

TiNi donated two FrangiBolt actuators to DINO. One FrangiBolt is being used to restrain the CTD deployment panel and the other to restrain the FITS solar array. The FrangiBolt is a bolt that is designed to fracture. This bolt is placed inside an actuator that expands upon heating until the bolt snaps in half. Both ends of the fractured bolt need to be contained so as not to harm other subsystems inside the spacecraft and to prevent unnecessary space debris. Space Grant students designed support hardware in order to satisfy these requirements. For example, each FrangiBolt is housed such that the fractured bolts are permanently contained and their kinetic energy after fracture is absorbed by springs.

Starsys donated a third actuator for the antenna deployment, which is a High Output Paraffin, HOP, actuator. This device is a titanium can containing paraffin that expands causing a pin to be pulled slowly and smoothly. In order to utilize one HOP for two antennas, Space Grant students designed supporting hardware. Starsys engineers also donated time for reviewing mechanical designs, even those not necessarily related to the HOP.

3.5 Planetary Systems Corporation

Planetary Systems Corporation (PSC) is donating the Lightband system that will be used to actuate the boom deployment. This will be used to deploy the gravity gradient boom, and is identical to the system being used for the separation of DINO from the Internal Cargo Unit (ICU). PSC has also provided mentorship at the Nanosat III reviews.

3.6 Lockheed Martin

Lockheed Martin is donating solar cells for the body mount solar arrays. These solar cells were designed and manufactured in house at Lockheed Martin, and are the innovative design remains proprietary information. However, Lockheed Martin provides advising in designing support hardware and will leave the final integration of these panels to Space Grant students.

4 K-12 Outreach

K-12 outreach is very important to the DINO project, and is perhaps one of the strongest components of Space Grant as a whole. An individual outreach team leader organizes outreach activities that are to be facilitated by volunteers. These volunteers are the very same students who do all of the engineering work for Space Grant satellite projects. Over the last two years DINO student volunteers have facilitated various outreach activities that have involved at total of 2,509 K-12 students. This does not include the activities run by students involved in non-DINO projects. Several K-12 students are counted more than once because some have participated in multiple activities including tours, interactive activities, classroom demonstrations, summer workshops, and many other similar endeavors.

Space Grant is not only interested in the quantity of students reached, but also the quality in which they are reached. Space Grant targets students who demonstrate the greatest need for exposure to science and engineering. These students are generally found at low-income schools attended by under-represented minority students and/or financially challenged students. Understandably, these schools receive priority although there are countless requests for outreach activities from a variety of schools. One way this is accomplished is through the recent commitment to adopt one elementary school per semester in order to supplement their science program with a four-week after-school activity program based on space technologies. This has now been done for each of the last three semesters.

The schools that were adopted so far have been part of the Mathematics, Engineering, and Science Achievement, (MESA), program, <http://www.cmesa.org>. This program is intended to serve K-12 schools that are in need of certain educational or financial resources. The schools that have been adopted thus far are Spangler Elementary in Longmont, Colorado (Fall - 2003), Fitzmorris Elementary in Aurora, Colorado (Spring - 2004), and Loma Linda Elementary in Longmont Colorado (Fall - 2004). Each of these programs lasted four weeks, and was developed around space technology, engineering, and the scientific process as related to the DINO project.

The number of K-12 students exposed to engineering concepts and space for each month over the last two years can be seen in Figure 5 below.

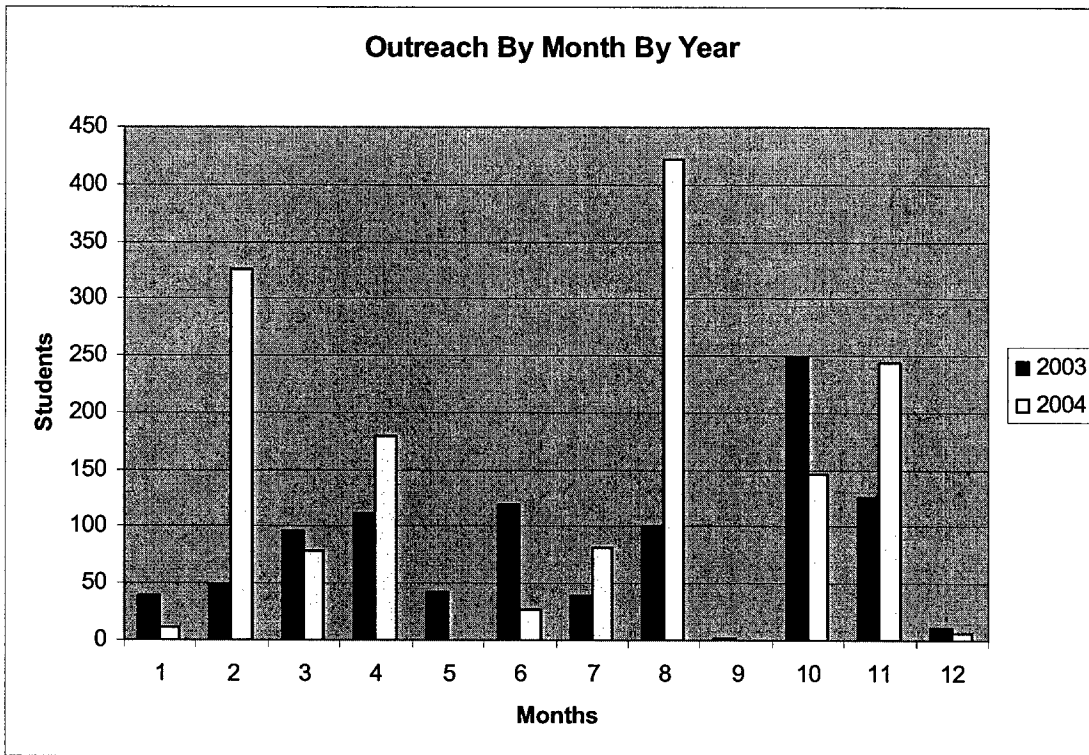


Figure 5: Outreach Numbers by Month

Appendix A – List of Acronyms

AIAA	American Institute of Aeronautics and Astronautics
AFRL	Air Force Research Laboratory
AFOSR	Air Force Office of Scientific Research
CTD	Composite Technologies and Development
DINO	Deployment and Intelligent Nanosat Operations
EMC	Elastic Memory Composite
FITS	Foldable Integrated Thin-film Stiffened
GSFC	Goddard Space Flight Center
HOP	High Output Paraffin
ICU	Internal Cargo Unit
MESA	Mathematics, Engineering, and Science Achievement
MLI	Multi Layer Insulation
PSC	Planetary Systems Corporation



Subsystem Description

DINO-PWR-PRT-SYSDS, Rev. A

Written by:
Mike Wong

Prepared for:
Nanosat III

Table of Contents

1	Scope.....	4
1.1	Identification.....	4
1.2	Document Maintenance.....	4
1.3	Systems Overview.....	4
1.4	Document Overview.....	5
1.5	Referenced Documents.....	5
2	Power Generation.....	6
3	Batteries.....	6
3.1	Power Storage	
3.2	Primary 9V Deployment Battery	
4	Mission.....	Error! Bookmark not defined.
5	EPS Controls	
6	EPS Control Card	
7	Charge Control	
8	Pulse Width Modulator	
9	Power Lines	
10	Grounding	
11	Safety	
12	Inhibits	
13	Power Structure	
	Appendix A – List of Acronyms.....	11

1 Scope

1.1 Identification

This document applies to the DINO project, a project undertaken by the Colorado Space Grant Consortium at the University of Colorado at Boulder. This project is part of the Nanosatellite III Program sponsored by the Air Force Office of Scientific Research (AFOSR), Air Force Research Laboratory (AFRL), Association of Aeronautics and Astronautics (AIAA), and Goddard Space Flight Center (GSFC).

1.2 Document Maintenance

This document falls under the DINO document control requirements as specified under the DINO Configuration Management plan. All changes and updates must be made in accordance with the DINO CM plan.

1.3 Systems Overview

The purpose of the student-led Deployment and Intelligent Nanosatellite Operations (DINO) mission is to determine cloud heights from space, evaluate the performance of intelligent operations, and assess deployment technologies for nanosatellites including a gravity-gradient boom, memory composite hinges, and thin-film solar arrays.

1.4 Document Overview

The system is direct energy transfer with a secondary lithium-ion battery for the main satellite, a primary 28V battery for the deployable devices, a main solar array the Foldable Integrated Thin-film Stiffened (FITS) and body mount solar array. The body mount solar array will have a start up 12V start up string that will go power up the satellite upon release from the shuttle. The batteries shall have a three-fault tolerance inhibit system to prevent the satellite from turning on prematurely. The expected efficiency of the entire system is estimated to be 80%. The system will provide voltage lines of 5, +12, -12 and 28. The system will use up to 120W of power while using 70W during regular operations. The system is designed for a mission life of one year, while the expected duration of the mission is six months. The satellite must remain off until it leaves the Internal Cargo Unit (ICU) and no deployment can occur until after the satellite is a safe distance away from the shuttle. The system's design is proprietary by Ball Aerospace Technologies Corporation (BATC). The EPS system will be located on the zenith plate of the satellite. A power control card will provide functions of charge control, power conditioning, conversion and distribution. The EPS system will use a star node configuration-grounding scheme with the center node being the EPS system. The EPS system will take commands from C&DH through an RS-422 serial line. Health and status will be sent to C&DH when requested. EPS will also receive a status signal from C&DH to determine if it is operational. When the signal is not received within a 10-minute time

span power to C&DH will be turned off and reestablished two seconds after power us cut. The system shall have four modes of operations: normal daytime operations, normal nighttime operations, deployment mode and safe mode.

1.5 Referenced Documents

None

2 Power Generation

The satellite will be power by the FITS solar array provided by Microsat Systems inc. The FITS will provide a minimum of 90W during end of life with an expected value of 19V. The FITS are 8% efficient and is expected to increase in efficiency when the satellite is delivered for flight. The FITS is series of Gallium-copper cells connected together to form strings. The FITS will be folded up and unable to provide power to the satellite until it is deployed by a frangibolt. The deployment of the FITS will be completed within a 30 second time frame. The FITS is a single solar array with a minimum of 4 strings going into the EPS card. The FITS shall last for the entire mission duration of 6 months and be designed to last for the mission goal of 1 year. One of the solar array strings shall be capable of being pulse width modulated to a increase the systems efficiency. By pulse modulating the string it will allow the system to receive the needed power and let the excess power dissipate into heat on the solar array.

The body mount solar array shall be capable of supporting the satellite should the FITS be unable to provide the power needed. Due to the constraints of surface area and cell efficiency the maximum power the body mount will produce is 25W. The body mount array shall be place upon four of the side panels. The body mount will contain a string specification to startup the satellite. The startup string will have a voltage of 12V and will be located on 2 of the side panels. The body mount array shall be inhibited by the EPS card with a MOSFET switch while the startup string shall be inhibited by the separation switches of the lightband.

3 Batteries

3.1 Power Storage

The system will store power in lithium-ion polymer cells with a capacity of 4Ahr and nominal voltage 3.7V and a maximum voltage of 4.1. The main battery will be composed of 4 lithium-ion cells connected in series and have a nominal voltage of 14.8V. The lithium cells will be the main battery for the satellite. The battery is sized to last three eclipse periods before charging is needed and has an expected life of 2,000 cycles of charging and discharging. The battery shall be discharge to 75% of its maximum capacity at the end of the three eclipse periods. The battery shall not be discharged below 60% capacity. The battery will lose all capacity once it is discharged completely and discharging below 60% will cause major capacity loss.

The battery will have a current monitor, a voltage monitor, voltage monitors for each cell and 2 sets of thermal couple: 1 set for flight and the other for ground support equipment. The charge plan for the battery is to perform sub-capacity charging to 95% for the default of the mission, occasionally charge the battery to 100% to recharge the battery to full capacity and charge the battery to 103% to recover capacity of battery near the end of the mission. Ball will certify the battery in their facilities with the assistance of CSGC students. The inhibit scheme will require 1 inhibit on the negative leg and 3 on the positive leg to satisfy the three fault tolerance requirement.

3.2 Primary 9V Deployment Battery

Six 9V alkaline cells will power the deployable devices. The battery cells will be configured as shown in figure 1. Each cell has a mass of 50 grams and the entire assembly will have a total mass of 300 grams. The battery will be flown fully charged and is expected to have 1 inhibit on the negative leg and 3 on the positive leg. This is done to comply with NASA safety standards and prevent any early deployments of the devices. The battery will be independent from the rest of the satellite and is meant for a one-time use so it will not be charged. This battery will be used only to trigger the HOPS, lightband system, frangibolts and the memory hinges. The battery shall be capable of supplying 1.4A at anytime during the deployment. The devices shall be deployment one at a time and all deployments are to be completed during the first week of the mission. These batteries shall have the air vents pointed up to satisfy NASA safety requirements. The battery shall have a voltage monitor, a current monitor and one thermal couple placed in the center of the battery configuration.

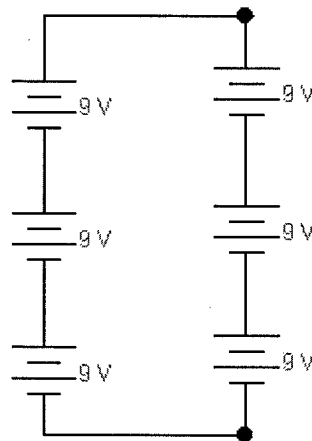


Figure 1

4 Mission

The system must provide power to the satellite for the mission duration of 3,500 cycles (approximately six months) and power for the mission goal of 7,000 cycles. The satellite shall be in an ISS orbit and must comply with shuttle safety standards. The primary battery must power the satellite for three eclipse times of 35 minutes each. The satellite will be in the sunlight for an average time per orbit 55 minutes. The power system will test and exhibit the technologies of MicroSat Inc., BATC, Broad Reach Engineering and Spaceworks Corporation.

5 EPS Controls

The system will take samples of all of the monitors and sends the information when requested by C&DH. The system shall depend upon the C&DH to give instructions on what tasks to perform. The EPS card will be connected to C&DH through a RS-422 line. The EPS shall have total control over the solar arrays, the charge control and the Power on Reset while C&DH will have control over the power switches and monitor data. The EPS shall monitor a signal from C&DH to determine its current status. If the signal is not received in a time span of 10 minutes the EPS system shall open the switch supplying power to the flight computer to cause a reset. The power shall be turned off for two seconds and power will be restored. EPS will go into a default mode until the C&DH instructs the system otherwise.

All switches on the system are controlled by a high or low signal. A high signal of 5V will close a switch and complete the circuit. A low signal of 0V will open the switch causing a break in the circuit. All switches except for the C&DH switch will remain open until it is instructed to close. The C&DH switch will remain closed until instructed to open. This is done to ensure the system will turn on once the satellite leaves the ICU and it makes the Power On Reset (POR) easier to design. The inhibits used are latching relays that are open until instructed to close and once instructed to close the latching relays remain closed.

6 EPS Control Card

The EPS control card shall use a PIC microcontroller to control the functions on the card. The microcontroller will communicate with C&DH through an RS-422 serial line. EPS will send health and status of the card to C&DH when requested. EPS shall control a watchdog timer to turn off the power to C&DH when a monitored heartbeat signal is not received for a time span of 10 minutes. The heartbeat signal will be sent over the RS-422 serial line as well as a dedicated I/O line. When the signal is not received EPS shall cut power to C&DH for two seconds and then restore power. For the microcontroller to handle all of the I/O signals on the EPS card expander chips will be used to increase the amount of I/O the PIC can process. The EPS card shall control all functions of the solar array, the FITS, the PWM and the charge control.

The MPU used for the EPS card will be a PIC16C77. The MPU uses RISK architecture and 35 word instructions. It is a 8-bit microcontroller with a 12-bit A/D and three timers. The capture feature is 16-bit with a maximum resolution of 12.5 ns. The compare feature is 16-bit with a resolution 200 ns. The MPU also provides support for high/low speeds and a 9-bit address mode supporting Universal Synchronous Asynchronous Receiver Transmitter.

7 Charge Control

The control card will have three settings for charging the main battery. The sub-capacity charge will charge the battery at 1.7A until the voltage reaches 95% of its capacity. This is done to increase the power efficiency in the system and prevent the cells from overcharging. The full-capacity charging will charge the battery stack until the battery is fully charged once again. This is done to maintain the capacitance and to help the battery cells maintain similar characteristics. The overcharge will charge the battery to 103% to extend the life of the battery when the cells start to degrade. To ensure the battery is charged to the appropriate level a comparator will be used to control the charging. Once the voltage level exceeds the upper limit on the comparator charging will be turned off. The comparison voltage will be altered according to the desired charge mode.

8 Pulse Width Modulator

The pulse width modulator (PWM) is a MOSFET switch that will be toggled to produce a desired average current. Using a PWM increases the efficiency of the power system by supplying the system with the amount of power required and leaving the excess power to be dissipated into heat on the solar array. The PWM open switches until power draw is constant then toggle switches until a stable power use is established. The PWM will adjust itself to supply the satellite with enough power. The PWM will be controlled only by the EPS microcontroller.

9 Power Lines

The system will have voltage lines of 5, +12, -12 and 28. The power supplies for the 12V line shall be rated to 30W and the 5V line shall be rated to 25W. A battery rated to 2.1 Ahr at 27V will source the 28V power lines.

10 Grounding

DINO shall use a star pattern for its grounding scheme. The center node of the star pattern shall be the EPS card and all return paths will go to the EPS card. The EPS card shall have a 3 Mohm resistance between itself and the structure.

11 Safety

NASA's safety documents state that all power sources must have at least 3 inhibits to prevent the sources from being turned on prematurely. One inhibit must be on the negative leg. The batteries DINO intends to use will be lithium-ion polymer chemistry, it will require 4 inhibits. The main and secondary battery will both be fully charged and requires higher safety precautions. The solar arrays will only need 1 inhibit because the satellite will be in an ICU, there will be no light for the solar array to power the satellite and that can be counted as an inhibit. More details on how the lithium-ion batteries will pass safety concerns will be provided by Ball Aerospace. The 28V battery will also use 4 inhibits as well due to the fact it will be charged during the launch. The 28V battery will be in an enclosed box and contain a venting hole to let out any gases that will cause hazards to the system. Inhibits for the solar array and batteries will trigger once the micro switches close, that will give power to the essential systems. The other inhibits will be controlled by the EPS card by commands from C&DH.

12 Inhibits

The EPS card shall use latching relays as the inhibits for the batteries and MOSFET switches for the loads of the satellite. The latching relays are used for the battery because they can handle large amounts of current and remain in their current position until instructed to change. Once the latching relays are closed they will remain closed to minimize risk should the EPS card come across a failure. MOSFET switches are used for the loads due to their simplicity and the switches default to an open state. All switches and inhibits are controlled by the EPS micro-controller, the switches and relays respond to a high low signal of 5 and 0V

13 Power Structure

The power structure will be fabricated by SpaceWorks and delivered to CSGC. CSGC will determine the dimensions and basic outline of the structure. SpaceWorks shall determine the power structures composition, properties, fabrication and tooling. The power panel will be the entire zenith panel of the satellite. The power panel shall integrate itself with the structure and provide mounting for the boom and the rest of the satellite. The structure will also house the battery assembly and dissipate the heat generated by the power system. The structure shall be design to account for the light band separation and the deployment of the boom.

The structure shall be composed of a graphite fiber reinforced epoxy resin and space qualified epoxy. The main panel shall consist of MS1D and MS4A. The power panel will have a radius of 39.77cm, a thickness of 1.91 cm and have a mass of approximately 2.10 kg. The structure shall have an aluminum interface with the satellite side panels for integration. The structure shall be conductive with the rest of the satellite.

Appendix A – List of Acronyms

ADCS- Attitude Determination and Control System
BATC – Ball Aerospace Technologies Corp.
C&DH –Command and Data Handling
COMM- Communications
CSGC – Colorado Space Grant Consortium
EPS – Electrical Power System
FITS – Foldable Integrated Thin-film Solar
ICU - Integrated Cargo Unit
PWR- Power

DINO Science Subsystem Stereoscopic Imaging: Gradient-Based Stereoscopic Algorithm

Pascal Getreuer

A major goal in the DINO Satellite project is to implement stereoscopic imaging based on photographs from the on board digital cameras. In order to reduce the amount of data transmitted to ground, most of the stereoscopic processing is to be done on the satellite itself. In previous reports, we developed the pre-processing necessary to compensate for camera orientations and nonlinear lens distortions. This report covers specifically the theory of the stereoscopic algorithm, basic implementation, optimizations, and demonstration of the algorithm's results on real photograph.

The goal in stereoscopic imaging is to find the local horizontal and vertical translations between two images. Stereoscopic imaging is one of the earliest and most actively investigated topics in computer vision; this is a non-trivial problem. A great pitfall in attempting stereoscopic imaging is the assumption that matching individual pixels between the two images yields the translation. The amount of local information at each point is insufficient to solve the matching problem; if the similarity were to be maximized for each point in isolation, the result would be noisy and inconsistent. Instead, a multi-scale approach is necessary. Another difficulty is that directly comparing pixel intensities is unstable. In practice, individual cameras have differing additive and multiplicative intensity factors, thus comparisons must be made in another way.

Implementation Concerns

As most of the processing is to be done on the satellite, in addition to the algorithm's reliability, some concerns are algorithmic complexity, workspace memory, code memory, floating-point operations, and MATLAB to C++ translation. In addition, the amount of data transmitted to the ground is a significant concern. While these issues seem to be more of the software group's interest, the computational intensity of this algorithm requires collaboration and careful thought for effective realization on DINO's computer system. Approaches to some of these implementation challenges will be proposed.

Gradient-Based Stereoscopic Imaging

The stereoscopic imaging algorithm discussed in this report is based on Scharstein's [3] gradient-based approach. The basic procedure is

- Pre-processing filtering
- Approximating image gradients
- Multi-scale aggregation and matching
- Post-processing filtering

In the (optional) pre-processing step, bandpass filtering and edge enhancement improve the image clarity in the matching steps. Image gradients are approximated for use in the matching criterion. The actual matching is done by finding the best match measure for every translation for every pixel for multiple scales through aggregation of a similarity measure over local neighborhoods. A rough translation map results from this main procedure. In post-processing, occlusion boundary effects are reduced with edge enhancement and constant depth extrapolation fills in unmatched regions.

Measures for Matches

Stereoscopic imaging is often based on two separate measures for matching at a point, a “confidence” measure and a “difference” measure. Given the intensity gradients \vec{g}_1 and \vec{g}_2 ,

$$\frac{1}{2} (\|\vec{g}_1\|_2 + \|\vec{g}_2\|_2)$$

measures the confidence of a match while

$$\|\vec{g}_1 - \vec{g}_2\|_2$$

measures the difference. While many algorithms consider the two measures separately, Scharstein’s particular algorithm combines them into one measure of the “evidence” of a local match

$$E = \frac{1}{2} (\|\vec{g}_1\| + \|\vec{g}_2\|) - \alpha \|\vec{g}_1 - \vec{g}_2\| \quad (1)$$

where α is a parameter to tune the selectivity of the matching. According to Scharstein, $\alpha = 1$ is a good choice and its exact value does not significantly change the results.

Approximating Gradients

The evidence measure (1) requires the intensity gradients of both images. Let $I_1(x, y)$ be the intensity of the first image at pixel (x, y) and similarly let $I_2(x, y)$ be the intensity for the second image. The gradients can be approximated with the Sobel filter, which is composed of a derivative filter along one direction and a prefilter in the orthogonal direction. This construction provides smoothness over simple differencing.

$$\frac{\partial}{\partial x} I_i(x, y) \approx I_i(x, y) * \begin{bmatrix} -1 & 0 & 1 \\ -2 & 0 & 2 \\ -1 & 0 & 1 \end{bmatrix} \quad \frac{\partial}{\partial y} I_i(x, y) \approx I_i(x, y) * \begin{bmatrix} 1 & 2 & 1 \\ 0 & 0 & 0 \\ -1 & -2 & -1 \end{bmatrix} \quad (2)$$

An alternative are Simoncelli’s filters, designed such that the derivative filter is a good approximation of the derivative of the prefilter. The 3×3 horizontal filter is

$$\begin{bmatrix} 0.2242 \\ 0.5516 \\ 0.2242 \end{bmatrix} \times [-0.4553 \quad 0 \quad 0.4553]$$

and the 5×5

$$\begin{bmatrix} 0.0357 \\ 0.2489 \\ 0.4308 \\ 0.2489 \\ 0.0357 \end{bmatrix} \times [0.1077 \quad -0.2827 \quad 0 \quad 0.2827 \quad 0.1077]$$

For both the Sobel and Simoncelli filters, Scharstein recommends also applying a light smoothing filter such as a Gaussian filter with $\sigma = 0.5$ pixels to the gradient approximation to attenuate quantization errors.

Aggregation

Combining the evidence measure (1) and gradient approximation (2), the evidence for a local match at point (x, y) for translation δ is

$$E_\delta(x, y) = \frac{1}{2} (\|\nabla I_1(x, y)\| + \|\nabla I_2(x + \delta_x, y + \delta_y)\|) - \alpha \|\nabla I_1(x, y) - \nabla I_2(x + \delta_x, y + \delta_y)\| \quad (3)$$

As stated earlier, the goal is *not* to match isolated points but to maximize the similarity between neighborhoods. Thus, we must aggregate the evidence measure $E_\delta(x, y)$ in a local neighborhood. One possibility is a Gaussian filter with standard deviation σ ,

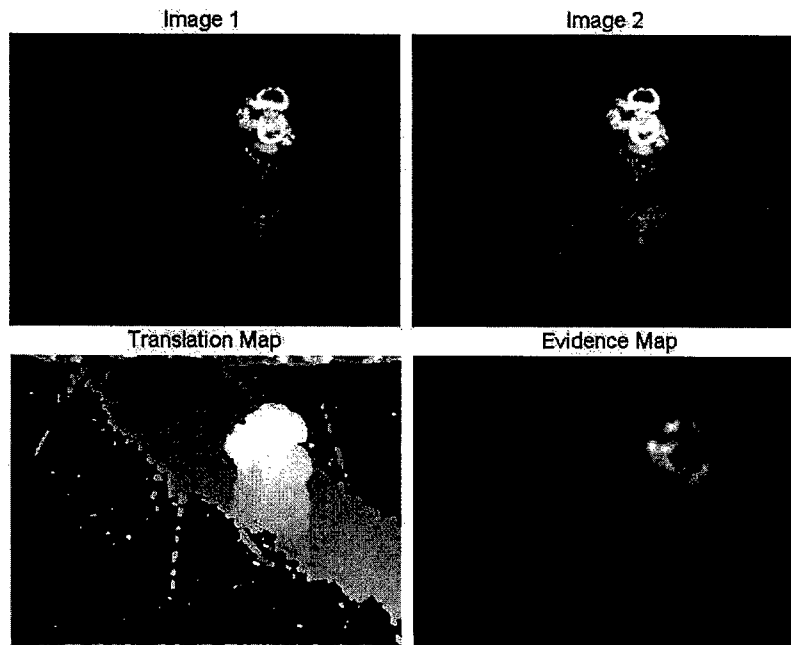
$$\text{GaussianFilter}(E_\delta)(x, y) = E_\delta(x, y) * \frac{1}{2\pi\sigma^2} e^{-(x^2+y^2)/(2\sigma^2)} \quad (4)$$

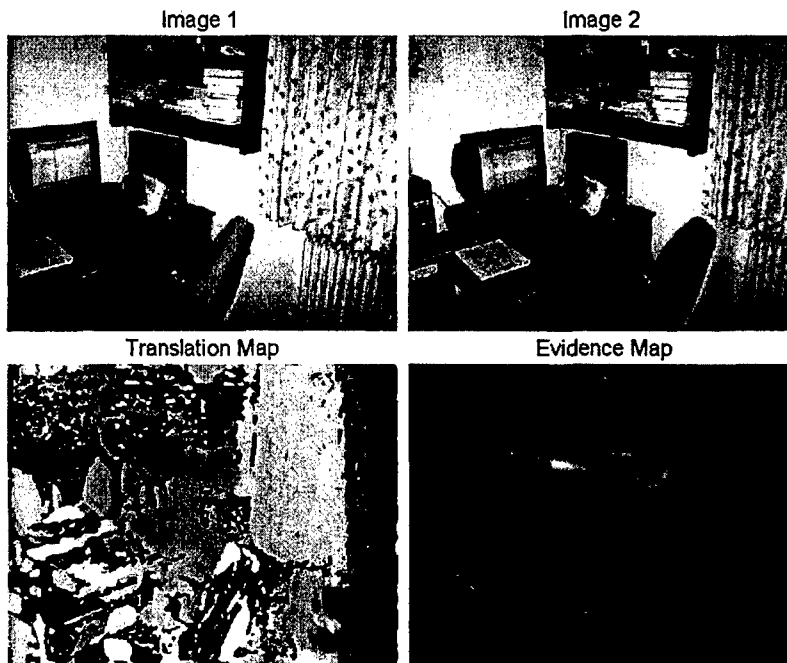
With the smoothed evidence map, matching is done at multiple scales. The best δ in some range is found for each pixel at varying neighborhood sizes. This approach suppresses false matches and fills in less textured areas at the larger scales, and can identify sharper features at finer scales. For the 512×384 pixel test images, a scale at $\sigma = 2.2$ and at $\sigma = 7$ were used.

Aggregation is based on the assumption that the translation δ is almost the same for neighboring pixels, observing that typical natural scenes are composed of solid, continuous surfaces. Discontinuities at object edges and occlusion boundaries disrupt this assumption and result in bleeding and blurring artifacts in the translation map. Occlusion boundaries are the biggest problem in aggregation stereo methods, however, the effects can be cleaned up somewhat in post-processing.

Experimental Results

The aggregation step is the bulk of the algorithm's work, resulting with a rough translation map of size $N_x \times N_y$. Points where the evidence measure (1) is negative for all attempted translation are left "unmatched" in the translation map. Here are some raw translation maps produced by my MATLAB implementation of the stereoscopic algorithm on real photographs (scaled to 512×384 pixels). In the images below, lighter shades in the translation maps are closer, darker are further, and black marks unmatched regions. The evidence at each point for the best translation is shown with lighter shades indicating stronger matches. Notice that more textured regions correspond to better evidence measures.



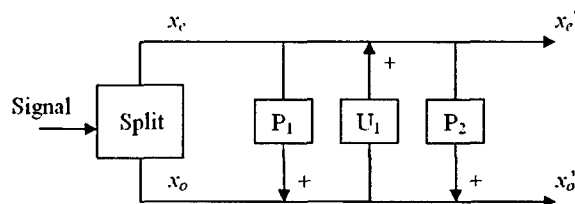


Translation Map Compression

Due to the limited transmission rate, the data sent to the ground must be under 20 kilobytes (20480 bytes). For a translation map of size $N_x \times N_y$ using one byte per pixel, the largest square map possible is only 143×143 . For better resolution, it is necessary to compress the translation map.

One promising method for lossy and lossless image compression are integer-to-integer wavelet transforms. Wavelet transforms typically outperform JPEG DCT-based compression. Furthermore, JPEG suffers from blocking artifacts, and as post-processing includes edge-enhancement, this is not acceptable. Integer-to-integer wavelet transforms can be performed in place using only integer operations; they are computationally efficient.

Wavelets factored into a Lifting Scheme are performed through a sequence of “predict” and “update” stages.



The input signal x is first split into the even x_e and odd x_o components. Then the first predict stage is applied to x_o ,

$$x'_o = x_o + x_e * P_1$$

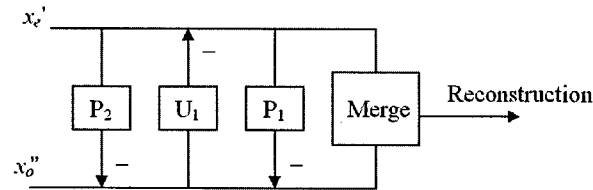
where P_1 is a FIR (convolution) filter. Next, the first update stage is applied to x_e ,

$$x'_e = x_e + x'_o * U_1$$

The process continues with a second update stage,

$$x_o'' = x_o' + x_e' * P_2$$

In general, the lifting can continue further with alternating predict and update stages. Once the signal passes through all the stages, x_e are the approximation coefficients and x_o are the detail coefficients. The approximation coefficients are often scaled larger to weight their greater significance relative to the detail coefficients. The inverse transform simply subtracts the stages in reverse,



Because only one stage is changed at a time, the Lifting Scheme transform is always reversible – even with nonlinear stage filters. In particular, to perform the transform with only integer operations, integer-to-integer wavelet transforms round the filtered sequences before adding. For an integer input signal, the inverse yields perfect reconstruction.

Adams and Kossentini [1] use a brute-force search for Lifting Scheme biorthogonal wavelets with all dyadic rational coefficients with good wavelet properties. The wavelets provide strong frequency localization and vanishing moments optimized for the purpose of image compression. The results from their search include

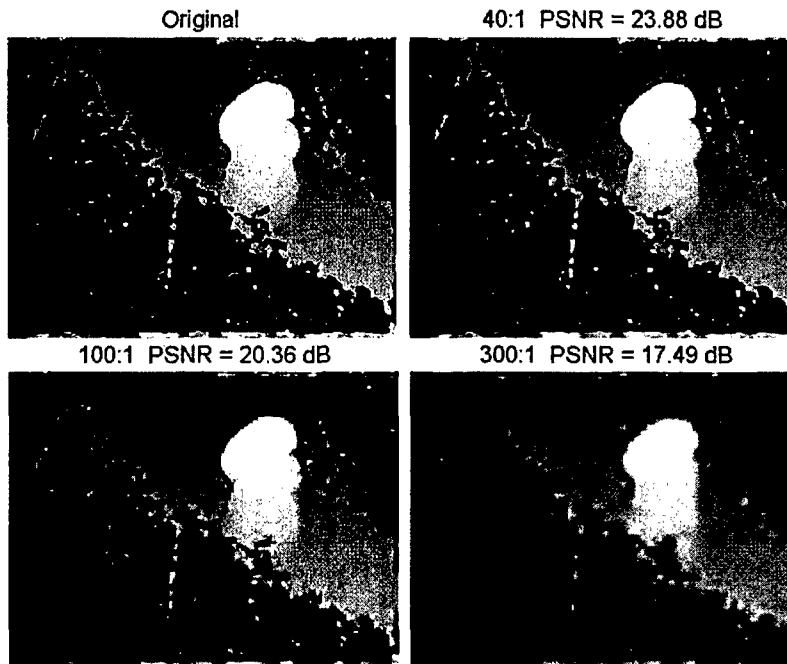
$$\begin{array}{l}
 5/11 \quad \left\{ \begin{array}{l} P_1(z) = \frac{1}{2}(-z - 1) \\ U_1(z) = \frac{1}{4}(1 + z^{-1}) \\ P_2(z) = \frac{1}{32}(z^2 - z - 1 + z^{-1}) \end{array} \right. \\
 6/14 \quad \left\{ \begin{array}{l} P_1(z) = -1 \\ U_1(z) = \frac{1}{32}(-z + 16 + z^{-1}) \\ P_2(z) = \frac{1}{32}(z^2 - z + z^{-1} - z^{-2}) \end{array} \right. \\
 13/7 \quad \left\{ \begin{array}{l} P_1(z) = \frac{1}{32}(3z^2 - 19z - 19 + 3z^{-1}) \\ U_1(z) = \frac{1}{32}(-z + 5 + 5z^{-1} - z^{-2}) \end{array} \right.
 \end{array}$$

5/11 and 6/14 are designed such that they can be performed with only additions and bit shifts. 13/7 requires integer multiplications but has slightly stronger compression capabilities. Adams and Kossentini do not define how to scale the approximation coefficients. My own experimentation found $\sqrt{2}$ to be a good scaling factor for these wavelets, however, for computational efficiency, 2 works reasonably well.

Wavelet-based compression will be performed on the translation map in the following steps

- Perform an integer-to-integer wavelet transform on the translation map to some level of decomposition (third to sixth level)
- Threshold all wavelet coefficients below some magnitude to zero
- Apply run-length encoding to the resulting coefficients to compress long sequences of zeros

With this approach, it is computationally efficient and algorithmically simple to compress translation maps. With wavelet image compression, it is realistic to yield 20:1 compression ratios with nearly imperceptible loss in quality. For smoother input images, this ratio can be higher yet. In order to meet the 20 kilobyte limit, a 1024×768 pixel translation map would need at least 39:1 compression. Below is a demonstration of this with the translation map found earlier at various thresholding ratios using the 5/11 wavelet. The actual data compression ratios depend on the particular run-length encoding method used.



Even at extreme thresholding ratios, the dominant low-scale information is retained. Notice that the image degrades smoothly – no blocking artifacts. Wavelet compression performs well for high quality/low compression ratios as well as for low quality/high compression ratios.

Improvements

The difficulty in aggregation stereoscopic methods using the right neighborhood size. Using too big of a neighborhood more frequently violates the smooth translation assumption while too small of a neighborhood is more likely to falsely match and produce inconsistent translations. One approach is to first perform aggregation as described, and then to use the edges in the resulting translation map to make a second pass of aggregation with neighborhoods fitting within these edges. Diffusion stereoscopic methods iterate aggregation in a similar manner. Such methods are yet more intense than simple aggregation, but they significantly improve effects at edges and occlusion boundaries.

A computationally cheaper (but lower quality) alternative to diffusion methods is to filter the aggregation results as post-processing. Because these operation can be done without the original photographs, the DINO Satellite can transmit the raw translation map to the ground for further manipulation. For refining object edges, instead of Scharstein's method of Canny edge detection and then thresholding, an alternative is the nonlinear bilateral filter [2]. As both diffusion and post-processing are fine-tuning done on the aggregation results, these topics will be discussed in further detail later once the current aggregation-only implementation is established.

Appendix A – Approximations

With the high computational intensity of the stereoscopic algorithm, Scharstein includes methods to speed up some of the more costly operations. As the aggregation step of the algorithm costs most of the processing time, the focus is on speeding up the particular operations involved. Significant optimizations can be made by approximating the L_2 norm with an “octagon” norm and applying another trick to approximate Gaussian filtering.

Approximating the L_2 Norm

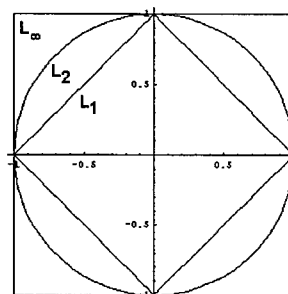
In evaluating the evidence measure (1), the stereoscopic algorithm involves calculating many vector L_2 norms.

$$\|x\|_2 = \left(\sum_i x_i^2 \right)^{1/2}$$

Depending on the hardware, the square root can be very costly. Scharstein proposes a clever combination of the L_1 and L_∞ norms to approximate the L_2 norm. These two are easier to compute than the L_2 norm.

$$\|x\|_1 = \sum_i |x_i| \quad \|x\|_\infty = \max_i |x_i|$$

Geometrically, the set of all $x \in \mathbb{R}^2$ such that $\|x\|_2 = 1$ lie on the unit circle. In the L_1 norm, vectors such that $\|x\|_1 = 1$ lie in a diamond shape within the unit circle. The vectors such that $\|x\|_\infty = 1$ lie in a square containing the unit circle.



The approximation combines the L_1 and L_∞ norms into an octagon norm. $\|x\|_{oct} = 1$ is an octagon fitting closely to the unit circle.

$$\begin{aligned} \|x\|_{oct} &= \frac{2}{1 + \sqrt{4 - \sqrt{8}}} \left[(\sqrt{2} - 1) \|x\|_1 + (2 - \sqrt{2}) \|x\|_\infty \right] \\ &\approx 0.3978 \|x\|_1 + 0.5626 \|x\|_\infty \end{aligned}$$

For its simplicity, this low-cost approximation is very close – within 4% of the L_2 norm everywhere.

Approximating Gaussian Filter Convolution

Scharstein notes that it is much faster to use “box filters” instead of a Gaussian filter in the aggregation step. Applying the “box filter” of size $(2B_x + 1) \times (2B_y + 1)$:

$$\begin{aligned} \text{BoxFilter}(E_\delta)(x, y) &= E_\delta(x, y) * \frac{1}{(2B_x+1)(2B_y+1)} \begin{bmatrix} 1 & 1 & \dots & 1 \\ 1 & 1 & & \vdots \\ \vdots & & \ddots & \vdots \\ 1 & \dots & \dots & 1 \end{bmatrix} \\ &= \frac{1}{(2B_x+1)(2B_y+1)} \left[\sum_{j=1}^{y+B_y} \left[\sum_{i=1}^{x+B_x} E_\delta(i, j) - \sum_{i=1}^{x-B_x} E_\delta(i, j) \right] \right. \\ &\quad \left. - \sum_{j=1}^{y-B_y} \left[\sum_{i=1}^{x+B_x} E_\delta(i, j) - \sum_{i=1}^{x-B_x} E_\delta(i, j) \right] \right] \end{aligned} \quad (5)$$

The above computation has nearly the same operations count for any box size $B_x \times B_y$. While the Gaussian convolution requires $O(N_x N_y w^2)$ for a filter size $w \times w$, the computational complexity of the box filter as in (5) does not depend on the filter size. Especially for wide neighborhoods, it is much faster to use box filters. The Gaussian filter can be efficiently approximated by three or four box filters in sequence [4]. Potentially, other smoothing filters could be approximated as well. Scharstein observes that a more localized cone-shaped weighting has advantages over Gaussian filter; it may be useful to investigate various filter shapes and their efficient box filter approximation.

Appendix B – MATLAB Code

GradientStereo.m

```
function [T,EMax] = GradientStereo(Img1,Img2,Translation)
%GRADIENTSTEREO Gradient-Based Stereoscopic Vision
% T = GradientStereo(Img1,Img2,Translation)
%
% Find the translation map T from Img1 and Img2. Translation
% specifies the set of horizontal displacements to test.
%
% Implementation by Pascal Getreuer March 2004

N = size(Img1);

if length(N) ~= 2 | ndims(Img2) ~= 2
    error('Only two-dimensional images allowed.');
```

```
end

if N ~= size(Img2)
    error('Images must be the same size.');
```

```
end

% approximate image gradients
Kernel = [-1,0,1;-2,0,2;-1,0,1]; % Sobel filter
%Kernel = [0.2242;0.5516;0.2242]*[-0.4553,0,0.4553]; % Simoncelli filter
Kernel = conv2(Kernel,GaussianFilter(0.5,3,3)); % light smoothing

Grad1X = conv2(Img1,Kernel,'same');
Grad1Y = conv2(Img1,Kernel','same');
Grad2X = conv2(Img2,Kernel,'same');
Grad2Y = conv2(Img2,Kernel','same');

GradMag1 = sqrt(Grad1X.^2 + Grad1Y.^2);
GradMag2 = sqrt(Grad2X.^2 + Grad2Y.^2);

% aggregation
FineScale = GaussianFilter(2.2,5,5)*2.2; % smaller neighborhood
CoarseScale = GaussianFilter(7,14,14)*7; % larger neighborhood

EMax = zeros(N); % evidence map for best matches
T = zeros(N); % translation map
E = zeros(N);
clf; shg;
```



```

for delta = Translation    % loop through translations
    % evidence measure, E(x,y) = confidence - difference
    E = (GradMag1 + ShiftImage(GradMag2,delta))*0.5 -...
        sqrt((Grad1X - ShiftImage(Grad2X,delta)).^2 + (Grad1Y - ShiftImage(Grad2Y,delta)).^2);

    E2 = conv2(E,FineScale,'same');    % fine-scale matching
    i = find(E2 > EMax);
    EMax(i) = E2(i);
    T(i) = delta;

    E2 = conv2(E,CoarseScale,'same');    % coarse-scale matching
    i = find(E2 > EMax);
    EMax(i) = E2(i);
    T(i) = delta;

    % display current translation map
    imagesc(T); colormap(gray); axis equal; axis off;
    drawnow;
end

return;

```

ShiftImage.m

```

function Img = ShiftImage(Img,Shift)
%SHIFTIMAGE Translate Img horizontally by Shift

[SizeY,SizeX] = size(Img);
Img = [(ones(Shift,1)*Img(:,1))',Img(:,max(1,1-Shift):min(SizeX,SizeX-Shift)),...
        (ones(-Shift,1)*Img(:,SizeX))'];

return;

```

GaussianFilter.m

```

function f = GaussianFilter(Sigma,Nx,Ny)
%GAUSSIANFILTER Gaussian convolution filter
% f = GaussianFilter(Sigma,N) makes a one-dimensional filter
% f = GaussianFilter(Sigma,Nx,Ny) makes a two-dimensional filter

if nargin == 3
    f = exp(-(-Nx:Nx).^2/(2*Sigma^2))/(Sigma*sqrt(2*pi));
    f = exp(-(-Ny:Ny).^2/(2*Sigma^2))/(Sigma*sqrt(2*pi))*f;
else
    f = exp(-(-Nx:Nx).^2/(2*Sigma^2))/(Sigma*sqrt(2*pi));
end

return;

```

References

- [1] M. Adams & F. Kossentini. *Low-Complexity Reversible Integer-to-Integer Wavelet Transforms for Image Coding*, in Proc. of IEEE Pacific Rim Conference on Communications, Computers, and Signal Processing, Victoria, BC, Canada, pp. 177-180, Aug. 1999.
- [2] F. Durand & J. Dorsey. *Fast Bilateral Filtering for the Display of High-Dynamic-Range Images*, proceedings of the 29th annual conference on Computer graphics and interactive techniques, 2002.
- [3] D. Scharstein. *View Synthesis Using Stereo Vision*. Lecture Notes in Computer Science, Vol. 1583, Springer-Verlag Heidelberg, 1999.
- [4] W. Wells. *Efficient synthesis of Gaussian filters by cascaded uniform filters*, IEEE Trans. PAMI, Vol. 8(2), pp. 234-239, 1986.



DINO Cloud Detection Algorithm

DINO-SCI-RPT-CLDS, Rev. B

Written by:
Paul Kolesnikoff
Loren Schuessler

Prepared for:
Nanosat III

Table of Contents

1	Scope.....	4
1.1	Identification.....	4
1.2	Document Maintenance.....	4
1.3	Systems Overview.....	4
1.4	Document Overview.....	4
1.5	Referenced Documents.....	4
2	Introduction.....	4
3	The Algorithm.....	5
4	Conclusion:.....	9

1 Scope

1.1 Identification

This document applies to the DINO project, a project undertaken by the Colorado Space Grant Consortium at the University of Colorado at Boulder. This project is part of the Nanosatellite III Program sponsored by the Air Force Office of Scientific Research (AFOSR), Air Force Research Laboratory (AFRL), Association of Aeronautics and Astronautics (AIAA), and Goddard Space Flight Center (GSFC).

1.2 Document Maintenance

This document falls under the DINO document control requirements as specified under the DINO Configuration Management plan. All changes and updates must be made in accordance with the DINO CM plan.

1.3 Systems Overview

The purpose of the student-led Deployment and Intelligent Nanosatellite Operations (DINO) mission is to determine cloud heights from space, evaluate the performance of intelligent operations, and assess deployment technologies for nanosatellites including a gravity-gradient boom, memory composite hinges, and thin-film solar arrays.

1.4 Document Overview

This document will go over how DINO plans to determine clouds in pictures.

1.5 Referenced Documents

List any reference documents here.

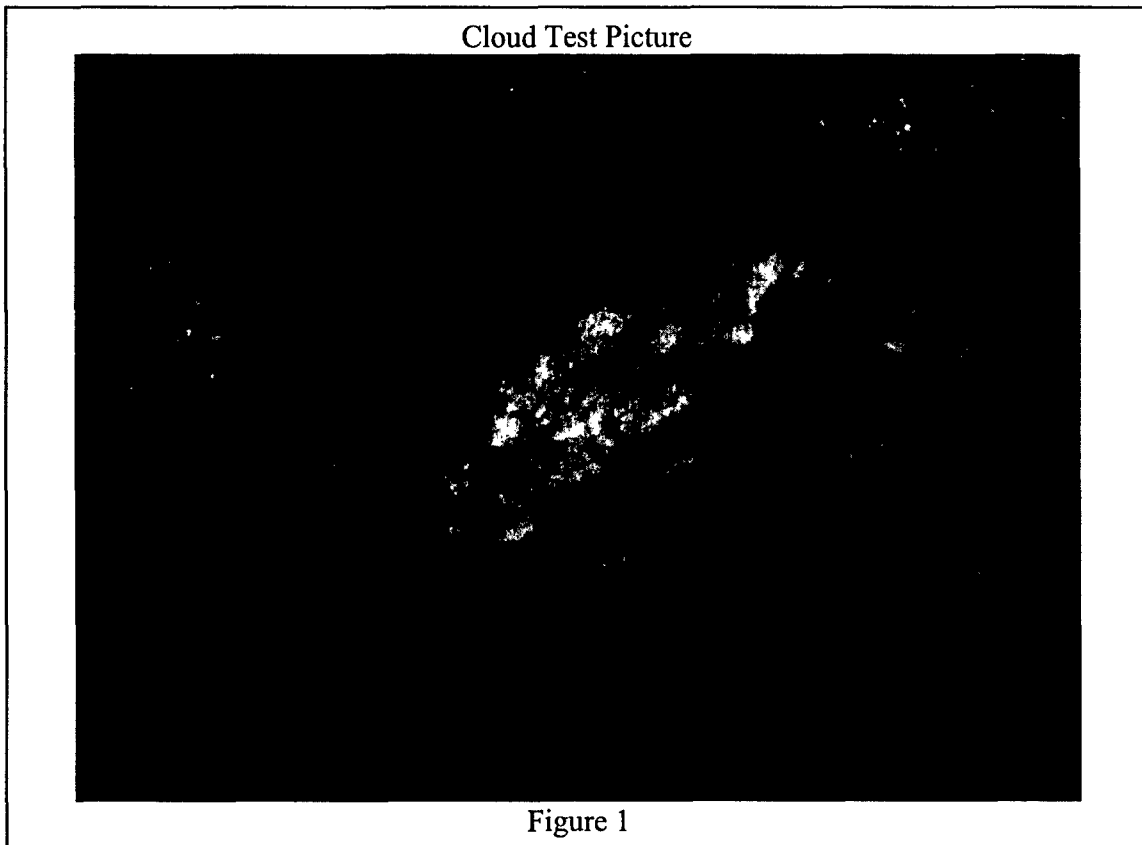
2 Introduction

The purpose of the DINO science mission is to generate topographic maps of the tops of clouds. Obviously, in order to do this, the pictures must have clouds in them. The DINO satellite will use the forward-looking camera to take a series of pictures in a low-resolution preview mode to search for clouds. This paper will cover the algorithm to be used to analyze these low-resolution pictures for the existence of clouds.

3 The Algorithm

During the mission, the DINO spacecraft will be in low-earth orbit. As a result, it will be in constant motion. This means that only the leading edge of the preview picture needs to be analyzed for the existence of a cloud. This is because any clouds in the trailing edge of the preview picture will have already passed by the spacecraft centerline. In addition, due to the spacecraft's speed, there are only ten seconds available to get the preview picture, analyze it, switch the camera to high resolution mode, and take the high resolution picture. As a result, the algorithm needs to be efficient to meet the time constraints.

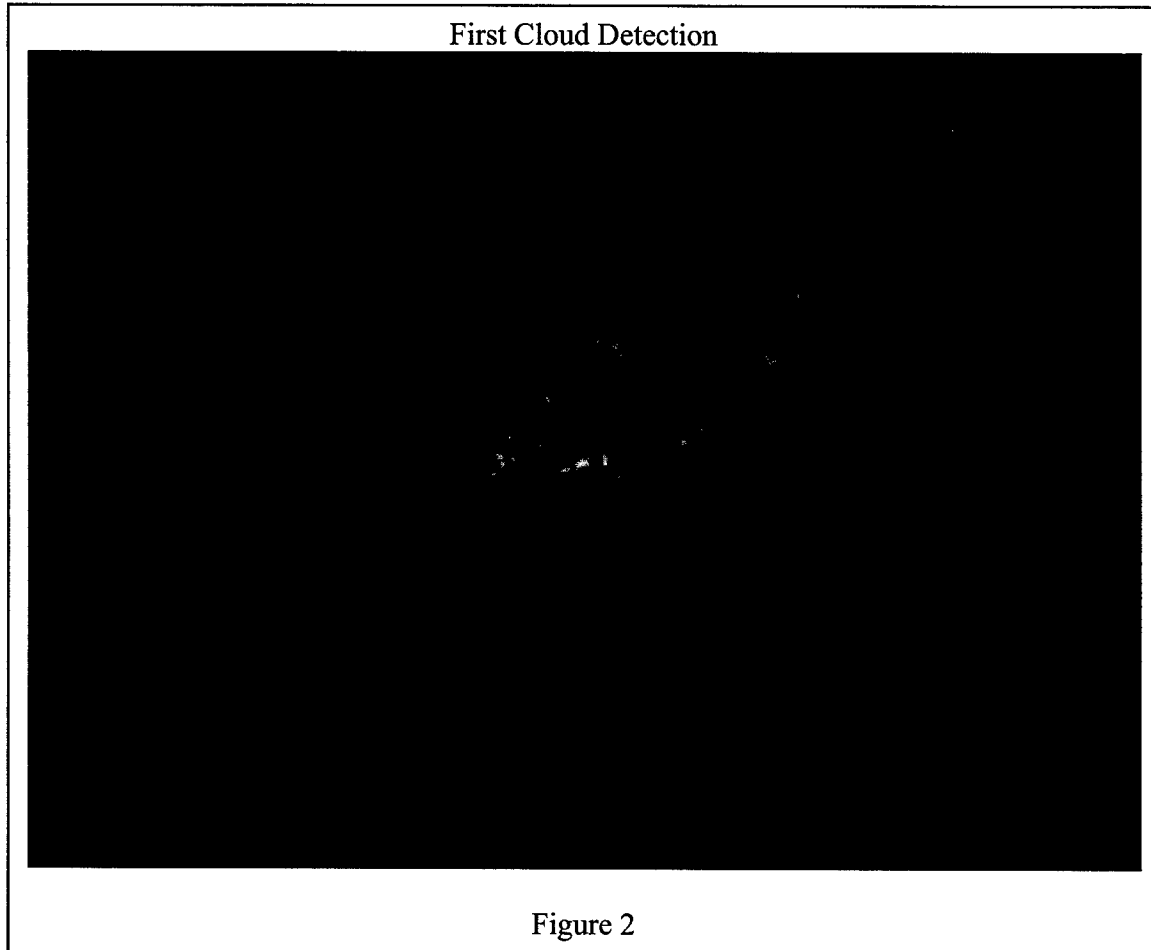
The goal of the cloud-detection algorithm is to derive a figure of merit for the existence of clouds in a picture. To test the cloud-detection algorithm, the picture shown in Figure 1 was used.



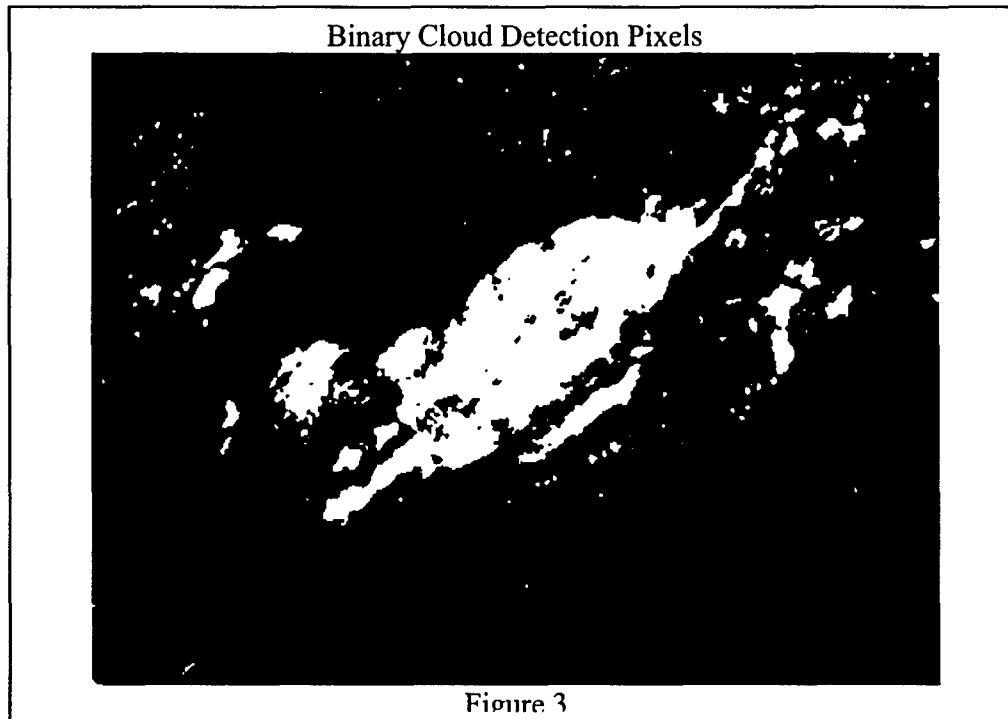
One possible approach is to use a mask to give credit to white pixels that are adjacent to other white pixels as shown here.

$$P_c = \begin{bmatrix} 255 & 255 & 255 \\ 255 & 255 & 255 \\ 255 & 255 & 255 \end{bmatrix} \bullet \begin{bmatrix} P_{i-1,j-1} & P_{i-1,j} & P_{i-1,j+1} \\ P_{i,j-1} & P_{i,j} & P_{i,j+1} \\ P_{i+1,j-1} & P_{i+1,j} & P_{i+1,j+1} \end{bmatrix} \quad (1)$$

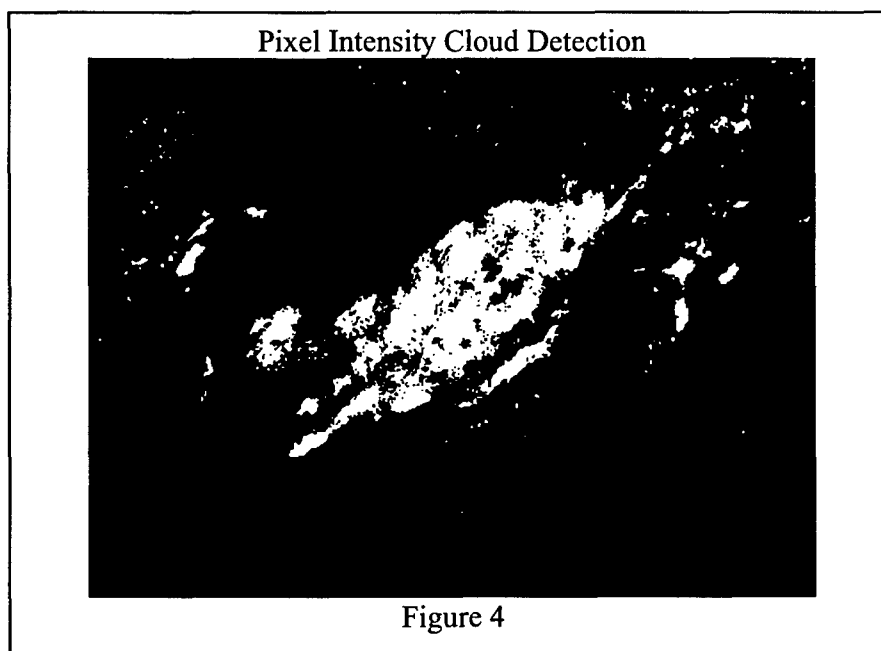
Where P_c is a matrix which gives the intensity for the (i,j)th pixel in the picture and all of its surrounding pixels. In order to measure for white, this matrix multiplication would have to be done for all three colors. Then, the elements of the rows and columns for each color would be added up to get one figure of merit for each pixel. Then, a threshold level is set and all pixels below the threshold are set to zero and all points above the threshold are scaled to a maximum value of 255 as shown in Figure 2.



Although this does show the cloud shapes, the cloud could be given a little more recognition by merely converting all pixels above the threshold to a maximum intensity and all pixels below the threshold to a minimum intensity. This was done in Figure 3. This allows the algorithm's interpretation of clouds in the picture to be readily identified.



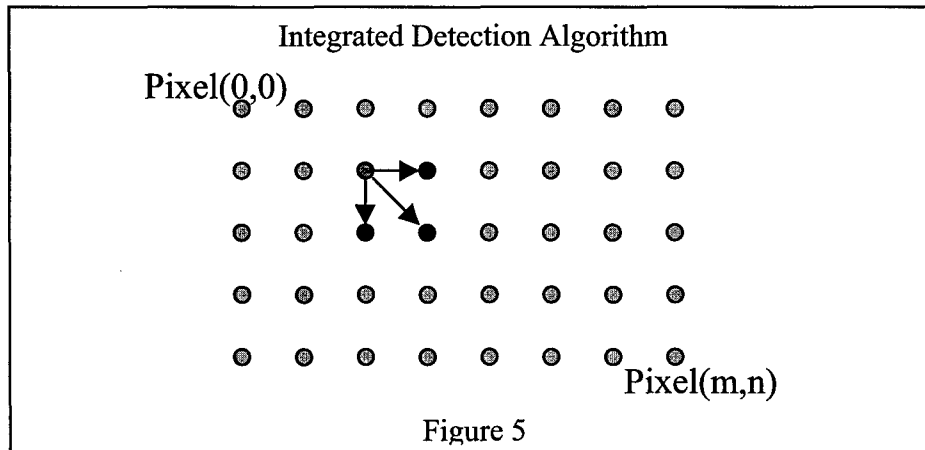
At this point, however, the computational intensity of this method should be considered. For each pixel, it requires 27 multiplications. Given the time constraints on this algorithm, another method was sought to detect clouds. Since clouds are white, all three colors are nearly equal. A check was made and, even in the gray regions of the clouds, this color balance remains. In addition, most terrestrial features do not have this sort of color balance. Therefore a check was made to determine if merely checking that all three color intensities were above a particular threshold would accurately detect clouds. The results for minimum pixel intensity for each color of 90 are shown in Figure 4.



This method clearly detects the clouds with a nearly two order of magnitude reduction in computational intensity.

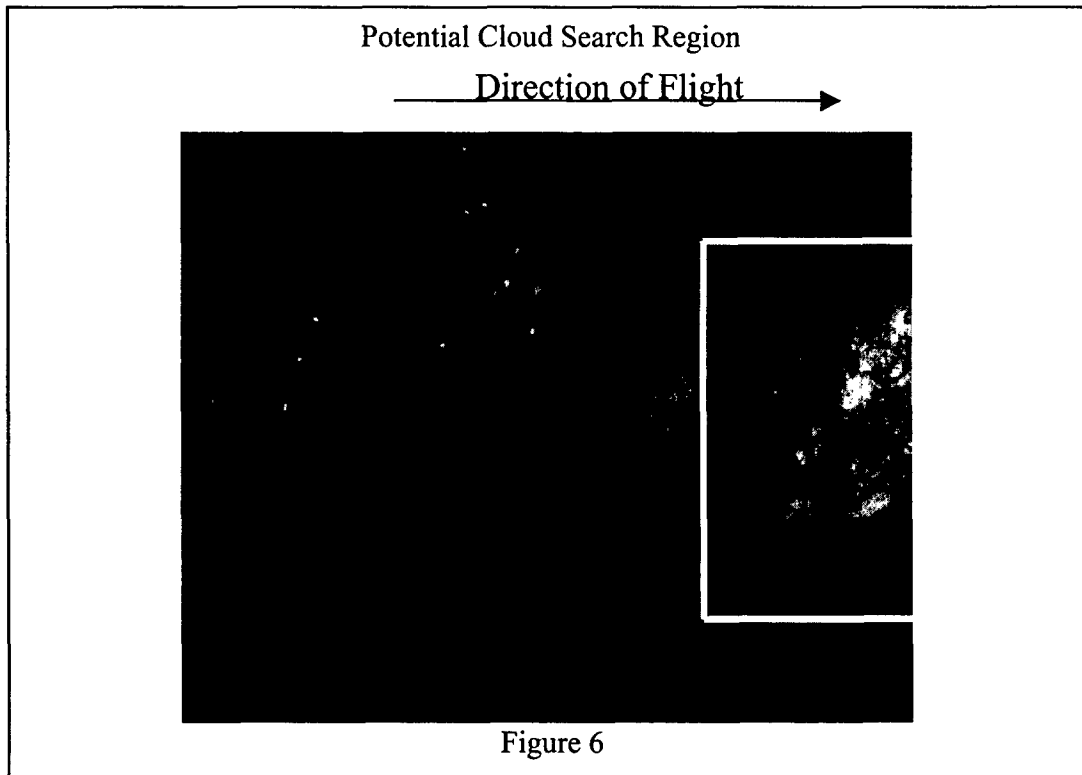
Now, a figure of merit for a cloud in the preview picture can be obtained. Again, extra credit should be given for white pixels that are next to white pixels. If all white pixels were given a value of 1 and all non-white pixels were given a value of 0, then a simple addition of each pixel with its right-hand and lower neighbors (including the diagonal pixel) would produce a maximum value of 4 for each pixel. Hence, a maximum value of 4 times the number of pixels in the picture would be the maximum figure of merit that an entirely cloudy picture would produce.

At this point, a threshold level is needed to determine when a cloud exists in the picture. The picture shown in Figure 1 has good cloud coverage and yet is only 8% of the maximum figure of merit. Therefore, a lower limit of 3% is probably reasonable. This also means that the maximum figure of merit for a given picture size could be determined ahead of time and the calculations structured such that the white detection and the figure of merit addition occur simultaneously as shown in Figure 5. Then, as soon as the 3% limit is crossed, the detection process could be stopped.



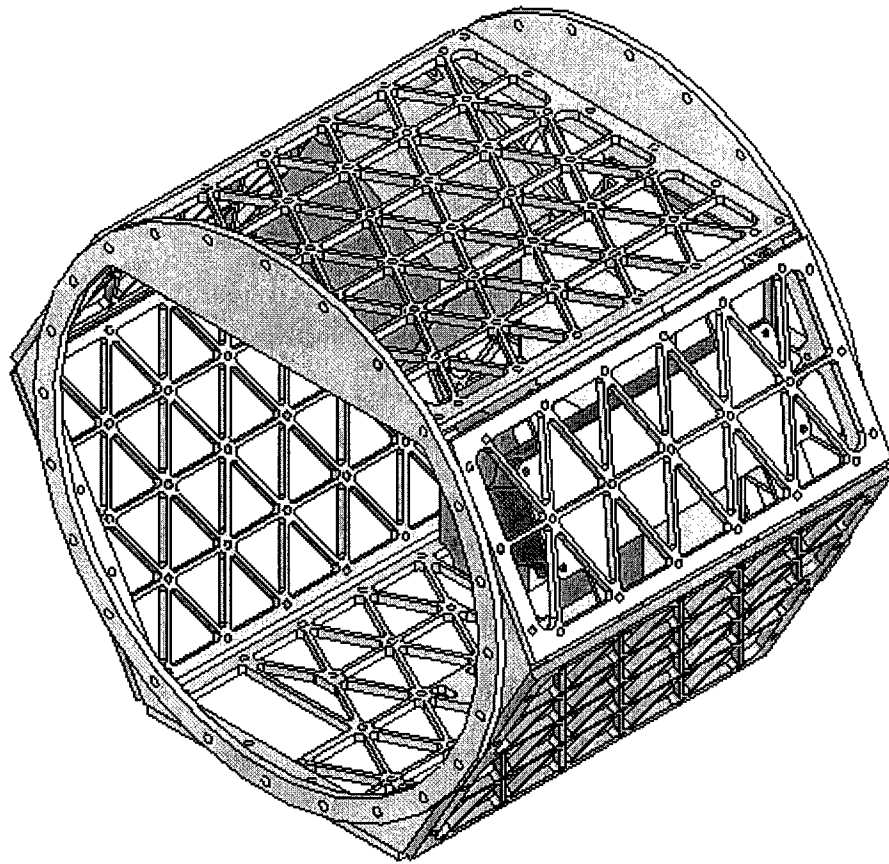
As Figure 5 shows, when testing a pixel, a pixel would first be tested to see if it is white (all three colors above the threshold). Then, if it is white, its three neighbors to the right and bottom would be checked to see if they are white. Finally, the total number of white pixels in this test group (up to 4) is added to the running total for the picture. When the running total exceeds 0.03 times the maximum possible total, a cloud is detected and the cloud search is aborted.

Another consideration is that, ideally, the cloud will be centered in the picture. Therefore when searching the preview picture for a cloud, only the leading edge and the center 60% of the picture should be searched as shown in Figure 6. Remember that the maximum figure of merit is based only on the number of pixels in the test region, not the total number of pixels in the picture.



4 Conclusion:

This paper has given a method of detecting the existence of a cloud in a picture. Techniques for improving the computational efficiency of this technique were also given.



ANALYSIS OF DINO

PROCEDURE:

The Analysis was primarily attempted in ANSYS first. The ANSYS version which is installed at the University of Colorado at Boulder is the Student version and does not support more than 32000 nodes. The analysis was carried out on individual panels, and then the full assembly was analyzed. ANSYS could not create a refined enough mesh for the analysis. Hence we looked at COSMOS Works which is compatible with Solid Works, as a potential option to run the analysis. All the parts have gone through extensive frequency analysis in COSMOS Works. It has been seen that we are well above the benchmark of 100 Hz. All the parts were meshed using the tetrahedral mesh option provided from COSMOS Works. The mesh for each of these panels, and also the Full Assembly has gone through extensive refinement procedures and then had their analysis done.

PROBLEMS FACED:

The main problem first was inability of ANSYS to analyze the panels, due to its restriction on the number of nodes. I had a lot of trouble getting space on my account here at the Integrated Teaching and Learning Laboratory (ITLL). COSMOS Works was also having troubles running the full assembly. I had to remove the torque rod assembly from the full assembly because it had interferences and COSMOS Works could not handle those. It was not so critical to the analysis since the torque rod assembly did not form major chunk of the mass of the structure. One of the boxes and its corresponding lids needed to be taken off due to some interference too. One of the lids was modified because COSMOS Works could not handle the tolerances for the mesh. The space allocation for the analysis was also an issue, since the simulation used to just hang up in the same spot each time. According to what the disk space allocations menu showed, there was free space on the account, but COSMOS Works, was unable to find the needed space for the analysis. Neither did the Technical Support at the ITLL know what was needed to be done, nor did anyone at MCAD, (The firm that provides technical support at University of Colorado, Boulder). On discussing the problem with the Technical support group at MCAD, they did give me some pointers as to what can be done to simulate the whole analysis.

The analysis ran after 9 long days, and we had good results.

The results follow this order.

The results for each of the individual panels will be shown first, they will be arranged in the following format. The first mode shape of each of these panels is documented. The deformation followed by the displacement plot. The full assembly is documented last.

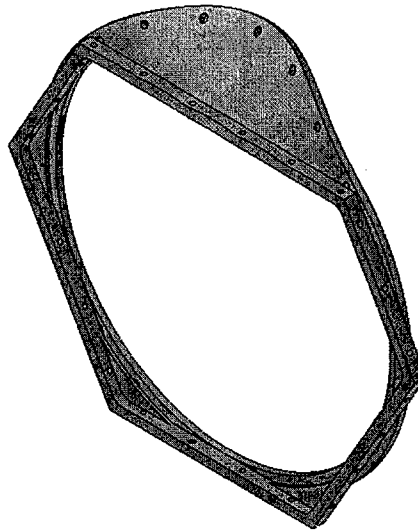
The panels follow the order:

- 1) Bottom Panel
- 2) Large Panel
- 3) Side Panel
- 4) Small Panel
- 5) Top Panel

And then last but not the least the whole Assembly.

Bottom Panel: First Mode=1247.5 Hz Deformation Plot:

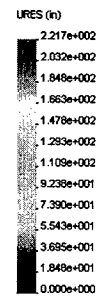
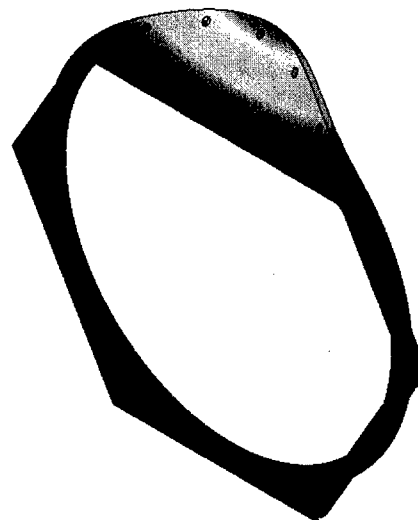
Model name: BOTTOM PANEL
Study name: BOTTOM PANEL
Plot type: Frequency-Plot1
Mode Shape: 1 Value = 1247.5 Hz
Deformation Scale: 0.0078845



Educational Version. For Instructional Use Only

Displacement Plot:

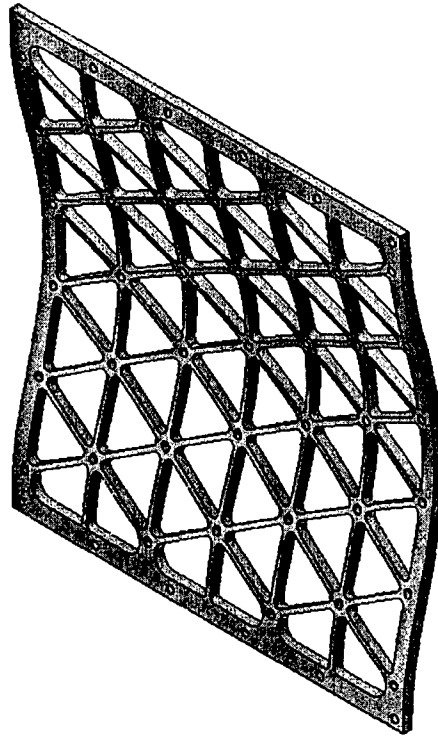
Model name: BOTTOM PANEL
Study name: BOTTOM PANEL
Plot type: Frequency-Plot1
Mode shape: 1
Deformation Scale: 0.0078845



Educational Version. For Instructional Use Only

Large Panel: First Mode = 310.66 Hz Deformation Plot:

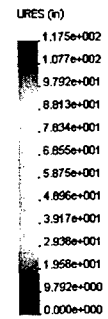
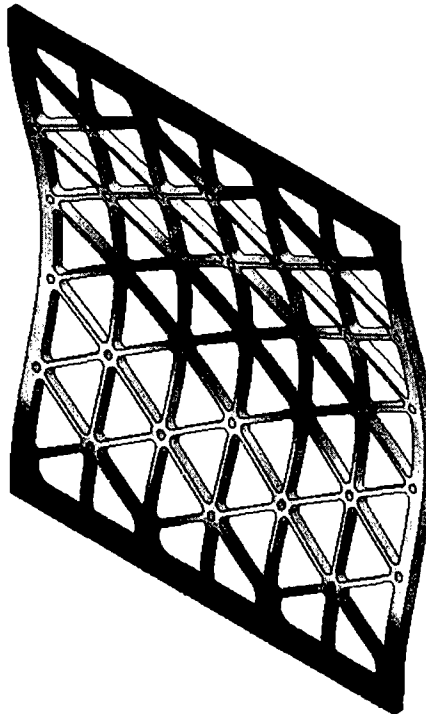
Model name: LARGE SIDE PANEL
Study name: large panel
Plot type: Frequency-Plot1
Mode Shape: 1 Value = 310.66 Hz
Deformation Scale: 0.0102122



Education Version - For Instructional Use Only

Displacement Plot:

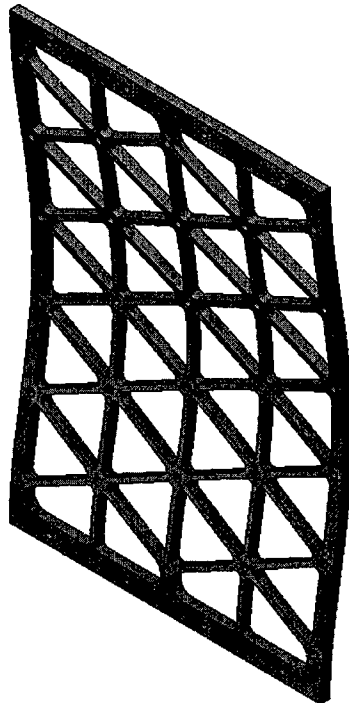
Model name: LARGE SIDE PANEL
Study name: large panel
Plot type: Frequency-Plot1
Mode shape: 1
Deformation Scale: 0.0102122



Education Version - For Instructional Use Only

Side Panel: First Mode = 276.65 Hz Deformation Plot:

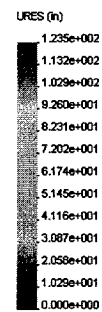
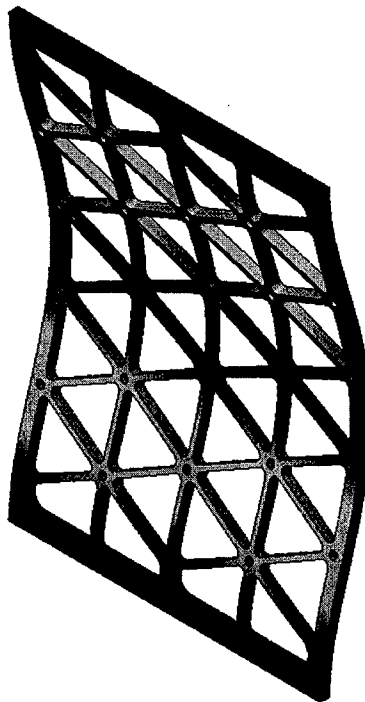
Model name: SIDE PANEL
Study name: analysis forside panel
Plot type: Frequency-Plot1
Mode Shape: 1 Value = 276.65 Hz
Deformation Scale: 0.005298



Educational Version. For Instructional Use Only

Displacement Plot:

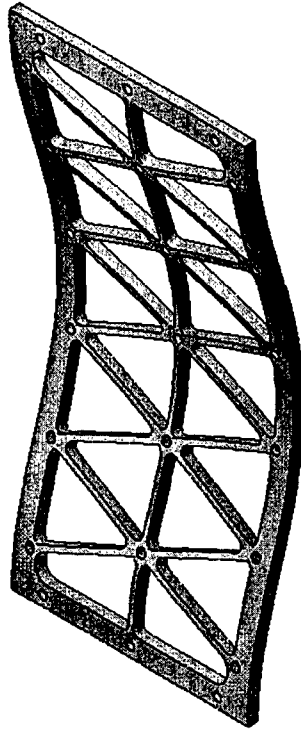
Model name: SIDE PANEL
Study name: analysis forside panel
Plot type: Frequency-Plot1
Mode shape: 1
Deformation Scale: 0.00971888



Educational Version. For Instructional Use Only

Small Panel: First Mode = 305.23 Hz Deformation Plot:

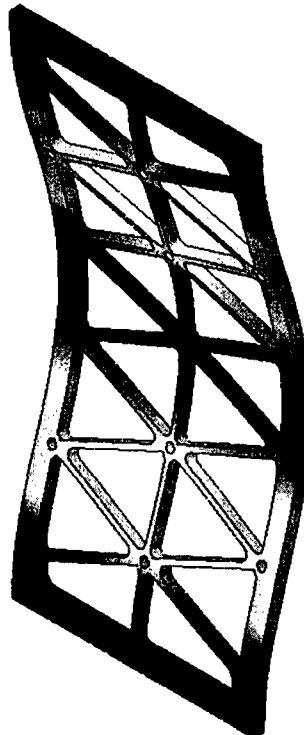
Model name: SMALL SIDE PANEL THIN
Study name: SMALL PANEL
Plot type: Frequency-Plot1
Mode Shape: 1 Value = 305.23 Hz
Deformation Scale: 0.00854172



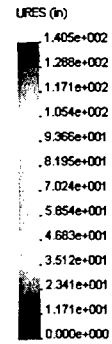
Educational Version - For Institutional Use Only

Displacement Plot:

Model name: SMALL SIDE PANEL THIN
Study name: SMALL PANEL
Plot type: Frequency-Plot1
Mode shape: 1
Deformation Scale: 0.00854172

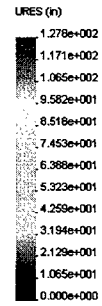
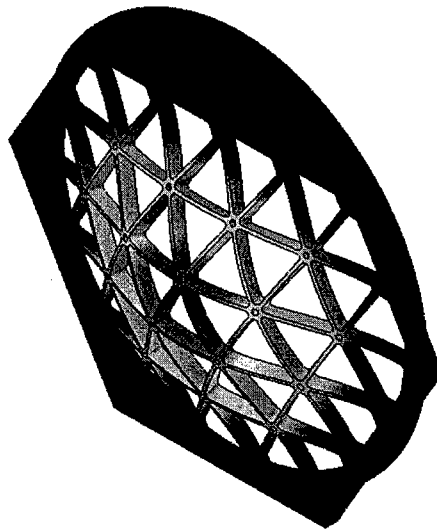


Educational Version - For Institutional Use Only



Top Panel: First Mode =699.85 Hz Deformation Plot:

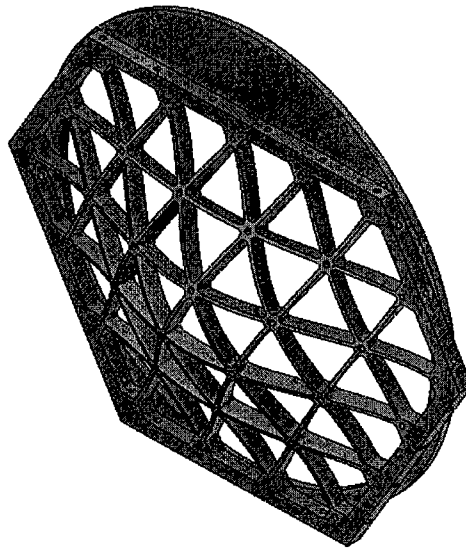
Model name: TOP PANEL
Study name: TOPPANEL
Plot type: Frequency-Plot1
Mode shape: 1
Deformation Scale: 0.0136366



Educational Version. For Instructional Use Only

Displacement Plot:

Model name: TOP PANEL
Study name: TOPPANEL
Plot type: Frequency-Plot1
Mode Shape: 1 Value = 699.85 Hz
Deformation Scale: 0.0136366

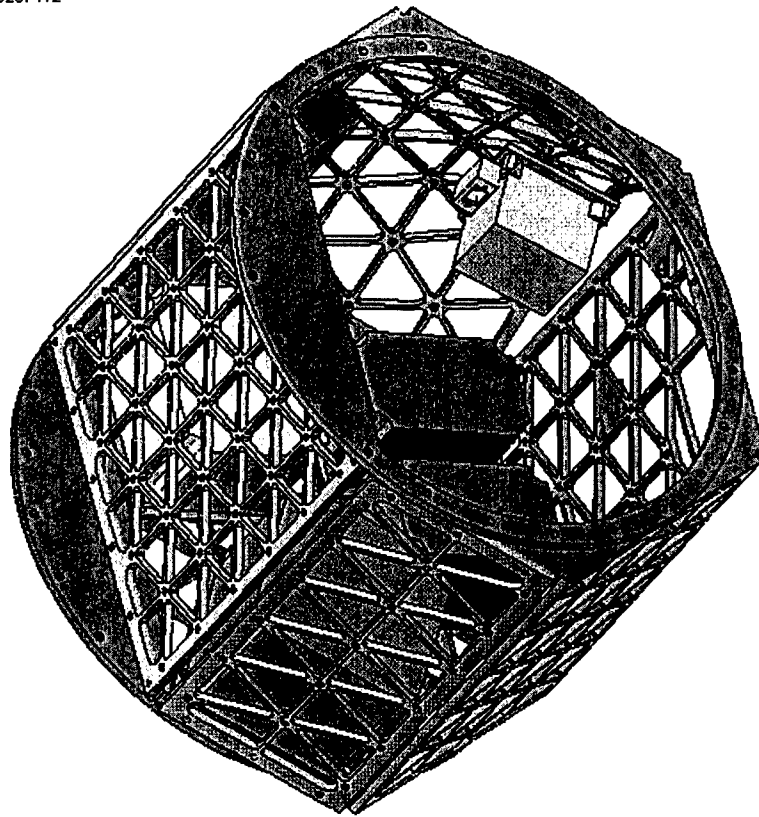


Educational Version. For Instructional Use Only

Full Assembly: First Mode = 328.78 Hz

Deformation Plot:

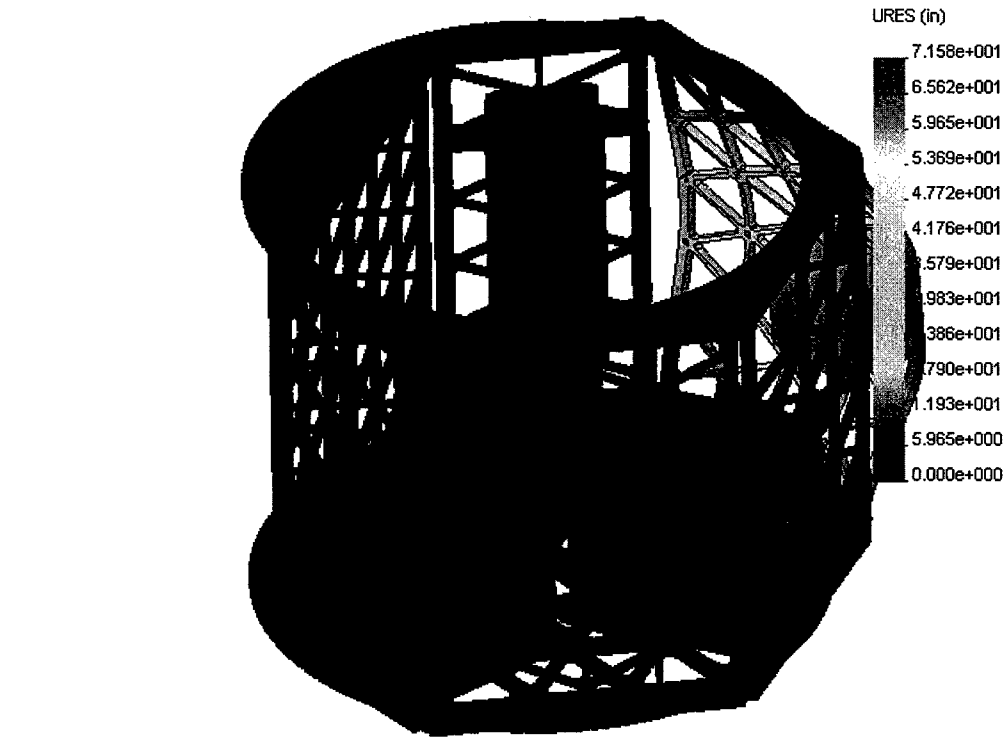
Model name: Full Assembly2
Study name: full assembly
Plot type: Frequency-Plot1
Mode Shape: 1 Value = 328.78 Hz
Deformation Scale: 0.0287412



Educational Version. For Instructional Use Only.

Displacement Plot:

Model name: Full Assembly2
Study name: full assembly
Plot type: Frequency-Plot1
Mode shape: 1
Deformation Scale: 0.0287412



Educational Version. For Instructional Use Only

ACKNOWLEDGEMENTS:

[1] Professor: Steve Wichman. (Space Grant College, University of Colorado, Boulder)

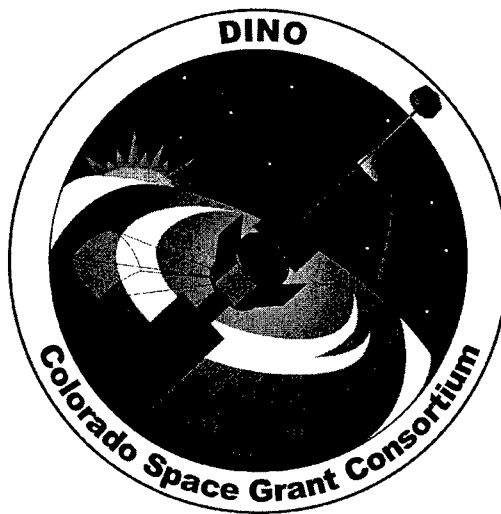
[2] Technical Support: ITLL

John Perry

Brad Dunkin

[3] Technical Support: MCAD

[4] Justin Reilly, Team Lead, Structures, DINO



Flight Software Algorithm Report
DINO-SW-RPT-ALG, Rev. A

Written by:
Cory Maccarrone

December 12, 2004

Prepared for:
Nanosat III

Table of Contents

1	Scope	3
1.1	Identification	3
1.2	Document Maintenance	3
1.3	Systems Overview	3
1.4	Document Overview	3
1.5	Referenced Documents	3
2	Overview	3
2.1	Science Analysis	3
2.2	Attitude and Determination	4
3	Science Algorithms	4
3.1	Cloud Detection	4
3.2	Stereoscopic Imaging	5
3.3	Cloud Classification	6
3.4	Testing	6
3.4.1	Cloud Detection Testing	7
3.4.2	Stereoscopic Imaging Testing	7
3.4.3	Cloud Classification Testing	7
4	ADCS Algorithms	8
4.1	SGP4 Orbital Propogator	8
4.2	Actuator Control Law	8
4.3	Testing	8
A	List of Acronyms	10

1 Scope

1.1 Identification

This document applies to the DINO project, a project undertaken by the Colorado Space Grant Consortium at the University of Colorado at Boulder. This project is part of the Nanosatellite III Program sponsored by the Air Force Office of Scientific Research (AFOSR), Air Force Research Laboratory (AFRL), Association of Aeronautics and Astronautics (AIAA), and Goddard Space Flight Center (GSFC).

1.2 Document Maintenance

This document falls under the DINO document control requirements as specified under the DINO Configuration Management plan. All changes and updates must be made in accordance with the DINO CM plan.

1.3 Systems Overview

The purpose of the student-led Deployment and Intelligent Nanosatellite Operations (DINO) mission is to determine cloud heights from space, evaluate the performance of intelligent operations, and assess deployment technologies for nanosatellites including a gravity-gradient boom, memory composite hinges, and thin-film solar arrays.

1.4 Document Overview

This document covers the implementation and testing of the various algorithms used in the flight software for science analysis and the Attitude and Determination Control System (ADCS).

1.5 Referenced Documents

No documents referenced.

2 Overview

There are two main areas in the flight software where algorithmic calculation is necessary: the science analysis, and the ADCS system for navigational control.

2.1 Science Analysis

There are three main algorithms used in the science analysis: cloud coverage detection, stereoscopic imaging, and cloud classification. The cloud coverage detection algorithm makes use of the hue and saturation values of each pixel in the image, as well as that of each neighboring pixel, to determine whether that pixel is part of a cloud or not. The stereoscopic imaging algorithm takes two images taken from different angles and determines their depth from the cameras. Using the known altitude of the satellite, the heights of the clouds above Earth's surface can then be determined. Finally, the cloud classification algorithm takes a picture

of the clouds, determines the area within the image that the clouds reside, then using a neural network architecture, attempts to determine the classification of the cloud.

2.2 Attitude and Determination

The attitude and determination system installed in the flight software consists of several different parts that interconnect:

- The orbital propagator, which takes orbital parameters supplied by NORAD and extrapolates them into the future to provide a predicted model of the orbit. This allows for orbital data to be sent only once every week instead of constantly, and provides the satellite with a better model of comparison with sensor readings.
- Magnetic field look-up table. The look-up table is also provided by NORAD and provides us with the means to find our location above the Earth's surface given a pattern of magnetic readings observed from the satellite's magnetometers.
- Actuator control law. This is the final stage of the control of the system, in which all observed and calculated data is brought together to determine which torque-rods need to be turned on, and for what duration of time.

3 Science Algorithms

The science analysis is made up of three main algorithms: Cloud coverage detection, stereoscopic imaging, and cloud classification.

3.1 Cloud Detection

The cloud detection algorithm is a very simple saturation and lightness comparison algorithm. The algorithm in pseudo-code is described below.

```

function CLOUD-DETECT( image ) returns a percentage of cloud cover
  score ← 0
  for each pixel p in image from left to right, top to bottom do
    result = PROCESSPIXEL( pred, pgreen, pblue )
    if result = True then do
      ptotal ← 1
      score ← score + 1
      for each pixel q below, to the right, and diagonally down-right of p do
        score ← score + qtotal
  return score / imagesize * 4

```

Figure 1: The cloud detection algorithm used in the science analysis

Here, *image* is the raw image taken from the camera, and reduced into an array of 3-bit RGB (Red Green Blue) components for each pixel. Each pixel has a score associated with it, and if PROCESSPIXEL returns *True* for a given pixel, its score is set to 1, and the global total is increased by 1. Then, for each surrounding pixel, if their values are 1 as well, the total score is incremented for each surrounding pixel. This gives a total score for the image as four times the number of pixels in the image. The percentage of cover then is a weighted percentage that takes into account surrounding pixels below and to the right of the pixel being examined.

The PROCESSPIXEL function is shown in the next figure. This function simply examines the components of a pixel in terms of its red, green, and blue color components, and returns *True* if the saturation and lightness are enough to satisfy conditions for a cloud.

```

function PROCESSPIXEL( pixel p ) returns True if in a cloud, False otherwise
  average ← (pred + pgreen + pblue)/3
  if average ≥  $\alpha$  then do
    saturation ← MAX(pred, pgreen, pblue) - MIN( pred, pgreen, pblue ) / average
    if saturation ≤  $\beta$  then return True
  return False

```

Figure 2: The PROCESSPIXEL function that checks each pixel's saturation and lightness against set thresholds

In the first part of this function, the average of the three color components is taken and compared against a threshold percentage α . If that passes, the saturation is taken and compared against a threshold percentage β . If both tests pass, the function returns positive, indicating that the pixel is white enough to be considered part of a cloud. Otherwise it returns negatively.

In both of these functions, the value of the pixel components is taken to be a value between 0 and 1. A good value of α seems to be 0.35, while a good value for β seems to be 0.25. These values have been experimentally determined, and have produced the best cloud detection results.

3.2 Stereoscopic Imaging

The stereoscopic imaging algorithm used on DINO is built in-house by Pascal Getreuer for the specific goal of detecting heights of clouds without imposing a high order of computational requirements on the flight computer. The algorithm itself is based on Scharstein's¹ gradient-based approach.

There are four main parts to the procedure of the algorithm:

1. Pre-processing filtering
2. Approximating image gradients
3. Multi-scale aggregation and matching
4. Post-processing filtering

¹D. Scharstein. *View Synthesis Using Stereo Vision*. Lecture Notes in Computer Science, Vol. 1583, Springer-Verlag Heidelberg, 1999.

Outlined in Pascal's work are the methods of performing each of these steps, as well as processor-saving approximations and test results. See [insert doc name here] for more details.

3.3 Cloud Classification

The cloud classification algorithm used is based on a simple back-propagation neural network training algorithm. The pseudo-code of this algorithm is shown below².

```

function BACK-PROP-LEARNING( examples, network ) returns a neural network
  inputs: examples, a set of examples, each with input vector x and output vector y
           network, a multilayer network with  $L$  layers, weights  $W_{j,i}$ , activation function  $g$ 

  repeat
    for each  $e$  in examples do
      for each node  $j$  in the input layer do  $a_j \leftarrow x_j[e]$ 
      for  $l = 2$  to  $M$  do
         $in_i \leftarrow \sum_j W_{j,i} a_j$ 
         $a_i \leftarrow g(in_i)$ 
      for each node  $i$  in the output layer do
         $\Delta_i \leftarrow g'(in_i) \times (y_i[e] - a_i)$ 
      for  $l = M - 1$  to  $1$  do
        for each node  $j$  in layer  $l$  do
           $\Delta_j \leftarrow g'(in_j) \sum_i W_{j,i} \Delta_i$ 
          for each node  $i$  in layer  $l$  do
             $W_{j,i} \leftarrow W_{j,i} + \alpha \times a_j \times \Delta_i$ 
      until some stopping criterion is satisfied
  return NEURAL-NET-HYPOTHESIS(network)

```

Figure 3: The back-propagation algorithm for learning in multilayer networks.

The details of this algorithm can be found in chapter 20 of *Artificial Intelligence: A Modern Approach*, second edition, by Russel and Norvig. Our particular implementation of this algorithm takes for each example a gray-scale image of a cloud, produced from the cloud-detection algorithm above. Using 250 to 500 training examples, the weights of each unit in the network is trained and stored into a file. Then, during use, each picture is classified against these pre-calculated weights and a result comes out of the network.

3.4 Testing

The easiest method of testing these algorithms is to take images of clouds taken at known distances, pass them to the algorithms, and verify the results. This is one of many methods we will use to verify that the algorithms written operate as expected.

Following is a summary of the testing plans we have, any testing we have already performed, and any results we have obtained.

²Algorithm and code taken from figure 20.25, Russel and Norvig: *Artificial Intelligence: A Modern Approach*, Second Edition, 2003

3.4.1 Cloud Detection Testing

The cloud detection algorithm has undergone the most testing of all of the algorithms. Used in two balloon-Sat missions, results indicated that clouds on the Earth were reliably and accurately detected from pictures taken from flight-model cameras. Returned percentages are accurate and indicative of how much actual cloud cover exists in each image. False detections were found to be at a minimum, but occurred mainly over buildings and arid plains (both areas of high luminosity and low saturation).

The results of one analyzed picture is shown below:

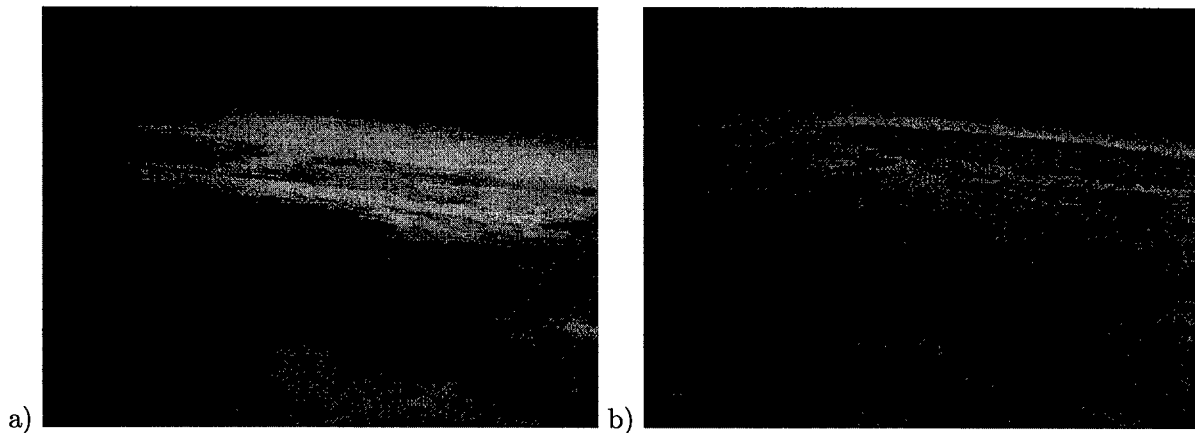


Figure 4: a) Original picture taken with SupportSAT II, b) processed image. Detected clouds are highlighted in green

3.4.2 Stereoscopic Imaging Testing

At the time of writing, no formal testing has been performed on the stereoscopic imaging of clouds. However, plans have been formulated to verify the algorithm using a very precise angle-table with objects set at fixed, known distances. Equipment and expertise is being donated from Ball Aerospace, Inc. to aid us in this testing.

3.4.3 Cloud Classification Testing

Initial testing of the cloud classification algorithm has shown promising results. We have determined that using the currently established infrastructure will require a relatively fast computer to do analysis of clouds, as the algorithm is very computationally intense. Initial results have shown one image classified in as little as 10 minutes to as much as an hour, depending on the parameters used in the algorithm. Further testing will be performed with a wider range of cloud formations, and in the end we will be using the algorithm in our ground software to analyze black-and-white images returned from our cloud detection algorithm on board the satellite.

4 ADCS Algorithms

The ADCS system installed on DINO is a complex, closed-loop system that is designed to autonomously determine and correct for the positioning of the satellite while in orbit. There are two main algorithms used within this system: The orbital propogator, and the actuator control law.

4.1 SGP4 Orbital Propogator

The SGP4 algorithm is an orbital propogation algorithm that is used to help orient the satellite. Given measurements of the satellite's position and orbit at a certain time (orbital parameters given to us in TLE format), the algorithm is able to calculate where the satellite is in its orbit based on the elapsed time since the measurements were taken.

The code for the algorithm was given to us in FORTRAN and translated by the DINO software team into native Python. The equations were broken up into functions based on what information they provide (e.g. calculating the effects of atmospheric drag and gravitation, or solving Kepler's equations). In this way, calculations could be tested part of the way through an iteration to help in diagnosing errors.

4.2 Actuator Control Law

This is the final stage of the control of the system, in which all observed and calculated data is brought together to determine which torque-rods need to be turned on, and for what duration of time. Figure 5 details the flow of the control law with the rest of the system.

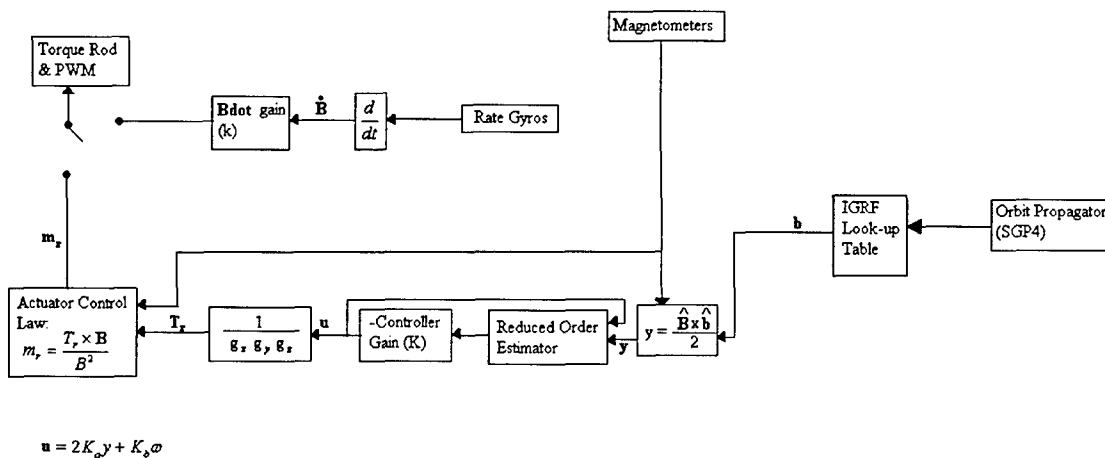


Figure 5: Flow chart of the ADCS control logic

4.3 Testing

Testing the SGP4 algorithm has been fairly straight forward. Provided with the code for the algorithm was a test case with the inputs and outputs of the algorithm to verify the implementation. This was used to create a spreadsheet for the creating of additional test cases and to provide test values for intermediate calculations in the algorithm. The spreadsheet performs the same calculations that the Python implementation does,

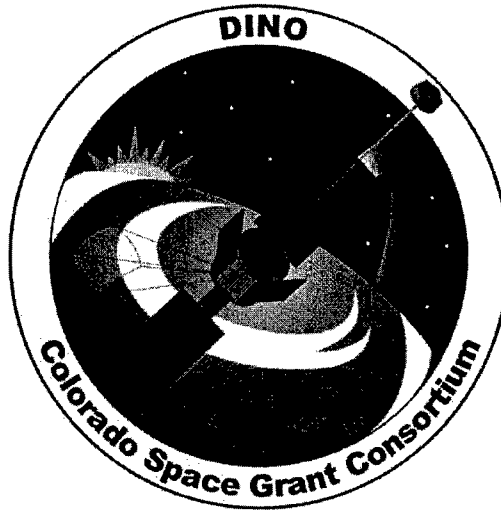
and in the same order. Using this spreadsheet, finding correct values for any calculation in the algorithm is made trivial, and provides an easy way to test the software.

To date, much of the algorithm has performed as expected. Additional testing is being performed to maximize the accuracy of each of the calculations produced by the algorithm.

No formal testing of the actuator control law has been completed to date. However, procedures employing the use of stringent test simulators will be used to confirm the output of the system. We will also use real NORAD orbital information in these simulations during satellite day-in-the-life testing to verify that the control law works as expected.

A List of Acronyms

Acronym	Meaning
ADCS	Attitude and Determination Control System
RGB	Red Green Blue. This is the order of color components in a pixel of color
SGP4	An orbital propagation algorithm developed for NORAD to be used with TLEs in predicting future orbital parameters.
TLE	Two-Line Elements. This is a set of data provided by NORAD containing information about the orbit of the satellite.



TC74 - Modifying, Testing and Mounting

DINO-THR-RPT-SENSOR, Rev. A

Written by:
Nicole Demandante

Prepared for:
Nanosat III

Table of Contents

1	Scope.....	4
1.1	Identification.....	4
1.2	Document Maintenance.....	4
1.3	Systems Overview.....	4
1.4	Document Overview.....	4
1.5	Referenced Documents.....	4
2	TC74.....	4
3	TC74 Placement.....	4
3.1	Address TC74A0-5.0VAT.....	5
3.2	Address TC74A2-5.0VAT.....	5
3.3	Address TC74A3-5.0VAT.....	5
3.4	Address TC74A5-5.0VAT.....	5
3.5	Address TC74A7-5.0VAT.....	5
4	Adding a Capacitor.....	6
4.1	Reason.....	6
4.2	Attaching Capacitor to TC74.....	6
4.2.1	Materials	6
4.2.2	Procedure	6
5	Testing.....	6
6	Mounting TC74.....	6
6.1	Epoxy.....	6
6.2	Mixing Epoxy.....	6
6.2.1	Materials	6
6.2.2	Procedure	6
6.2.3	Mounting	7

1 Scope

1.1 Identification

This document applies to the DINO project, a project undertaken by the Colorado Space Grant Consortium at the University of Colorado at Boulder. This project is part of the Nanosatellite III Program sponsored by the Air Force Office of Scientific Research (AFOSR), Air Force Research Laboratory (AFRL), Association of Aeronautics and Astronautics (AIAA), and Goddard Space Flight Center (GSFC).

1.2 Document Maintenance

This document falls under the DINO document control requirements as specified under the DINO Configuration Management plan. All changes and updates must be made in accordance with the DINO CM plan.

1.3 Systems Overview

The purpose of the student-led Deployment and Intelligent Nanosatellite Operations (DINO) mission is to determine cloud heights from space, evaluate the performance of intelligent operations, and assess deployment technologies for nanosatellites including a gravity-gradient boom, memory composite hinges, and thin-film solar arrays.

1.4 Document Overview

This document describes the TC74 thermal sensor.

1.5 Referenced Documents

List any reference documents here.

2 TC74

The TC74 is a serially accessible, digital temperature sensor particularly suited for low cost and small form factor applications. Temperature data is converted from the onboard thermal sensing element and made available as an 8-bit digital word. Communication with the TC74 is accomplished via a 2-wire SMBus/I2C compatible serial port. This bus also can be used to implement multi-drop/multi-zone monitoring. Temperature resolution is 1°C with a ± 3 C accuracy from 0C to +125C.. Conversion rate is a nominal 8 samples/sec. During normal operation, the quiescent current is 200 μ A. During standby operation, the quiescent current is 5 μ A. The TC74 are static sensitive.

3 TC74 Placement

There are five different addresses for the TC74. Each SMBus/I2C can have only one TC74 of each address.

3.1 Address TC74A0-5.0VAT

- Camera 1
 - o Due to the limited space on the electronics inside the Camera 1 box it was decided the TC74 would be mounted of the wall of box as near the camera as possible.
- TNC
 - o TC74 will be mounted to the back of one of the TNC boards.
- Radio
 - o TC74 will be mounted on radio board near the antennae.
- Solar Panel One

3.2 Address TC74A2-5.0VAT

- Camera 2
 - o Due to the limited space on the electronics inside the Camera 1 box it was decided the TC74 would be mounted of the wall of box as near the camera as possible.
- Tip Mass Comm (TMC)
 - o TC74 will be mounted on the board by the antennae.
- Solar Panel Two

3.3 Address TC74A3-5.0VAT

- Magnetometer
 - o TC74 will be mounted on the wall of the box due to the small size of the magnetometer.
- Power Panel 1
 - o TC74 will be mounted on the EPS board by the micro controller.
- Frangibolt One
- FITS

3.4 Address TC74A5-5.0VAT

- Solar Panel Three
- Power Panel 2
 - o TC74 will be mounted on the EPS board by the DC-DC converters.
- Frangibolt Two
- FITS

3.5 Address TC74A7-5.0VAT

- Solar Panel Four
- ADCS box
 - o TC74 will be mounted on the A/C converter due to its abundance of space.

4 Adding a Capacitor

4.1 Reason

A 0.1 microfarad capacitor was attached to each TC74 in order to eliminate noise.

4.2 Attaching Capacitor to TC74

4.2.1 Materials

- (20) 0.1 microfarad capacitors
- (20) TC74s

4.2.2 Procedure

- Make sure the leads of the TC74 are clean and free of debris
- Solder capacitor to lead number 3 (ground) and lead number 5 (data)

5 Testing

Each TC74 was tested with the flight computer individually. The average reading was 31.1 degrees Celsius when tested in a room temperature environment. The largest deviation was 4 degrees Celsius.

6 Mounting TC74

6.1 Epoxy

3M Scotch – Weld 2216 B/A Gray Epoxy Adhesives are flexible, two-part, room temperature curing epoxies with high peel and shear strengths.

6.2 Mixing Epoxy

6.2.1 Materials

- Epoxy Part A (accelerator)
- Epoxy Part B (base)

6.2.2 Procedure

- Mix 7 parts weight of Accelerator with 5 parts weight of Base.
- Stir mixture with stir stick for 2 minutes or until mixture is of a uniform color.
- Work life is 90 minutes at room temperature (74 deg. F).

6.2.3 Mounting

- Make sure TC74 and mounting surface is free of dirt and debris.
- Cover back of TC74 with epoxy.
- Cover desired area or surface with epoxy making sure to completely cover all metal leads on board.
- Place TC74 on desired location and hold in place for 2 minutes.
- Wipe excess epoxy off board with wet cloth.
- Keep TC74 in a horizontal position to avoid slipping.
- Wait 24 hours for epoxy to dry.
- Taping sensor in place is permissible



Tip Mass

DINO-TM-RPT-TM, Rev. A

Written by:
Siddharth Shetty
Anders Fornberg

Prepared for:
Nanosat III

Table of Contents

1	Scope.....	4
1.1	Identification.....	4
1.2	Document Maintenance.....	4
1.3	Systems Overview.....	4
1.4	Document Overview.....	4
1.5	Referenced Documents.....	4
2	The Wireless Link.....	4
2.1	Specifications.....	5
2.2	Radio Propagation Tests.....	5
2.2.1	Procedure for Test 1	5
2.2.2	Results for Test 1	5
2.2.3	Conclusion:	6
2.2.4	Procedure for Test 2	6
2.2.5	Results for Test 2	6
2.2.6	Conclusion	8
2.3	Interface Customization.....	8
3	Science Incorporated on the Tip Mass.....	10
3.1	Tip Mass Science Hardware.....	10
3.1.1	Rate Gyros	10
3.1.2	Rate Gyros Testing	10
3.1.3	Accelerometers	11
3.1.4	Accelerometers Testing	12

1 Scope

1.1 Identification

This document applies to the DINO project, a project undertaken by the Colorado Space Grant Consortium at the University of Colorado at Boulder. This project is part of the Nanosatellite III Program sponsored by the Air Force Office of Scientific Research (AFOSR), Air Force Research Laboratory (AFRL), Association of Aeronautics and Astronautics (AIAA), and Goddard Space Flight Center (GSFC).

1.2 Document Maintenance

This document falls under the DINO document control requirements as specified under the DINO Configuration Management plan. All changes and updates must be made in accordance with the DINO CM plan.

1.3 Systems Overview

The purpose of the student-led Deployment and Intelligent Nanosatellite Operations (DINO) mission is to determine cloud heights from space, evaluate the performance of intelligent operations, and assess deployment technologies for nanosatellites including a gravity-gradient boom, memory composite hinges, and thin-film solar arrays.

1.4 Document Overview

This document explains the interfaces existing on the Tip Mass module:

- Tip Mass radio interface with the Microcontroller
- Microcontroller interface with the On-board motion sensors

AND the radio interface with the Flight computer on the main satellite module

1.5 Referenced Documents

<http://rex.colorado.edu/svn/dino/trunk/hardware/tipmass/schematic.pdf>

<http://rex.colorado.edu/svn/dino/trunk/hardware/tipmass/aux-schematic.pdf>

2 The Wireless Link

Wiser 2400 (802.11b) radios provide conversion of serial (RS-232) data interface to the 802.11b wireless interface. The serial end of the interface will connect to the flight computer (on the main satellite module) and the microcontroller (PIC16C77 on the Tip Mass side). The wireless interface will provide the link between the flight computer and the Tip Mass separated by a distance of 6m as shown in Figure 1.

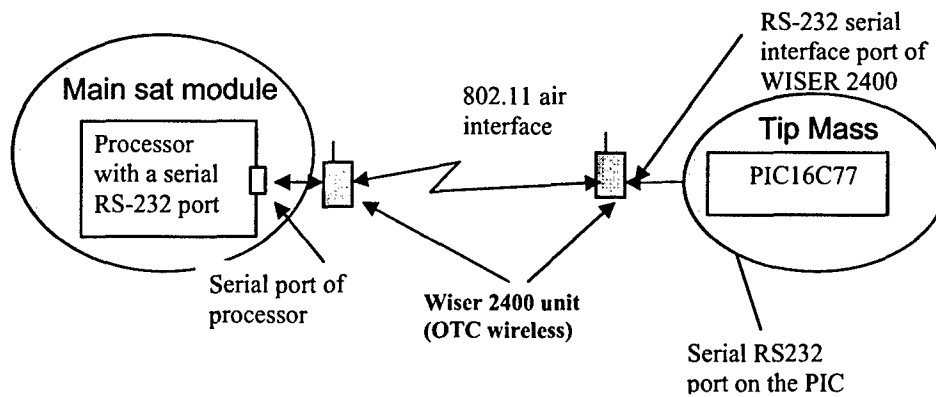


Figure 1

2.1 Specifications

Specifications of the Wisier 2400 radios:-

- Frequency: ISM band (2.4GHz – 2.495GHz)
- Voltage, current: 5v, max 480mA (in transmit mode)
- Data rate: Configured for 115K baud
- Weight : 2.0 ounces
- Antenna type: Integrated dipole antenna (omni-directional) with ~2dBi gain

2.2 Radio Propagation Tests

2.2.1 Procedure for Test 1

The radios were tested in a no-obstruction environment. The orientation of the two radios was switched from Vertical (V) to Horizontal (H) and the subsequent measurements were recorded at increasing distances.

Table 1 summarizes the measurements.

2.2.2 Results for Test 1

Table 1

Distance	wiser1-V, wiser2-V	wiser1-H, wiser2-H	wiser1-V, wiser2-H	Wiser1-H, wiser2-V
	signal level (dbm)	signal level (dbm)	signal level (dbm)	signal level (dbm)
(m)				
12	-71	-67	-76	-62
20	-71	-71	-72	-72
33	-78	-78	-75	-75

2.2.3 Conclusion:

The losses were higher than that estimated using Link Power budget but were low enough to sustain an error-free transmission for a significant distance range. The omnidirectional antenna assures that the signal level is satisfactory for any orientation of the radios with respect to each other.

2.2.4 Procedure for Test 2

The second set of radio measurements were made with the radios enclosed in an isogrid/metal box. The isogrid can induce a faraday cage effect for the 2.4GHz frequencies. This was performed because the final structure will have the radio enclosed in a metal box (although the design will have a provision for the antenna (dipole) to be protruding out of the box) mounted on an isogrid.

2.2.5 Results for Test 2

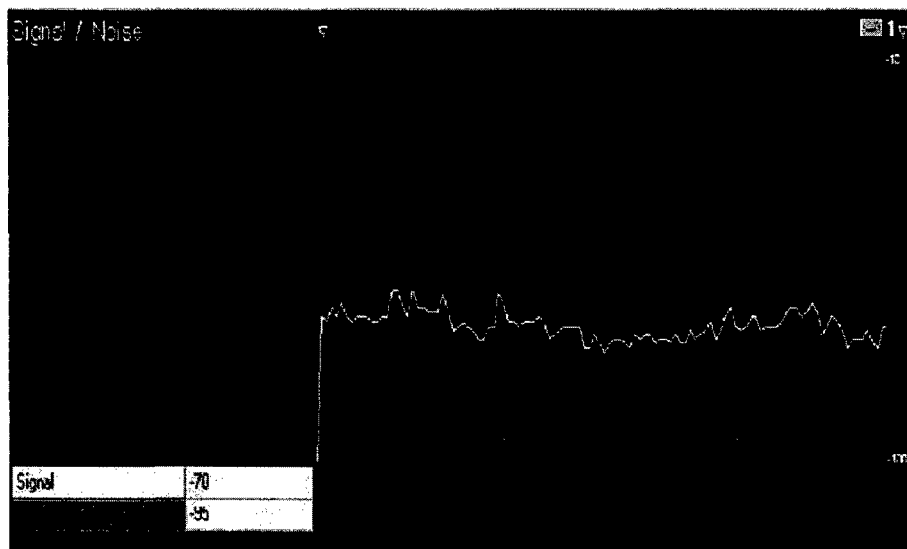


Figure 2

- Signal level: -70dBm
- Radio placed in the open (without obstruction)
- Signal level measurements taken all around a circle of radius 8-8.5m
- Signal range:-65dbm to -73dbm
- Frame transmission rate at 11Mbps

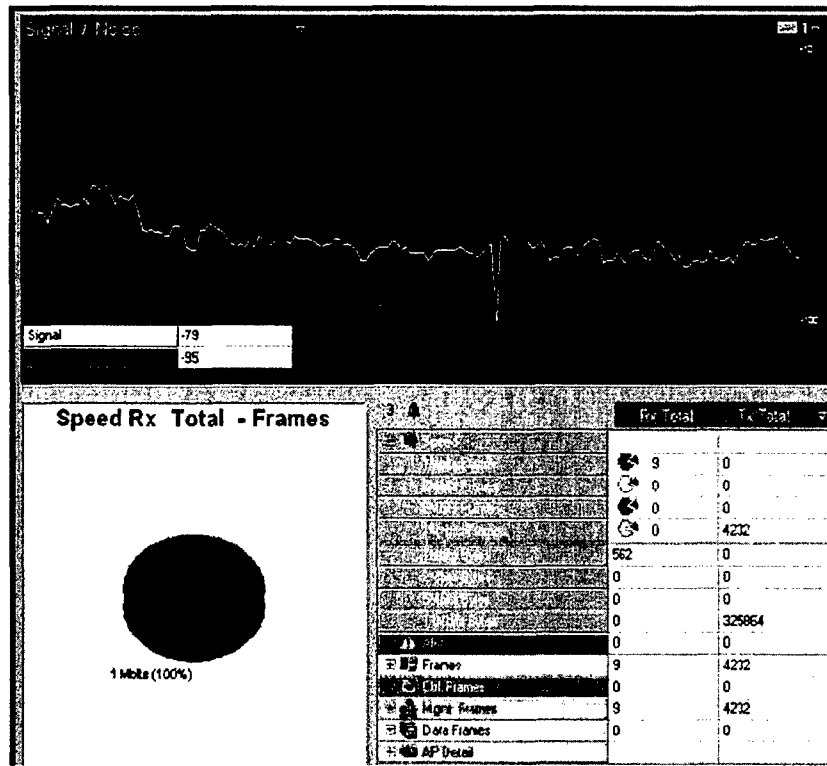


Figure 3

- Radio placed under the solid metal plate.
- Signal level measurements taken all around a circle of radius 8-8.5m
- Signal range:-76dbm to -81dbm
- Frame transmission rate at 11Mbps

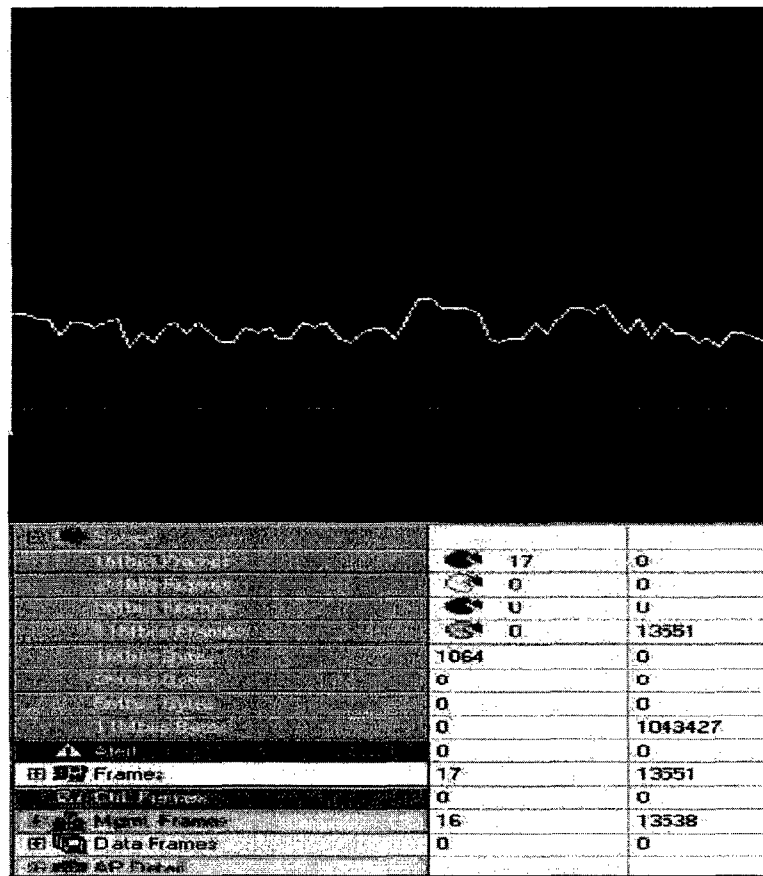


Figure 4

- Radio placed between the solid metal plate and the ‘isogrid’
- Signal level measurements taken all around a circle of radius 8-8.5m
- Signal range:-78dbm to -82dbm
- Frame transmission rate at 11Mbps

2.2.6 Conclusion

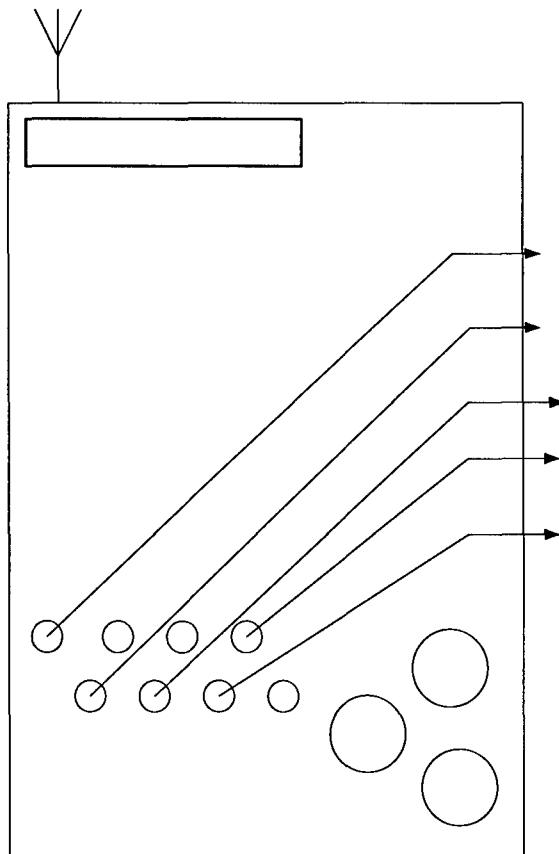
Under simulated conditions the radio performed well for the link distance expected in the deployed state. A distance margin is also accounted for.

2.3 Interface Customization

The Wiser 2400 radios were modified to meet the interface requirements at the serial connections. There were two serial connections for the two radio units respectively:-

- On the Tip Mass, interface with the PIC
- On the main satellite module, interface with the Flight computer

Figure 5 shows the internal pin configuration for the Wiser 2400 radio PCBs.



LABEL

Figure 5

The pin-outs for the radio are shown above. Table 2 maps pins 1-8 in the above figure to the pins provided on the flight computer for the Tip Mass communication system

Table 2

Radio	Fight Computer
Pin 2 (Tx)	
Pin 3 (Rx)	
Power +5V	
Pin 5 and Power GND	

Table 3 provides the mapping between the pins 1-8 on the radio side and the PIC16 C77

Table 3

Radio	PIC16 C77
Pin 2 (Tx)	Pin14 (DOUT1)
Pin 4 (Rx)	Pin 13 (RIN1)
Pin 3 (RTS)	Pin 7 (DOUT2)
Pin 5 (CTS)	Pin 8 (RIN2)

3 Science Incorporated on the Tip Mass

The Tip Mass Science board measures rate of rotation and acceleration on all 3 axis, which will allow for accurate recreation and modeling of the deployment of the Tip Mass module. The measurements are accomplished through the use of 3 rate gyros and 2 dual axis accelerometers.

3.1 Tip Mass Science Hardware

3.1.1 Rate Gyros

The Rate Gyros are the ADXRS150EB $\pm 150^\circ/\text{s}$ Single Chip Yaw Rate Gyros. It was decided to use these gyros because of the familiarity with these devices from other space grant projects. The ADXRS150 deliver an analog output signal that's voltage is proportional to the angular rate of rotation about the axis normal to the top surface of the package, see Figure 6. This signal is then converted into a digital signal and stored in a data log on the Tip Mass, to be later sent to the main DINO module. The package used is Tip Mass science has the rate gyro on a factory mounted evaluation board, which was decided on because it would be easier to integrate and mount on the Tip Mass PCB board.

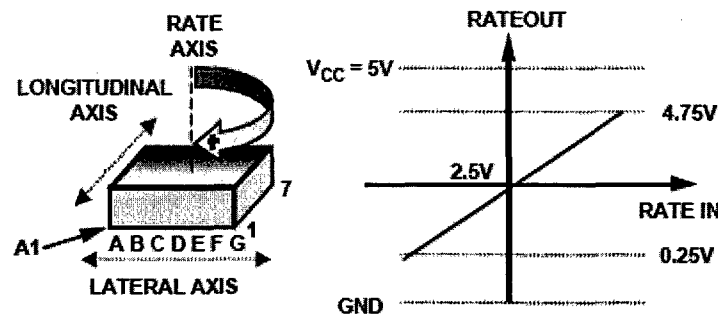


Figure 6: RATEOUT Signal Increases with Clockwise Rotation

3.1.2 Rate Gyros Testing

The rate gyro circuitry was constructed on a "prototyping board" with the corresponding components. A voltmeter was placed in the output of the circuit. Variable power supplies were utilized to simulate the input voltages of the +5VDC power supplies. The circuit was then rotated in each direction to verify correct response of the rate gyro. The rate gyro was also verified to have insignificant drift by placing it in a stable atmosphere (i.e. not rotating) and taking data for 48 hours. The following figure, Figure 7 displays the results of this test.

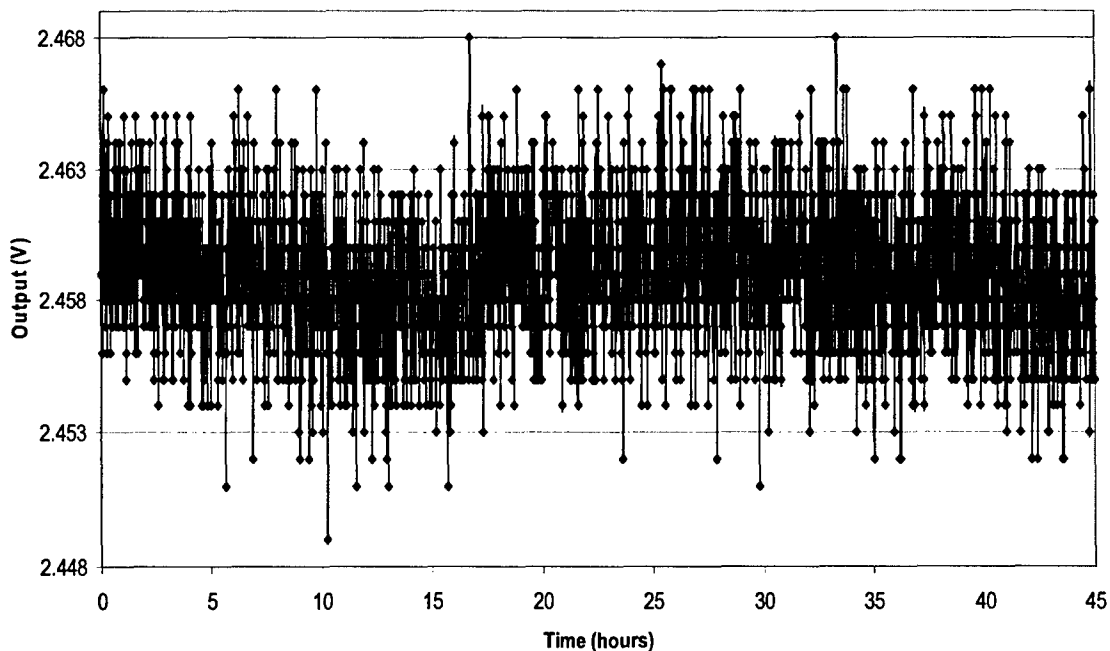


Figure 7: Rate Gyro 48hr Test Results

The rate gyro had no drift when average value of the output is taken. The null rate is approximately 2.5VDC and will have to be taken from the individual rate gyros before launch to verify the values in software. This value will also be affected by the signal conditioning circuitry. The circuits were tested individually in the same manner after they were manufactured and populated. After testing, the circuits were functionally tested with the completed Tip Mass electronics.

3.1.3 Accelerometers

The two dual axis accelerometers used on Tip Mass are the ADXL311 ± 2 g Dual Axis Accelerometers. The ADXL311 can measure both dynamic acceleration (e.g., vibrations) and static acceleration (e.g., gravity). The output is an analog voltage that is proportional to the acceleration. The high accuracy and small acceleration range is achieved because of the slow deployment of the Tip Mass, which is expected to be at its maximum less than 1 g. See Figure 8 for functional block diagram.

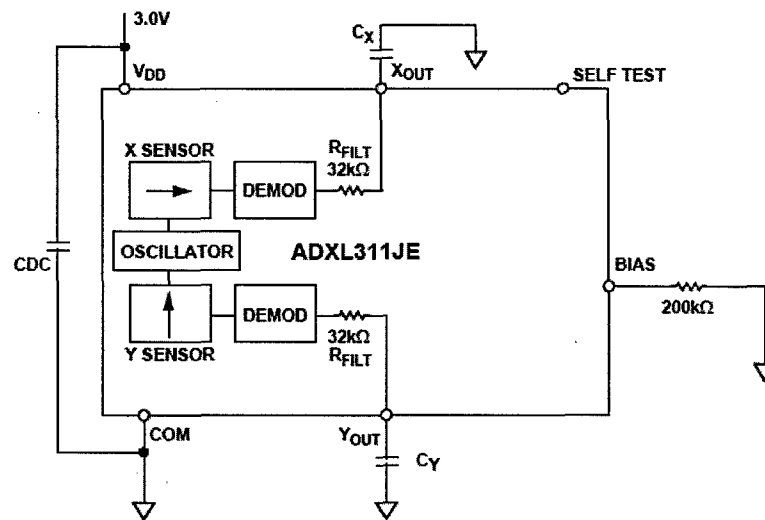


Figure 8: Functional Block Diagram of Accelerometers

3.1.4 Accelerometers Testing

The accelerometers were all individually hooked up to an oscilloscope and each was verified for proper operations. The null rate is approximately 2.5 VDC, and using the earth's gravitation force it was viewed that the actual range of measurable acceleration for these devices is approximately ± 4 g, high then the rated ± 2 g. From this it was determined that, using 8 bit encoding, that an obtainable resolution of 15 mg is achievable.